

International Journal on

Advances in Life Sciences



The *International Journal on Advances in Life Sciences* is published by IARIA.

ISSN: 1942-2660

journals site: <http://www.ariajournals.org>

contact: petre@aria.org

Responsibility for the contents rests upon the authors and not upon IARIA, nor on IARIA volunteers, staff, or contractors.

IARIA is the owner of the publication and of editorial aspects. IARIA reserves the right to update the content for quality improvements.

Abstracting is permitted with credit to the source. Libraries are permitted to photocopy or print, providing the reference is mentioned and that the resulting material is made available at no cost.

Reference should mention:

International Journal on Advances in Life Sciences, issn 1942-2660
vol. 15, no. 1 & 2, year 2023, http://www.ariajournals.org/life_sciences/

The copyright for each included paper belongs to the authors. Republishing of same material, by authors or persons or organizations, is not allowed. Reprint rights can be granted by IARIA or by the authors, and must include proper reference.

Reference to an article in the journal is as follows:

<Author list>, "<Article title>"
International Journal on Advances in Life Sciences, issn 1942-2660
vol. 15, no. 1 & 2, year 2023, <start page>:<end page> , http://www.ariajournals.org/life_sciences/

IARIA journals are made available for free, proving the appropriate references are made when their content is used.

Sponsored by IARIA

www.aria.org

Copyright © 2023 IARIA

Editor-in-Chief

Les Sztandera, Thomas Jefferson University, USA

Editorial Advisory Board

Åsa Smedberg, Stockholm University, Sweden

Piero Giacomelli, SPAC SPA -Arzignano (Vicenza), Italia

Ramesh Krishnamurthy, Health Systems and Innovation Cluster, World Health Organization - Geneva, Switzerland

Anthony Glascock, Drexel University, USA

Hassan Ghazal, Moroccan Society for Telemedicine and eHealth, Morocco

Hans C. Ossebaard, University of Twente, the Netherlands

Juergen Eils, DKFZ, German

Trine S Bergmo, Norwegian Centre for Integrated Care and Telemedicine, Norway

Anne G. Ekeland, Norwegian Centre for Integrated Care and Telemedicine / University Hospital of North Norway |

University of Tromsø, Norway

Kari Dyb, Norwegian Centre for Integrated Care and Telemedicine / University Hospital of North Norway |

University of Tromsø, Norway

Hassan Khachfe, Lebanese International University, Lebanon

Ivan Evgeniev, TU Sofia, Bulgaria

Matthieu-P. Schapranow, Hasso Plattner Institute, Germany

Editorial Board

Dimitrios Alexandrou, UBITECH Research, Greece

Giner Alor Hernández, Instituto Tecnológico de Orizaba, Mexico

Ezendu Ariwa, London Metropolitan University, UK

Eduard Babulak, University of Maryland University College, USA

Ganesharam Balagopal, Ontario Ministry of the Environment, Canada

Kazi S. Bennoor, National Institute of Diseases of Chest & Hospital - Mohakhali, Bangladesh

Trine S Bergmo, Norwegian Centre for Integrated Care and Telemedicine, Norway

Jorge Bernardino, ISEC - Institute Polytechnic of Coimbra, Portugal

Tom Bersano, University of Michigan Cancer Center and University of Michigan Biomedical Engineering
Department, USA

Razvan Bocu, Transilvania University of Brasov, Romania

Freimut Bodendorf, Universität Erlangen-Nürnberg, Germany

Eileen Brebner, Royal Society of Medicine - London, UK

Julien Broisin, IRIT, France

Sabine Bruaux, Sup de Co Amiens, France

Dumitru Burdescu, University of Craiova, Romania

Vanco Cabukovski, Ss. Cyril and Methodius University in Skopje, Republic of Macedonia

Yang Cao, Virginia Tech, USA

Rupp Carriveau, University of Windsor, Canada

Maiga Chang, Athabasca University - Edmonton, Canada

Longjian Chen, College of Engineering, China Agricultural University, China
Dickson Chiu, Dickson Computer Systems, Hong Kong
Bee Bee Chua, University of Technology, Sydney, Australia
Udi Davidovich, Amsterdam Health Service - GGD Amsterdam, The Netherlands
Maria do Carmo Barros de Melo, Telehealth Center, School of Medicine - Universidade Federal de Minas Gerais (Federal University of Minas Gerais), Brazil
Kari Dyb, Norwegian Centre for Integrated Care and Telemedicine / University Hospital of North Norway | University of Tromsø, Norway
Juergen Eils, DKFZ, German
Anne G. Ekeland, Norwegian Centre for Integrated Care and Telemedicine / University Hospital of North Norway | University of Tromsø, Norway
El-Sayed M. El-Horbaty, Ain Shams University, Egypt
Ivan Evgeniev, TU Sofia, Bulgaria
Karla Felix Navarro, University of Technology, Sydney, Australia
Joseph Finkelstein, The Johns Hopkins Medical Institutions, USA
Stanley M. Finkelstein, University of Minnesota - Minneapolis, USA
Adam M. Gadomski, Università degli Studi di Roma La Sapienza, Italy
Ivan Ganchev, University of Limerick, Ireland / University of Plovdiv "Paisii Hilendarski", Bulgaria
Jerekias Gandure, University of Botswana, Botswana
Xiaohong Wang Gao, Middlesex University - London, UK
Josean Garrués-Irurzun, University of Granada, Spain
Hassan Ghazal, Moroccan Society for Telemedicine and eHealth, Morocco
Piero Giacomelli, SPAC SPA -Arzignano (Vicenza), Italia
Alejandro Giorgetti, University of Verona, Italy
Anthony Glascock, Drexel University, USA
Wojciech Glinkowski, Polish Telemedicine Society / Center of Excellence "TeleOrto", Poland
Francisco J. Grajales III, eHealth Strategy Office / University of British Columbia, Canada
Conceição Granja, Conceição Granja, University Hospital of North Norway / Norwegian Centre for Integrated Care and Telemedicine, Norway
William I. Grosky, University of Michigan-Dearborn, USA
Richard Gunstone, Bournemouth University, UK
Amir Hajjam-El-Hassani, University of Technology of Belfort-Montbéliard, France
Lynne Hall, University of Sunderland, UK
Päivi Hämäläinen, National Institute for Health and Welfare, Finland
Anja Henner, Oulu University of Applied Sciences, Finland
Stefan Hey, Karlsruhe Institute of Technology (KIT) , Germany
Dragan Ivetic, University of Novi Sad, Serbia
Sundaresan Jayaraman, Georgia Institute of Technology - Atlanta, USA
Malina Jordanova, Space Research & Technology Institute, Bulgarian Academy of Sciences, Bulgaria
Attila Kertesz-Farkas, University of Washington, USA
Hassan Khachfe, Lebanese International University, Lebanon
Valentinas Klevas, Kaunas University of Technology / Lithuaniaian Energy Institute, Lithuania
Anant R Koppar, PET Research Center / KTwo technology Solutions, India
Bernd Krämer, FernUniversität in Hagen, Germany
Ramesh Krishnamurthy, Health Systems and Innovation Cluster, World Health Organization - Geneva, Switzerland
Roger Mailler, University of Tulsa, USA

Dirk Malzahn, OrgaTech GmbH / Hamburg Open University, Germany
Salah H. Mandil, eStrategies & eHealth for WHO and ITU - Geneva, Switzerland
Herwig Mannaert, University of Antwerp, Belgium
Agostino Marengo, University of Bari, Italy
Igor V. Maslov, EvoCo, Inc., Japan
Ali Masoudi-Nejad, University of Tehran , Iran
Cezary Mazurek, Poznan Supercomputing and Networking Center, Poland
Teresa Meneu, Univ. Politécnica de Valencia, Spain
Kalogiannakis Michail, University of Crete, Greece
José Manuel Molina López, Universidad Carlos III de Madrid, Spain
Karsten Morisse, University of Applied Sciences Osnabrück, Germany
Ali Mostafaeipour, Industrial engineering Department, Yazd University, Yazd, Iran
Katarzyna Musial, King's College London, UK
Hasan Ogul, Baskent University - Ankara, Turkey
José Luis Oliveira, University of Aveiro, Portugal
Hans C. Ossebaard, National Institute for Public Health and the Environment - Bilthoven, The Netherlands
Carlos-Andrés Peña, University of Applied Sciences of Western Switzerland, Switzerland
Tamara Powell, Kennesaw State University, USA
Cédric Pruski, CR SANTEC - Centre de Recherche Public Henri Tudor, Luxembourg
Andry Rakotonirainy, Queensland University of Technology, Australia
Robert Reynolds, Wayne State University, USA
Joel Rodrigues, Institute of Telecommunications / University of Beira Interior, Portugal
Alejandro Rodríguez González, University Carlos III of Madrid, Spain
Nicla Rossini, Université du Luxembourg / Università del Piemonte Orientale / Università di Pavia, Italy
Addisson Salazar, Universidad Politecnica de Valencia, Spain
Abdel-Badeeh Salem, Ain Shams University, Egypt
Matthieu-P. Schapranow, Hasso Plattner Institute, Germany
Åsa Smedberg, Stockholm University, Sweden
Chitsutha Soomlek, University of Regina, Canada
Monika Steinberg, University of Applied Sciences and Arts Hanover, Germany
Les Sztandera, Thomas Jefferson University, USA
Jacqui Taylor, Bournemouth University, UK
Andrea Valente, University of Southern Denmark, Denmark
Jan Martijn van der Werf, Utrecht University, The Netherlands
Liezl van Dyk, Stellenbosch University, South Africa
Sofie Van Hoecke, Ghent University, Belgium
Iraklis Varlamis, Harokopio University of Athens, Greece
Genny Villa, Université de Montréal, Canada
Stephen White, University of Huddersfield, UK
Levent Yilmaz, Auburn University, USA
Eiko Yoneki, University of Cambridge, UK

CONTENTS

pages: 1 - 10

Exploring the Medical Caregivers' Perceptions of Technology Acceptance for an Online Speech and Language Assessment Application Among Stroke Patients

Awais Ahmad, Computer and Systems Science, Mid Sweden University, Sweden
Karin Ahlin, Service research Centre, Karlstad University, Sweden
Peter Mozelius, Computer and Systems Science Mid Sweden University, Sweden
Ali Hassan Sodhro, Department of Computer Science Kristianstad University, Sweden

pages: 11 - 19

Modeling of Animal Vibrissae: Adaptive Control of Multi-body Systems under Output Noise

Carsten Behn, Schmalkalden University of Applied Sciences, Germany
Moritz Scharff, Wilhelm-Franke-Str. 11, Dresden, Germany
Lukas Merker, Technische Universität Ilmenau, Germany

pages: 20 - 32

Designing a Low-Cost Early Diagnosis System Based on Deep Learning Monitoring the Development of Chronic Venous Disorder with Indirect Augmented Reality

Huseyin A. Erdem, Dokuz Eylül University, Turkey
Işıl Erdem, İzmir Institute of Technology, Turkey
Semih Utku, Dokuz Eylül University, Turkey

pages: 33 - 43

Step Measurement Using a Household Floor Mat and Shoe Sensors

Tomoko Funayama, Teikyo University of Science, Japan
Yasutaka Uchida, Teikyo University of Science, Japan
Yoshiaki Kogure, Teikyo University of Science, Japan

pages: 44 - 54

Possibility of Gait Analysis with MediaPipe and Its Application in Evaluating the Effects of Gait-assist Devices

Yasutaka Uchida, Teikyo University of Science, Japan
Tomoko Funayama, Teikyo University of Science, Japan
Yoshiaki Kogure, Teikyo University of Science, Japan

pages: 55 - 61

Examining the Relationship between COVID-19 Mobility and Eviction Rates in Philadelphia

Regina Ruane, The University of Pennsylvania, USA
Les Sztandera, Jefferson University, USA

Exploring the Medical Caregivers' Perceptions of Technology Acceptance for an Online Speech and Language Assessment Application Among Stroke Patients

Awais Ahmad
Computer and Systems Science,
Mid Sweden University,
Östersund, Sweden
e-mail: awais.ahmad@miun.se

Karin Ahlin
Service research Centre,
Karlstad University,
Karlstad, Sweden
e-mail: Karin.ahlin@kau.se

Peter Mozelius
Computer and Systems Science
Mid Sweden University,
Östersund, Sweden
e-mail: Peter.mozelius@miun.se

Ali Hassan Sodhro
Department of Computer Science
Kristianstad University
Kristianstad, Sweden
email: ali.hassan_sodhro@hkr.se

Abstract— Stroke is a globally increasing disease and speech and language deficiencies are common in stroke survivors. To facilitate medical caregivers in their professional work and to improve patients' quality of life, technology can play an important role. However, the use and acceptance of technology are uncertain and more research is needed in this direction. This study evaluates the technology acceptance and adoption of an online speech and language assessment application. The evaluation-focused Design Science Research strategy was adopted for that purpose. Two physiotherapists, one occupational therapist and three speech therapists participated in the study. The Unified Theory of Acceptance and Use of Technology (UTAUT) was used as the theoretical base for interview questions formation and data analysis. The study findings show that the suggested application is useful and easy to use; however, it should be better synchronised with speech therapists' daily work routines. The speech therapists stressed that the functionalities of the application should be designed in close collaboration with them, and it should be compatible with the already existing systems and services in place. Due to impairments after stroke, the patients have some specific preferences for software and hardware; such as a tablet with a touch pen is the preferred hardware. Additionally, the interface should have bigger text fonts and pictures, and highly contrastive colours in the graphics should be used for patients' convenience. The user's privacy and security, the patient's current health, and their previous knowledge and experience with technology were also found important determinants for the intention to use the given technology.

Keywords-Technology acceptance; Speech and language relearning; Unified Theory of Acceptance and Use of Technology (UTAUT); eHealth; Stroke.

I. INTRODUCTION

This study serves as an extension of a previously published paper wherein we delved into the perceptions of medical caregivers regarding the acceptance of technology for an online speech and language assessment application among stroke patients [1]. In this current study endeavour, we have undertaken a comprehensive and detailed analysis of the data, specifically focusing on the perspectives of speech

therapists. Furthermore, we have presented and discussed the related work more elaborately.

In the rapidly growing proportion of older adults in the global population, age-related chronic diseases are increasing [1], [2]. Stroke is a disease where survivors often suffer from both physical and mental impairments [3]. The impairments after stroke have a serious impact on patients' overall daily life quality and often a patient's friends and relatives are affected [4], [5]. Stroke impairments and rehabilitation after stroke can be divided into motoric, cognitive and speech disabilities [6]. This study focuses on speech impairments and the use of a technology-enhanced system to assess speech and language impairment and to find a relevant rehabilitation plan.

After a stroke, a patient's ability to read, write, speak and listen can be decreased to different degrees depending on how the stroke affected their brain [7]. Stroke patients' social and professional life is often severely affected, which can lead to an isolated and depressed state of mind. An important part of a successful rehabilitation process is early assessment of the speech and language impairments and to start relearning as soon as possible. Speech therapists often work with pen-and-paper-based assessment systems where calculating results, storing statistics, and measuring progress are time-consuming tasks. This study evaluates a prototype of the digitalisation of the pen-and-paper-based language assessment system 'A-ning'.

A-ning is a Swedish word that could be translated to English as a 'clue', symbolising the important idea of getting a clue to the mystery of which speech and language relearning activities the actual patient needs. The A-ning system has at least three user roles: stroke patients, speech therapists and health administrators. This first evaluation of the digital prototype only involves the speech therapist's perspective, and this must be followed up later by tests with the other user groups. Three speech therapists with long professional careers participated in the tests for this study, where interview questions and data analysis were based on the Unified Theory of Acceptance and Use of Technology (UTAUT) [8].

Despite the fact that several advanced and sophisticated technologies are available in the health sector, the use and acceptance of these technologies are doubtful and more research is needed to find the critical factors that might affect technology acceptance [9]-[13]. UTAUT model [14] has been widely used in research to evaluate the effectiveness and adoption of technology-enhanced systems [12], [15], [16]. This study is aimed to access and evaluate the technology acceptances of an eHealth application by using the UTAUT as a theoretical model.

The addressed research question was:

What is the technology acceptance of a speech and language assessment application from medical caregivers' viewpoint?

This study contributes to technology-enhanced speech and language relearning by co-creating and evaluating an online speech and language assessment application. The speech and language relearning process starts with an initial assessment to diagnose the patient's current speech and language deficiency. The manual assessment system is complex and time taking for speech therapists, which makes it difficult for already physically and mentally impaired patients to concentrate on the assessment exercises. Therefore, the assessment application was developed in close cooperation with speech therapists. The application was designed according to the gathered requirements from our previous study [17], and it was further developed according to the user's feedback in the article [1].

The remainder of the paper is structured as follows. An extended literature review is presented in Section II. In Section III, the UTAUT theory is presented as the theoretical framework of this study. An overview of the Speech and Language Assessment Application (A-ning) is given in Section IV. Section V describes the adopted methodology for this study, while the study results and the discussion about those results are presented in Sections VI and VII, respectively. Finally, the study conclusion and recommendations for future work are presented in Section VIII.

II. RELATED WORK

Several studies have been conducted previously to explore general technology acceptance factors in different areas of life [9], [17]-[21]. However, research on technology acceptance for speech and language relearning is scarce. Most of the studies have not considered the technology acceptance for patients with different types of disabilities. To our knowledge, this is the first study to find the critical factors for acceptance of speech and language relearning with the help of an interactive software application. X Zhou et al. argued in their study that the use of mobile applications is effective for speech rehabilitation after stroke [22], however, some other studies highlighted that the patient's eyesight is impaired after stroke [5], [23]; hardware with a bigger screen such as laptop or tablet is more efficient for the stroke patients

with an impaired vision [23]. Our study has, therefore, a broader scope where different kinds of hardware and software are considered. Many studies focused on the acceptance of ICT among older adults [18], [24]-[26].

Since stroke is most common in elderly people [16], some of our findings are similar to studies conducted for older adults. The notion of smart and pervasive healthcare for Swedish older patients is presented by [26]. It is further highlighted how much technology helps them to be active and alert in their daily normal routines. Authors in [27]-[29] emphasised the role of mobile devices for instance tablets to monitor people with aphasia, stroke, and neuron disorder diseases. It is easier to detect their falling position and get to know about location awareness in their homes and parks. Because mobile devices with sensors and gyroscopes and accelerometers in their bodies are more helpful in predicting such incidents. In [30], [31], the technology-driven relearning mechanism for speech and language patients is highly demanding to come back and regain their lost memories.

In this regard, design science is the key role player in providing state-of-the-art strategies and patterns of information collection and proper methods for its utilisation. Technological tools and trends have reshaped the entire world and COVID-19's critical situation at homes and workplaces. Online software and digital tools such as Zoom, Teams, skype and so on are key sources for video and teleconferences [32], [33]. It is essential to provide knowledge about technology and its proper utilisation to elderly and unaware people or individuals with critical diseases [32], [33]. Authors in [32], [33] also addressed the different ways of healthcare quality improvement with the help of emerging technological tools and evolutions. Researchers in [34], [35] presented technology-driven healthcare devices for data collection, classification, analysis and plotting for the proper recommendation to the experts and patients at the hospitals and medical centres.

Also, these wearable devices are helpful for the elderly and critical patients to measure their vital-sign signals for example, electrocardiogram (ECG), blood pressure and temperature. The technology revolution has made the lives of patients and healthcare comfortable and convenient, similarly [36] and [37] presents and discusses the role of internet-enabled therapy for problem analysis and mixed methods for clinical and healthcare analysis.

Healthcare experts in association with technology experts and data scientists interact and interpret the collected and classified data for better analysis and results which is quite necessary for smart medical uses-cases. An extensive review of the needs and acceptance rate of technology in today's world is addressed in [38], authors widely investigated the different tools, techniques, and methods for better and suitable recommendations to the medical centres. The role of mobile edge computing technology and IoT devices in healthcare for elderly and remote patients at cost-effective rates and simple ways is presented in [39], [40]. It is also

encouraged that the authors have proper training and awareness sessions for new users with clear benefits and consequences about the technology and its implications for the users.

Overall, the acceptance of online speech and language assessment applications is likely to be influenced by a complex interplay of factors, including perceived usefulness, perceived ease of use, social influence, perceived credibility, and perceived compatibility. As such, developers of these applications need to consider these factors when designing and marketing their products. Additionally, providing adequate training and support to users may also help to improve technology acceptance and adoption.

III. THEORETICAL FRAMEWORK: UNIFIED THEORY OF ACCEPTANCE AND USE OF TECHNOLOGY (UTAUT)

The UTAUT model was designed to assess user behaviour and intention to use technology [13]. It is a synthesis of eight different theories and models that were previously designed for technology acceptance including the Technology Acceptance Model (TAM), a widely acknowledged model to identify the intention to use the technology [11], [14], [27].

After comparing and synthesising those eight models, Venkatesh et al. [12] suggested that the intention to use technology depends upon four basic factors: performance expectancy, effort expectancy, social influence and facilitating conditions. Performance expectancy is explained in TAM as “perceived usefulness”, and effort expectancy is stated as “ease of use” in TAM. In other words, the UTAUT model can be seen as an extension of TAM as it adds two extra factors, social influence and facilitating conditions. Several studies highlighted that social influence such as the role of important others and facilitating conditions like education and training is important for technology acceptance [6], [23], [28], [29]. Therefore, the UTAUT model was preferred as the theoretical framework for this study. The UTAUT model suggests the following four technology acceptance elements.

A. Performance expectancy

Venkatesh et al. [12] defined performance expectancy as “the degree to which an individual believes that using the system will help him or her to attain gains in job performance” [13]. It is considered an important determinant of intention to use technology in many different studies [7]. Venkatesh et al. [12] highlight, the user should have a firm belief that the system will improve his/her productivity and performance, speed up the work tasks and it will make the work easier.

B. Effort expectancy

Effort expectancy describes the user’s belief in the ease of use of the system. Venkatesh et al. [12] stress that learning to operate the new system should be easy and quick, the use of the system should be effortless, and the interaction with the system should be understandable and clear. The system

should take less time and effort to perform mechanical operations such as data input [7].

C. Social influence

Venkatesh et al. [12] described social influence as “The degree to which an individual perceives that important others believe he or she should use the new system”. The beliefs of other influential and important people have a significant effect on the intention to use the system. In an organisation, the viewpoints of co-workers, supervisors and senior management play an important role in the acceptance of a technology-enhanced system.

D. Facilitating conditions

Venkatesh et al. [12] defined facilitating conditions as “The degree to which an individual believes that an organisational and technical infrastructure exists to support the use of the system”. The new system should be compatible and synchronised with the existing work routines and work style of the user. Guidance, clear instructions to use, and personalised support are the essential determinants for technology acceptance [7].

IV. SPEECH AND LANGUAGE ASSESSMENT APPLICATION (A-NING) OVERVIEW

Speech and language relearning start with an initial test of the patient’s communication loss after stroke; the test is called A-ning [30]. Despite the test being developed a long time ago (in 1995), it is still the most used and comprehensive test for language impairments in Sweden [31]. A-ning can be used by speech-language pathologists, teachers, and other professionals who work with individuals who have communication difficulties. The test is a standardised process conducted by speech therapists, and it consists of different assessment tasks. For example, the patient is asked to look at an image (see Figure 1) of an outdoor restaurant and describe the different activities there.



Figure 1. An example of a Patient’s task

Speech and language assessment applications typically use a range of assessment tools and techniques to evaluate

different aspects of an individual's speech and language skills. For example, these tools may include standardized tests, observation, and analysis of the individual's spoken and written language. During a session with the patient, the speech therapist gives some points from 0 to 5 on each task. Those points are then calculated according to different language categories and the average of all those categories is calculated to summarise the assessment, which is quite a time taking process. Figure 2 presents the manual evaluation after the test.

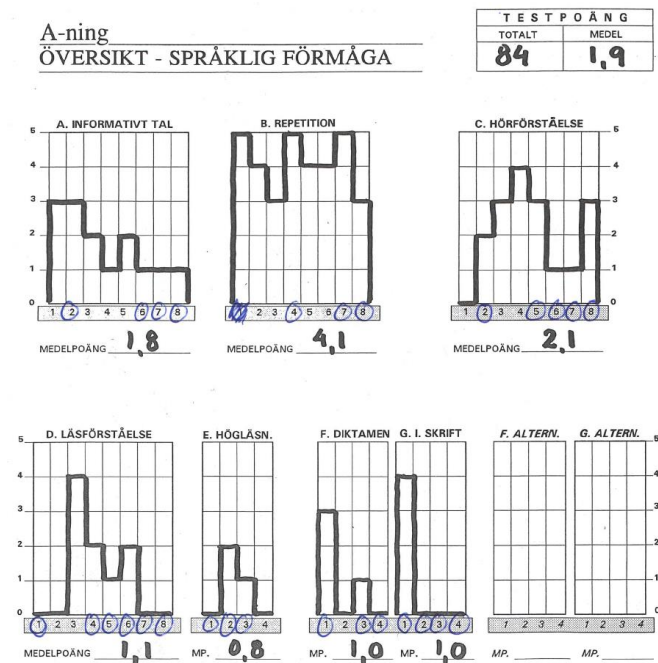


Figure 2. Manual and paper-pen-based evaluation

The speech therapists (Participants 1-3, Table 1) emphasised the need of converting this old paper-pen system to an online application. The application was co-created in close cooperation with speech therapists. As presented in Figure 3, after the session with the patient, the application presents auto-generated graphs.

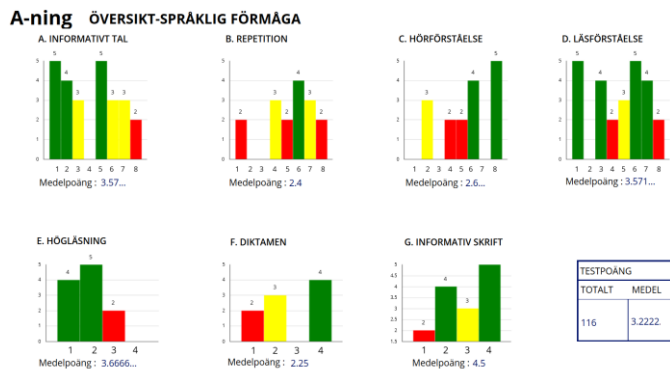


Figure 3. Digital Speech and Language Evaluation System

Each graph presents a set of exercises that are related to a specific category. Different colours in the graphs present a patient's deficiency level; the green colour presents minor impairments, the yellow colour presents mild impairments and the red colour presents some major impairments.

V. METHOD

To explore and evaluate the technology acceptance of an online aphasia assessment application, the Evaluation Focused Design Science Research strategy was followed [32]. The assessment application was developed in collaboration with speech therapists at regional municipality rehabilitation. Six therapists participated in the study. Their location and years of experience in speech and language rehabilitation are presented in the following Table 1.

TABLE I. STUDY PARTICIPANTS

Participants	Professional role	Region	Years of experience
Participant 1	Speech Therapist #1	Stockholm	25
Participant 2	Speech Therapist #2	Mid Sweden Region	4
Participant 3	Speech Therapist #3	Mid Sweden Region	5
Participant 5	Occupational Therapist	Mid Sweden Region	5
Participant 6	Physiotherapist #1	Mid Sweden Region	8
Participant 7	Physiotherapist #2	Mid Sweden Region	3

Participants 4-6 work at the mobile stroke-rehabilitation team at the regional hospital. They offer rehabilitation services at the patient's home for those who are living within the 70 Km range from the hospital. The main reason to involve these participants was to explore the effect of social influence on technology acceptance.

Following design science, the evaluation is conducted in two steps. First, the artefact was demonstrated for an initial evaluation and a detailed evaluation was conducted in the next step.

A. Demonstrate artefact

The purpose of this activity was to demonstrate and test the artefact in one case. In this activity, the application was tested and evaluated for technology acceptance with only one speech therapist (Participant 2). This type of initial

demonstration gives us an idea about how well the artefact addresses the identified problem in one scenario. Johannesson and Perjons [21] argue, if an artefact performs well in one case, there are some good possibilities that it might perform the same in many other cases.

Figure 4 presents an overview of the artefact demonstration activity. The activity was carried out in two sub-activities. First, a test case was designed that contains five tasks followed by some interview questions (see APPENDIX I). The interview questions were developed using UTAUT as base knowledge [7], [13].

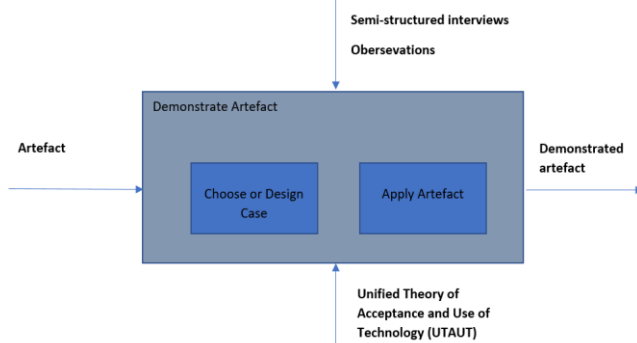


Figure 4. Demonstrate artefacts Activity

The activity was performed at the local municipality rehabilitation centre, one speech therapist (Participant 2) and all three researchers participated in this activity. After the session, the researchers discussed and analysed the data, and found that the application was effective for aphasia assessment; however, some changes and additional functions were suggested. The application was updated by implementing the suggested alterations and it was ready for a detailed evaluation.

B. Evaluate artefacts

After demonstrating the artefact, the next step was to make a detailed evaluation of the artefact. As suggested by Johannesson and Perjons [21], this activity aimed to evaluate whether the developed artefact solves the defined research problem or not. As presented in Figure 5, the activity was conducted in three sub-activities; analyse the context, select goals, and finally conduct the evaluation. The old aphasia evaluation system was paper-pen based while the new system is technology-enhanced; therefore, technology acceptance was analysed as a context and exploring technology acceptance of the new system was highlighted as an important goal for conducting the evaluation. As described in the artefact demonstration activity, UTAUT was used as theoretical base knowledge for data collection and analysis.

Four sessions were conducted with all three speech therapists. In both demonstration and evaluation activities, the same interview questions and evaluation tasks were used (See APPENDIX I). Because of Covid-19, some participants were working from home, therefore, three sessions were

conducted at the municipality rehabilitation centre, where two researchers participated online and only one researcher conducted the session at the rehabilitation centre. However, the last interview was entirely online where all the study participants and the researchers participated online. For data collection and recordings, the Zoom Meetings Platform was used [33].

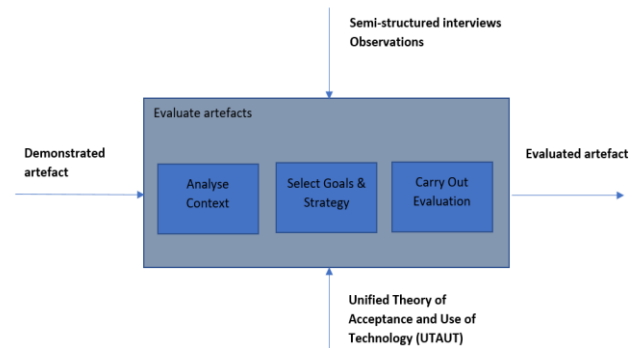


Figure 5. Evaluate artefacts Activity

Deductive thematic analysis was performed for data analysis [34]. First, the transcripts and audio recording were thoroughly examined and initial codes that were relevant to the technology acceptance of the artefact were selected. The defined codes were then categorised according to the determinant factors of the UTAUT model as initial themes. Thereafter, the important findings that were relevant to answer the research question were identified and presented in the findings section.

C. Ethical considerations

The rules and regulations from the Swedish Research Council (Codex) were followed for ethical considerations [35]. Before the interviews started, all the participants were informed that they could refuse to answer any question and cancel the interview at any time (before or during the interview). The privacy and anonymity of the study participants are also important to consider in research ethics where people are involved [36]. The interviews were recorded with the participants' permissions and their anonymity was ensured. The interview recordings were stored in a secure database at the university that is only accessible to the relevant study researchers.

VI. RESULTS

To evaluate the technology acceptance, the results were thematically analysed and categorised according to the UTAUT model's determinants: performance expectancy, effort expectancy, social influence and facilitating conditions. However, these categories were not enough to cover the contents of the interviews. Therefore, privacy and security, and previous knowledge and experience about technology were added as extra categories.

A. Performance expectancy

This category explains the perceived usefulness of the online assessment application. All the study participants mentioned that the online application is beneficial for speech and language assessment (Participants 1-3). The automatically generated points-based evaluation of language impairment was the most valued function in the application. The paper-pen-based and manual assessment involves several calculations that take a lot of time after the assessment session with patients (Participants 1, 2). Speech therapist 3 described,

“The manual evaluation system was time taking and boring; it takes 40 minutes for me to conclude the evaluation and to transfer it to the hospital journal system”.

The old paper and pen-based speech and language assessment system takes a lot of time to calculate the assessment points manually. After a session with the patient, the speech therapists have to do several calculations for diagnosing the patient’s impairment level. Thereafter, they transfer the gathered data to the hospital journal. Since the suggested online application makes these calculations digitally, it might be easy for speech therapists to transfer the patient's data to the hospital journal. Speech therapist 1 suggested that the application should be automatically connected to the hospital journal system so that manual data entry into the journal system could be avoided.

Speech therapist 1 mentioned, *“The assessment tasks and exercises with the patients are performed in a different order and the final evaluation is categorised in a totally different sequence of exercises. Therefore, it is quite hectic to rearrange everything after the session with the patient and to calculate every point in a different sequence.”* Figure 2 gives an overview of the paper-pen-based evaluation.

In the existing paper-and-pen-based system, the sequence of performing events is different from the categorisation of exercises for the final presentation which makes it difficult to calculate the evaluation points. Since the new system makes the calculation automatic and the speech therapists do not have to do it manually, it might ease their job. However, the same sequence of performing the exercises and calculating the points might increase the ease of use of the application. Speech therapists 1 and 2 also suggested; there should be separate folders for different categories with descriptive names and all the exercises related to the same category should be presented in their dedicated folder. Hence, it will be easy for them to manage and conduct the test.

Based on the speech therapist’s input during a session with the patient, the new calculation system diagnoses speech and language deficiency automatically. Participant 3 described that the new system will help her with point-based diagnosis, and save data digitally. Figure 3 demonstrates the new digital assessment system. All the speech therapists acknowledged the usefulness of these coloured graphs as they make it easy to discuss with patients their health conditions (Participants 1-3). The patients will get a better idea of their impairments in different language categories and it will be easy for speech therapists to highlight in which category the patients need to put some more effort (Participant 3).

B. Effort expectancy

This category explores the ease of use of the software application. Speech therapists 2 and 3 found the application easy to use and navigate, however, speech therapist 1 found it difficult to navigate through the different functionalities of the application.

Speech therapist 1 described, *“The system is easy to use, interactive and self-descriptive; I can perform the tasks without any help or guidance. However, all the sub-tasks need more tailor-made alterations to synchronise the system with the existing system.”*

Speech therapist 2 used the application for the first time and it was easy for her to navigate throughout the entire process. She was able to perform the functions easily without any help or guidelines; however, she emphasised better synchronisation with the workflow of the existing system. For example, the sub-tasks in each exercise should be designed according to the previous paper and pen-based system. In a later interview, speech therapist 1 also said that the application should be altered to fit their daily work routines.

An early user’s participation in system development and design also plays an important role in the technology acceptance of that system. During the interviews, it is observed that speech therapists 2 and 3 who were involved earlier (from the requirements identification phase), showed more interest and intention to use the system as compared to speech therapist 1 who participated only in the evaluation of the developed application.

A continuation of the performance expectancy is the new calculation system, where participants 1-3 discussed the necessity of individualising the traffic light metaphor as well as interpreting it. There is a need for individualising the speech training, both relating to the patient's current health condition and goal with the speech training. Based on the latter, the system should allow follow-ups and comparisons between the various test occasions. Speech therapists 1 and 2 declared that they hoped for the patient to improve, as shown in the statistics, and that the system should help them to increase the degree of difficulty at each test occasion. The ultimate goal should be to get a detailed assessment system that could find more linguistic defects. Speech therapists 1 and 2 declared that such a system would take at least five years to develop, but as brought up by Participant 1, there are several words and expressions in A-ning that today are obsolete and difficult to understand for younger patients and patients with a foreign background. An alternative is to update the existing A-ning system, or as suggested by Participants 2 and 3, the digitalisation could be carried out based on A-ning, but with the possibility to replace the A-ning tests with some other test system in the future.

The aforementioned is that statistics are the obvious gain of digitalising the assessment. To gain more efficiency there should be an overall workflow, with a starting point and the next assignment showing up, without interference. Participants 1 and 2 emphasise that they should be the ones choosing the assignments and that the order should be shown on an overview. All participants emphasised that there should

be possibilities to add individual notes, both for each assignment and on a general level, e.g., when an assessment is completed. Another important aspect of the system is that each category should be marked with one colour, improving the possibility to interpret the test results. One suggestion from Participants 1 and 2 is therefore to create folders with descriptive headlines, where assignments from each category could be stored

C. Social influence

This category explains the other co-workers' views about the usefulness of the system. The viewpoints of speech therapists' colleagues (Participants 4-6) were used to assess the social influence. Moreover, speech therapist 2 discussed the usefulness of the applications with their fellow therapists; all the co-workers acknowledged the usefulness and a positive intention to use the assessment application (Participant 2). Stroke patients feel comfortable and motivated by getting treatment in their home environment and living independently (Participants 4-6). The rehabilitation process is faster and more effective when the patients are at home with their significant others (Participants 3, 4-6). Since the application provides the possibility of online sessions, the application will be useful for the patients as well as for the speech therapists (Participant 1).

D. Facilitating conditions

This category discusses the availability of facilitating conditions such as technical infrastructure, education and training about the application functions, and personal support for the system. The requirements on technical infrastructure are several and focus on not solely converting the assessment from a paper-based assessment to a digital system. One example is the participants' emphasis on having different views for the patient and the speech therapist on every given occasion. Therefore, the patient's screen should show, e.g., one image, while the speech therapist should see several images and pick one for the patient. Another aspect is the possibility to change the size of the patient's image to offer him/her the best possible resolution.

One part of the assessment is for the patient to write, e.g., what is shown on the screen. Therefore, a touch pen is necessary, preferably on a tablet (Participants 1 - 3). The tablet's size should allow both the patient and speech therapist to write on it. On occasion, the speech therapist needs to give written instructions, adding requirements on immediate digital interaction. Another patient assignment describes what is shown on the screen and creates a story, preferably recorded. The recording also needs to be played for further evaluation by the speech therapist.

Previously described is that stroke patients often suffer from brain fatigue, offering small time slots of total energy. Therefore, there is a need to save the solved assignments and continue at another session not related to a specific speech therapist. Related to partly finished or fully finished assessment is the integration into any journal system. Participant 3 emphasises the importance of this requirement, describing that it takes 40 minutes of administration to cover this manually.

E. Privacy and security

Trust in the privacy and security of the users' data was also a matter of concern for the participants. One part of privacy and security is that other speech therapists should be able to see the results from one assessment to create efficiency in the flow of patients. Still, the patient's privacy and security should be in focus for the system. Somewhat contradictory to the patient's privacy and security is the involvement of relatives or other secondary users. The secondary users are essential, depending on the patient's condition and the wish for distance use. They should be able to help the patient, still not affecting the results of the assessment.

F. Previous knowledge and experience

The user's previous knowledge and experience with related technologies was another important factor for technology acceptance. During the interviews, it was observed that the participants who have previously used relearning applications in their work showed more interest in using the suggested application. The user's participation in the design and development also enhances their knowledge and interest in the given technology. The speech therapist (Participant 2) who was involved throughout the process of the application's co-creation showed the most enthusiasm and intention to use the application. However, the speech therapist (Participant 3) who was involved only in the evaluation phase, showed the least interest in using the application.

VII. DISCUSSION

The study aimed to explore the technology acceptance of the speech and language assessment application from medical caregivers' viewpoints. The technology acceptance evaluation conducted on the speech and language assessment application has shown promising results for its usefulness and efficiency in aiding speech therapists. One of the significant benefits of the application is the automated diagnosis system that has significantly reduced the workload of speech therapists. Additionally, the system has provided an instant tool for speech therapists to discuss impairments with their patients, resulting in a more comprehensive and efficient treatment process.

Furthermore, the online treatment functionality of the application has the potential to improve the quality of life and independent living for patients and their loved ones. The remote accessibility of treatment sessions eliminates the need for patients to travel, which can be particularly challenging for individuals with speech and language impairments.

However, despite the advantages of the application, the study revealed some critical factors that can impact its technology acceptance and adoption. The usability and usefulness of the application for speech therapists can be enhanced by proper synchronization with the existing system in place. This means that all tasks and sub-tasks in the application must align with the existing workflow, and they

should be designed and developed in close collaboration with speech therapists.

Moreover, the intention to use the technology is also influenced by early user participation in the system's development and design. Speech therapists who have been involved from the start of the application's development process have shown more interest in using the system compared to those who were only involved in the technology acceptance evaluation. Therefore, user participation and empowerment are crucial for the effective implementation of a technology-enhanced system.

Since the medical caregivers (speech therapists in the study context) play an important role in the patient's recovery and relearning, their viewpoints and participation in the system development are important [37]. The same phenomena are observed in this study; the participants with the most participation showed the most intention to use the application. The technology acceptance also depends upon the expected benefits of using the system. The unawareness of the potential benefits of a given technology and a fear to use that technology negatively affect the medical caregivers' performance expectancy [38]. Therefore, continuous technical support and training are of great importance.

There are several options while creating a digital version of the A-ning assessment system. One is to convert the paper-based system to a digital version, adding the feature of creating better possibilities for speech therapists to use statistics, both for individual patients or synthesising statistics for specific categories of patients or on an assignment level. The prototype adds such features, improving parts of the work for speech therapists. Another option is to, still based on the involvement of the speech therapists, create an online system, separating features for the speech therapists and the patient. Examples are immediate written interaction between the speech therapists and the patient's screen or showing different images. The development could be done in steps, where one initial step could be integrated into various journal systems, offering immediate efficiency for the speech therapist. Creating an online system relies on various technical solutions, like recording or writing on one screen and reading on another. The interaction of being in the same room simultaneously needs to be replaced by other interactions and be based on the patient's varying condition.

A-ning is the most frequently used and comprehensive test for speech and language impairment in Sweden, and all participants find the system to be of high quality. However, natural languages like Swedish are entities that change over time and the test vocabulary involves some words that today must be classified as obsolete. Important for the younger generation of patients in a country where 20% of the population has a foreign origin. In the same way, as a thesaurus needs continuous updating, a language test system also needs updating. This looks like the most realistic alternative for the moment since the development of a new test system would be both costly and time-consuming. Authors find the analogue A-ning system to be a thorough and high-quality test system and a good foundation for further digitalisation. Some obvious contributions to the language

relearning process in a further digitalised version of the system would be features for statistics and for measuring relearning progression.

The relationship between a user's personality and his/her behavioural intentions to use a given technology is complex and it depends upon several different factors. Such factors are, among others, trust in personal data security, personal integrity and privacy, previous experience with technology, and the willingness to learn new technologies. Moreover, the developed systems must be in line with social needs, highly compatible and flexible with clear guidance and coherent technology involvement [39], [40].

VIII. CONCLUSION

The study explored the acceptance of an online speech and language assessment application. The factors that might affect the adoption and use of technology were also discussed in the study. The online evaluation seems more effective and efficient than the traditional manual system for speech therapists and it enables independent living for the patients. To enhance the performance expectancy, the potential users (speech therapists) should be involved throughout the application development process and all the application functionalities should be comprehensively discussed with them. The intention to use the application depends upon patients' medical condition, active users' participation in the application development, trust in the privacy and security of personal data, and providing users with proper education and training about the system.

This evaluation was carried out with a speech therapist and caregiver perspective, which is an important part of the process. The next important step is to get the patient's perspective, in an evaluation that preferably also should involve some patients' relatives and friends. Furthermore, the multi-stakeholder approach should include administrative staff at health centres and hospitals to get their view on statistical features and security aspects. Finally, what seems like the most valuable contribution of a further digitalised system would be to implement more features for test result statistics, and for visualisation of relearning progression.

ACKNOWLEDGEMENT

We are grateful to stroke rehabilitation therapists and the communal rehabilitation centre for co-creating and evaluating the speech and language relearning application with us.

REFERENCES

- [1] A. Ahmad, K. Ahlin, and P. Mozelius, "Technology Acceptance of an Online Speech and Language Assessment Application for Stroke Patients-the Medical Caregivers' Viewpoints," in Tenth International Conference on Global Health Challenges (GLOBAL HEALTH 2021), Barcelona, Spain, October 3-7, 2021.
- [2] M. Freund et al., "Effectiveness of information and communications technology interventions for stroke survivors and their support people: a systematic review," *Disability and Rehabilitation*, pp. 1-16, 2021.

- [3] S. Palmcrantz et al., "An interactive distance solution for stroke rehabilitation in the home setting—A feasibility study," *Informatics for Health and Social Care*, vol. 42, no. 3, pp. 303–320, 2017.
- [4] Y. Guo et al., "The Unmet Needs of Community-Dwelling Stroke Survivors: A Systematic Review of Qualitative Studies," *International journal of environmental research and public health*, vol. 18, no. 4, p. 2140, 2021.
- [5] P. Mozelius, K. Ahlin, and A. Ahmad, "A game-based approach for motoric stroke rehabilitation: defining the requirements," in *ECGBL 2019*, vol. 13.
- [6] K. Ahlin, A. Ahmad, and P. Mozelius, "Determining Testbed Requirements for Technology Enhanced Speech Rehabilitation after Stroke—the Informed Co-workers' View Point," in *IARIA GLOBAL HEALTH International Conference on Global Health Challenges*, 2019.
- [7] M. Tousignant et al., "Satisfaction with in-home speech telerehabilitation in post-stroke aphasia: an exploratory analysis," *Journal of the International Society for Telemedicine and eHealth*, vol. 6, pp. e11-1, 2018.
- [8] V. Venkatesh, J. Y. Thong, and X. Xu, "Unified theory of acceptance and use of technology: A synthesis and the road ahead," *Journal of the association for Information Systems*, vol. 17, no. 5, pp. 328–376, 2016.
- [9] A. Ahmad and P. Mozelius, "On the Importance of Tailor-made Speech Relearning Software for Stroke Rehabilitation," in *ICT4AWE 2020*, vol. 6.
- [10] S. H. Fischer, D. David, B. H. Crotty, M. Dierks, and C. Safran, "Acceptance and use of health information technology by community-dwelling elders," *International journal of medical informatics*, vol. 83, no. 9, pp. 624–635, 2014.
- [11] A. H. Zai, J. G. Ronquillo, R. Nieves, H. C. Chueh, J. C. Kvedar, and K. Jethwani, "Assessing hospital readmission risk factors in heart failure patients enrolled in a telemonitoring program," *International journal of telemedicine and applications*, vol. 2013.
- [12] A. Kohnke, M. L. Cole, and R. Bush, "Incorporating UTAUT predictors for understanding home care patients' and clinician's acceptance of healthcare telemedicine equipment," *Journal of technology management & innovation*, vol. 9, no. 2, pp. 29–41, 2014.
- [13] A. Ahmad, Å. Cajander, B. Johansson, Y. Tiblom Ehrsson, and U. Långegård, "Designing for Human Well-Being: A Case Study with Informal Caregivers of Individuals with Cancer," in *Challenges of Trustable AI and Added-Value on Health*, IOS Press, 2022, pp. 214–218.
- [14] V. Venkatesh, M. G. Morris, G. B. Davis, and F. D. Davis, "User acceptance of information technology: Toward a unified view," *MIS quarterly*, pp. 425–478, 2003.
- [15] A. J. De Veer, J. M. Peeters, A. E. Brabers, F. G. Schellevis, J. J. Rademakers, and A. L. Francke, "Determinants of the intention to use e-Health by community dwelling older people," *BMC health services research*, vol. 15, no. 1, pp. 1–9, 2015.
- [16] V. L. Hanson, "Influencing technology adoption by older adults," *Interacting with Computers*, vol. 22, no. 6, pp. 502–509, 2010.
- [17] A. Ahmad, P. Mozelius, and K. Ahlin, "Speech and Language Relearning for Stroke Patients—Understanding User Needs for Technology Enhancement," in *Proceedings of Thirteenth International Conference on eHealth, Telemedicine, and Social Medicine (eTELEMED 2021)*, Nice, France, 2021.
- [18] S. T. Peek, E. J. Wouters, J. Van Hoof, K. G. Luijkx, H. R. Boeije, and H. J. Vrijhoef, "Factors influencing acceptance of technology for aging in place: a systematic review," *International journal of medical informatics*, vol. 83, no. 4, pp. 235–248, 2014.
- [19] C. Scott Kruse, P. Karem, K. Shifflett, L. Vegi, K. Ravi, and M. Brooks, "Evaluating barriers to adopting telemedicine worldwide: a systematic review," *Journal of telemedicine and telecare*, vol. 24, no. 1, pp. 4–12, 2018.
- [20] C. K. Or and B.-T. Karsh, "A systematic review of patient acceptance of consumer health information technology," *Journal of the American Medical Informatics Association*, vol. 16, no. 4, pp. 550–560, 2009.
- [21] L. de Vries, "Stroke Survivors general use of technical devices in their home environment and likelihood of using a potential digital application in their rehabilitation: A survey following Early Supported Discharge." 2020.
- [22] X. Zhou, M. Du, and L. Zhou, "Use of mobile applications in post-stroke rehabilitation: a systematic review," *Topics in stroke rehabilitation*, vol. 25, no. 7, pp. 489–499, 2018.
- [23] M. B. Garcia, "A Speech Therapy Game Application for Aphasia Patient Neurorehabilitation—A Pilot Study of an mHealth App," *International Journal of Simulation: Systems, Science & Technology*, vol. 20, 2019.
- [24] A. Ahmad and P. Mozelius, "Critical factors for human computer interaction of ehealth for older adults," in *Proceedings of the 2019 the 5th International Conference on e-Society, e-Learning and e-Technologies*, 2019, pp. 58–62.
- [25] S. H. Fischer, D. David, B. H. Crotty, M. Dierks, and C. Safran, "Acceptance and use of health information technology by community-dwelling elders," *International journal of medical informatics*, vol. 83, no. 9, pp. 624–635, 2014.
- [26] L. T. Vassli and B. A. Farshchian, "Acceptance of health-related ICT among elderly people living in the community: A systematic review of qualitative evidence," *International Journal of Human-Computer Interaction*, vol. 34, no. 2, pp. 99–116, 2018.
- [27] S. Wiklund Axelsson and A. Melander Wikman, "Ready for eHealth. Older Swedes' perceptions of eHealth Services: Using the PIADS scale as a predictor for readiness," *Technologies*, vol. 4, no. 3, p. 29, 2016.
- [28] K. Mallet et al., "RecoverNow: A patient perspective on the delivery of mobile tablet-based stroke rehabilitation in the acute care setting," *International Journal of Stroke*, vol. 14, no. 2, pp. 174–179, 2019.
- [29] J. Marshall et al., "Technology-enhanced writing therapy for people with aphasia: results of a quasi-randomized waitlist controlled study," *International journal of language & communication disorders*, vol. 54, no. 2, pp. 203–220, 2019.
- [30] E. Lindström and C. Werner, A-ning: neurolingvistisk afasiundersökning. Protokoll. Ersta högsk, 1995.
- [31] A. Ahmad, K. Ahlin, and P. Mozelius, "Technology-enhanced speech and language relearning for stroke patients—defining requirements for a software application development," in *11th Scandinavian Conference on Information Systems (SCIS2020)*, Sundsvall, Sweden, 2020.
- [32] P. Johannesson and E. Perjons, *An introduction to design science*. Springer, 2014.
- [33] M. M. Archibald, R. C. Ambagtsheer, M. G. Casey, and M. Lawless, "Using zoom videoconferencing for qualitative data collection: perceptions and experiences of researchers and participants," *International Journal of Qualitative Methods*, vol. 18, p. 1609406919874596, 2019.
- [34] V. Braun and V. Clarke, "Thematic analysis," 2012.
- [35] S. Eriksson, CODEX-Regler och riktlinjer för forskning. Forskning som involverar människan, 2015.
- [36] Kvale, S., & Brinkmann, S. (2014). *Den kvalitativa forskningsintervjun*. Lund: Studentlitteratur.
- [37] T. Simic, C. Leonard, L. Laird, J. Cupit, F. Höbler, and E. Rochon, "A usability study of internet-based therapy for naming deficits in aphasia," *American Journal of Speech-Language Pathology*, vol. 25, no. 4, pp. 642–653, 2016.

- [38] A. Vaezipour, D. Aldridge, S. Koenig, D. Theodoros, and T. Russell, “‘It’s really exciting to think where it could go’: a mixed-method investigation of clinician acceptance, barriers and enablers of virtual reality technology in communication rehabilitation,” *Disability and Rehabilitation*, pp. 1–13, 2021.
- [39] V. Venkatesh, J. Y. Thong, and X. Xu, “Unified theory of acceptance and use of technology: A synthesis and the road ahead,” *Journal of the association for Information Systems*, vol. 17, no. 5, pp. 328–376, 2016.
- [40] A. Ahmad et al., “Positive Design Framework for Carer eSupport: Qualitative Study to Support Informal Caregivers of Patients With Head and Neck Cancer in Sweden,” *JMIR Cancer*, vol. 9, no. 1, p. e45748, May 2023, doi: 10.2196/45748.

APPENDIX 1

A. Evaluation Tasks of A-ning application

1) Task 1

Preplanning for a new patient

- Create a new patient by giving information:
- First name: Awais
- Last Name: Ahmad
- Personal no. : 8111150000
- Speech therapist Name: Tove
- Select the exercises

2) Task 2

Performing the exercises A2, A6, A7, A8

- Complete the tasks for all the
- Select an exercise

- Write some comments in the comments box
- Give some points

3) Task 3

Describing the evaluation

I. Select the graph sign from the main page

II. Describe the evaluation for different categories

III. Describe the overall aphasia evaluation

4) Task 4

Changing the selected exercises during an ongoing evaluation

- Select some exercises, which are not selected
- Deselect some exercises, which are selected
- Update the Information

5) Task 5

- Resuming a previously started evaluation

B. Technology acceptance Interview questions

1) Question 1.

How easy-to-use was the system as compared to the old system?

2) Question 2

Which feature was difficult to use and what was easy to use?

3) Question 3

What are your recommendations to improve the interface?

4) Question 4

How do you see the usefulness of this system for patients and other speech therapists?

5) Question 5

What help do you need for the use of this system in terms of:

- Infrastructure
- Education/training

Modeling of Animal Vibrissae: Adaptive Control of Multi-body Systems under Output Noise

1st Carsten Behn

Schmalkalden University of Applied Sciences
Schmalkalden, Germany
c.behn@hs-sm.de

<https://orcid.org/0000-0001-7618-1926>

2nd Moritz Scharff

Wilhelm-Franke-Str. 11
Dresden, Germany
moritz.scharff@live.de

<https://orcid.org/0000-0002-1581-7668>

3rd Lukas Merker

Technische Universität Ilmenau
Ilmenau, Germany
lukas.merker@tu-ilmenau.de

<https://orcid.org/0000-0003-1931-0749>

Abstract—The reception of vibrations is a special sense of touch, important for many insects and vertebrates. The latter realize this reception by means of hair-shaped vibrissae all over the body, but especially arranged in the mystacial pad around the snout. Latest research activities focus on modeling these sensor components to explain some biological behaviors/features (Technical Biology) or to investigate their usage for technical applications for, e.g., object surface and/or shape detection (Bionics). In contrast to these works, we focus on the modeling of the dynamic operation modes to be applied for dynamic scanning patterns of objects. We set up a principal mechanical model of a single vibrissa to describe these modes of operation: passive and active vibrissae. They are either used passively to sense environmental forces, e.g., wind, or actively, when they are rhythmically moved to scan objects or surfaces. Consequently, the vibrissa inspired model has to allow for stabilizing and tracking control as well, but yet being able to detect (superimposed) solitary excitations. Hence, the biological paradigm exhibits some adaptive behavior, and so must the controller: to be adaptive in view of both the randomness of the external signals to be suppressed and the uncertainty of the system data.

Index Terms—vibrissa; modes of operation; adaptive control; uncertain system; tactile sensor

I. INTRODUCTION

Tactile sensor technology seems nowhere near from playing a key role in environmental exploration in mobile robotics, especially when compared to optical sensing technology. Taking a glance at the world of biology, the sense of touch provides necessary information for several species, e.g., mammals, especially nocturnal animals like rats. They exhibit a sophisticated tactile sense organ supporting tactile exploration which complements the visual and aural sensing: the mystacial vibrissae in the snout region, see Fig. 1.



Fig. 1. Mammals with vibrissae: a cat named ‘Alfred’ with whiskers (left), and a rat (right) [3].

The rats benefit from their vibrissae in different ways while they are moved in different modes of operation [1], [2]: they are involved in their social behavior, acquisition of food, locomotion, navigation [4], [5], detecting air flows [6]. They enable the rats to detect, localize and recognize objects near their faces [7], including detection of object features (orientation, shape, texture) [8], [9].

The mystacial vibrissae are arranged in an array of columns and rows around the snout, see Fig. 2.

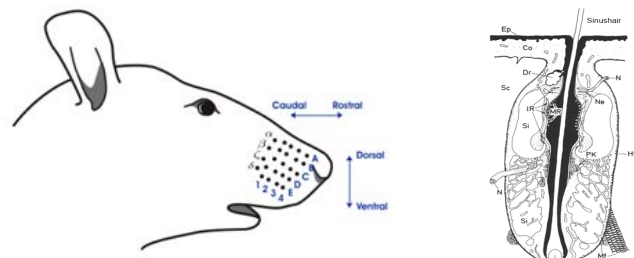


Fig. 2. Schematic drawing of the mystacial pad (left) [10], follicle-sinus-complex of a vibrissa (right) [11].

The vibrissa itself (made of dead material) is mainly used as a lever for the force transmission. But, in contrast to ordinary hairs, vibrissae are stiffer and have a hollow conical shape [10]. Each vibrissa in the mystacial pad is embedded in and supported by its own follicle-sinus complex (FSC), see Fig. 2, right. The FSC is characterized by its exceptional arrangement of blood vessels, neural bonding and muscles.

Despite the distribution and difference of the vibrissae in a mystacial pad with respect to their (varying) material and geometrical features (multi-layer system, slenderness, conical shape with inherent curvature inside this pad), we focus on a single vibrissa, its surrounding tissue, its functionality and mode of operation. For a more detailed overview see [12]. Due to [13], the surrounding musculature is divided in extrinsic and intrinsic one. The vibrissa can either be moved passively (e.g., by wind), or actively through alternate contractions of the intrinsic and extrinsic muscles. The resulting rhythmic pro- and retractions of the vibrissa, called whisking, are used to scan surfaces and objects [11]. Relevant information can be perceived by adjusting the frequency and amplitude of

the oscillation to each task. By observing rats accomplishing several types of exercises, Berg and Kleinfeld in [14] could distinguish two main *whisking patterns*: *exploratory whisking* when rodents explore their environment with large amplitude sweeps in a low frequency (5-15Hz) range, and *foveal whisking* when rodents palpate object surfaces with small amplitude, high frequency (15-25Hz) movements. Summarizing, the complex FSC- and muscle-system enables the rodents to use their vibrissae in two different ways (modes of operation):

- In the **passive mode**, the vibrissae are being deflected by external forces (e.g., wind). They return to their rest position passively — thus without any muscle activation.
- In the **active mode**, the vibrissae are swung back- and forward by alternate contractions of the intrinsic and extrinsic muscles. By adjusting the frequency and amplitude of the oscillations, the rodents are able to investigate object surfaces and shapes amazingly fast and with high precision [15].

But, how the animals convert these multiple contacts with single objects into coherent information about their surroundings remains unclear and is not of focus in this work. However, from the point of view from control theory, every biological sensory system has the ability to constantly adapt its sensitivity to its current environment in a way that empowers it to distinguish the relevant information out of the multitude of negligible stimuli (\rightarrow *adaptive system*). Several *control strategies* enhance the relevance-oriented stimulus processing:

- a feedback-loop (closed-loop control system) enables the rodents to immediately react to an object contact: they slow down the concerned vibrissae, diminishing the occurring wear-out effect on the hair [16], [17],
- depending on the mode (passive or active) and the expectations of the rodent, the neurons reaction is being suppressed, enhanced or left unaltered [18]–[20].

Therefore, this biological sensor system is highly interesting for applications in the field of autonomous robotics, since tactile sensors can offer reliable information, where conventional sensors fail (in dark, smoky or noisy environments).

In the following Section II, we give a very brief overview on mathematical models to describe the rigid-body motion of vibrissa-like mechanical systems. In Section III, we set up a simple model of a single vibrissa, derive the equations of motion for a stringent mathematical treatment. For this, we present some aspects of control theory for this systems in Section IV. We introduce a general system class this equations of motion belongs to and show some output feedback controllers mimicking the adaptive nature of the mentioned different modes of operation of a vibrissa. Numerical simulations in Section V show the effectiveness of these controllers in λ -tracking some reference signals such that the system is in a passive or active mode. The main difference to [1] is presented in Section VI, where we –additionally to new adaptors– focus on noise-corrupted outputs due to some measurement failures and show that the suggested adaptive tracking strategies still

work effectively. Section VII concludes the paper and closes with an outlook.

II. STATE OF THE ART - MODELING ANIMAL VIBRISSAE

An intensive literature overview of technical vibrissa models (rigid body and continuum) has been presented in [21]–[23]. Here, we briefly discuss some models therein, where we restrict the investigations to rigid body models, continuous models are in recent exploration.

The following summarizes the relevant information of the encountered mechanical models found in the literature for this paper.

- Mitchinson in 2004 [24] and 2007 [17] - *Model of the FSC*: Mitchinson's research group has developed a model of the FSC to increase the knowledge over this biological sensory system on the one hand, and on the other hand to promote the development of innovative and efficient tactile sensors. Following the anatomy in literature, the scientists modeled the various layers of the FSC, linking them with spring and damping elements to simulate the compliance of the biological tissue (see Fig. 3).

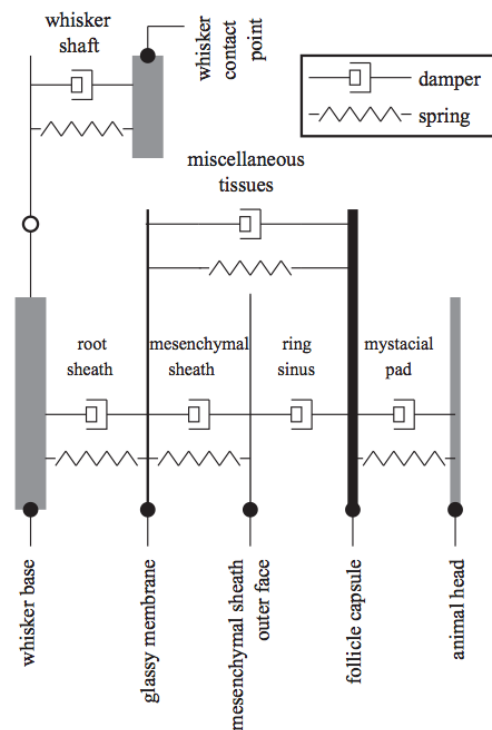


Fig. 3. Mechanical model of the FSC of [24].

- ⊖ too complex for a technical implementation
- ⊕ Determination of spring and damping coefficients for the FSC

- Berg in 2003 [14] - *Determination of the range of movement of the vibrissa*: The function of the musculature in the mystacial pad was investigated by Berg and Hill in [14]. They recorded electromyogram (EMG) activity from the intrinsic and extrinsic muscles while rats were

whisking, to characterize the pattern of muscular dynamics. The following observations were made during one whisking cycle, also see Fig. 4:

- the **protraction** of the vibrissa is caused by the contraction of the intrinsic muscle retracting the FSC (\rightarrow **angular deflection**),
- the **retraction** of the vibrissa is induced by the contraction of the extrinsic muscle retracting the vibrissa at skin level (\rightarrow **translatory shift**).

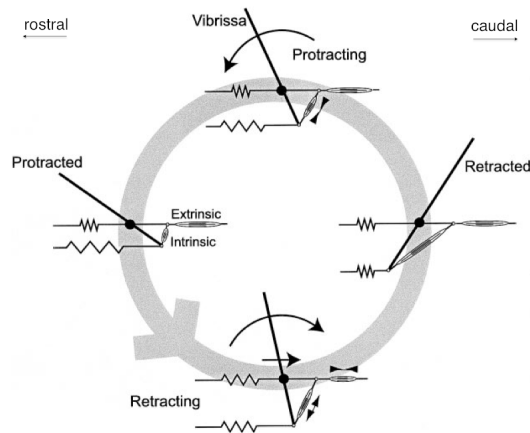


Fig. 4. Mechanical model relating cyclic vibrissa movements according to alternating intrinsic and extrinsic muscle contractions during whisking of [14].

Summarizing:

$$\hookrightarrow \varphi_{Rest} \approx 80^\circ$$

hence: angular deflection in rostral direction $\varphi_{rest} + 65^\circ$, angular deflection in caudal direction $\varphi_{rest} - 35^\circ$, translatory shift $\approx 5mm$ in caudal-rostral direction, translatory shift $\approx 3mm$ in dorsal-ventral direction

- Hill in 2008 [25] - *Model of the musculature in the mystacial pad*: The researchers developed a mechanical model of the vibrissa, focussing on the relationship between the various muscle contractions and the resulting vibrissa motion. Furthermore, three vibrissa / follicle units, linked by spring and damping elements, were incorporated in the model so that the influence of the intrinsic muscle slings on their neighboring follicles could also be considered, see Fig. 5.

The fact that a passively deflected vibrissa returns to its initial position without oscillating, implies that the mystacial pad is overdamped. Summarizing:

- ⊕ Implementation of intrinsic and extrinsic musculature
- ⊕ Simulating the viscoelastic properties of the skin
 - \hookrightarrow Determination of spring and damping coefficients for the skin
- ⊖ Negligence of the viscoelastic properties of the FSC
- ⊖ Connection between the follicles
 - \hookrightarrow leads to complex control strategy and high control effort

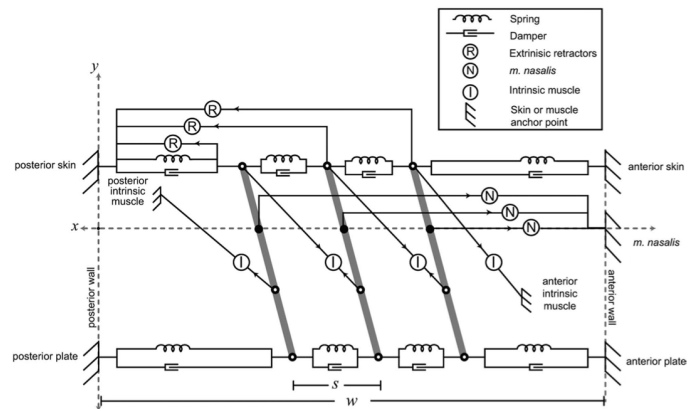


Fig. 5. Schematic drawing of the mechanical model of a row of three vibrissae in [25].

- models by Simony [26] and Haiderliu [27] in 2010 are too complex in their structure and neglected for discussion here
- Behn in 2013 [22] - *Model of stimulus transmission*
 - ⊕ Implementation of viscoelastic properties of FSC
 - ⊖ Negligence of the viscoelastic properties of the skin

The goal is *not* to recreate an exact copy of the biological system, but *to implement the specific characteristics of the vibrissa needed for the detection of useful information in challenging surroundings in a mechanical model*. Principally, the tenor of our investigations is from bionics: modeling live paradigms, exploiting corresponding mathematical models in order to understand details of internal processes and, possibly, coming to artificial prototypes (e.g., sensors in robotics). We point out that we focus on a single vibrissa and not on a tuft of various vibrissae as in [27].

III. A FIRST MODEL OF A SINGLE VIBRISSA

In this section, we present a first vibrissa-inspired sensor model and derive the corresponding equations of motion.

Following [13] and as mentioned in Section I, the vibrissa is supported by its FSC. Important parts of it are an enveloping chamber with controllable blood supply, and intrinsic and extrinsic muscles which control the vibrissa motions. This biological description suggests physical models as sketched in Fig. 6, and these then lead us to the mathematical model based on the pendulum device in Fig. 7.

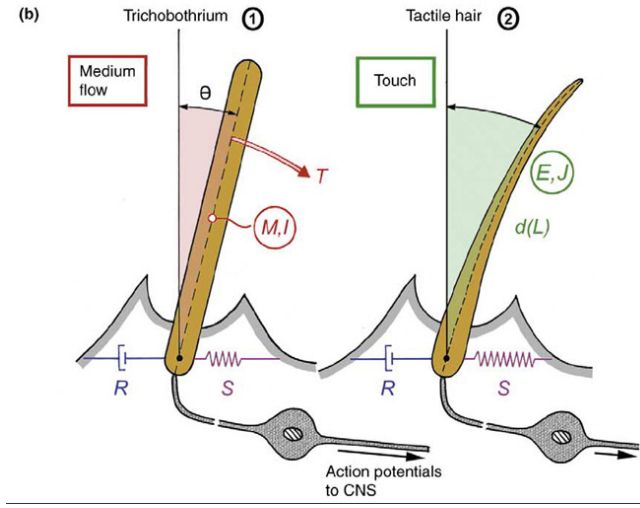


Fig. 6. Scheme of a vibrissa, [28].

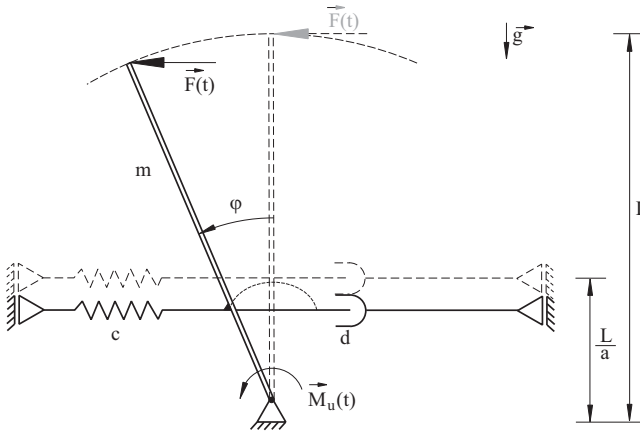


Fig. 7. A mechanical model of a vibrissa.

The model has a viscoelastic support (skin level) and is acted upon by a force excitation $F(\cdot)$ and a control torque $M_u(\cdot)$. The control torque is due to control impact by the musculature [13]. The equations of motion are given by the Principle of Angular Momentum:

$$J_0 \ddot{\varphi}(t) = \frac{L}{2} m g \sin(\varphi(t)) - \frac{L^2}{a^2} c \sin(\varphi(t)) \cos(\varphi(t)) - \frac{L^2}{a^2} d \cos(\varphi(t))^2 \dot{\varphi}(t) + L \cos(\varphi(t)) F(t) + M_u(t), \quad (1)$$

where $J_0 := \frac{1}{3} m L^2$ is the moment of inertia about the pivot. The output of the system is $y(t) = \varphi(t)$.

IV. MATHEMATICAL BACKGROUND

Dealing with sophisticated, biologically inspired systems, one cannot expect to have all information about it. Instead only structural properties are known. In doing so, we assume that internal data (e.g., mass, spring stiffness, and damping

ratio) are unknown. Furthermore, with respect to a changing, and therefore uncertain, environment, we assume the external excitations to be unknown which leads us to the treatment of *highly uncertain (control) system* of known structure given in (1). Note that this system belongs to the following general system class, firstly presented in [22]: finite-dimensional, nonlinearly perturbed, m -input $u(\cdot)$, m -output $y(\cdot)$ systems (MIMO-system) of relative degree two with known sign of the high-frequency gain G :

$$\begin{aligned} \dot{y}(t) &= A_1 \dot{y}(t) + f_1(s_1(t), y(t), z(t)) + G u(t), \\ \dot{z}(t) &= A_2 z(t) + A_3 \dot{y}(t) + f_2(s_2(t), y(t)), \end{aligned} \quad (2)$$

with initial conditions $y(t_0) = y_0 \in \mathbb{R}^m$, $\dot{y}(t_0) = y_1 \in \mathbb{R}^m$ and $z(t_0) = z_0 \in \mathbb{R}^{n-2m}$ and the following properties:

- dimensions $u(t) \in \mathbb{R}^m$, $A_1, G \in \mathbb{R}^{m \times m}$, $A_2 \in \mathbb{R}^{(n-2m) \times (n-2m)}$ and $A_3 \in \mathbb{R}^{(n-2m) \times m}$, $n \geq 2m$,
- $\text{spectrum}(G) \subset \mathbb{C}_+$, i.e., the spectrum of the high-frequency gain lies in the open right-half complex plane,
- $s_1 \in \mathcal{L}^\infty(\mathbb{R}_{\geq 0}, \mathbb{R}^q)$ and $s_2 \in \text{mathcal}L^\infty(\mathbb{R}_{\geq 0}, \mathbb{R}^q)$ can be thought of (bounded) disturbance terms, whereby $\mathcal{L}^\infty(\mathbb{R}_{\geq 0}, \mathbb{R}^q)$ is the space of measurable essentially bounded functions with infinity-norm, see [29],
- $f_1 : \mathbb{R}^q \times \mathbb{R}^m \times \mathbb{R}^{n-2m} \rightarrow \mathbb{R}^m$ and $f_2 : \mathbb{R}^q \times \mathbb{R}^m \rightarrow \mathbb{R}^{n-2m}$ are continuous and linearly affine bounded functions,
- $\text{spectrum}(A_2) \subset \mathbb{C}_-$, i.e., the spectrum of the high-frequency gain lies in the open left-half complex plane, which equals that the system is minimum phase, provided $f_1 \equiv 0$ and $f_2 \equiv 0$.

Using these descriptions, the reader can easily identify the components of (1) in the explanations given above. Some assertions are given in a more general way than presented in the equation of motion (1) to encompass more systems, which can be λ -tracked later in this paper.

Relative degree two means that the input u directly influences the second derivative of each output component.

To dominate this system with uncertain parameters, we have to design an adaptive controller which learns from the behavior of the system in automatically adjusting its (gain) parameters to achieve a desired control objective. Because the system is excited by unknown forces (e.g., possible wind from the environment), we try to design a universal feedback controller which adaptively compensates this unknown excitation and leaves the system in a desired operation pattern.

Since we are dealing with an uncertain, randomly perturbed, non-autonomous system, particular attention is paid to the adaptive λ -tracking control objective: determine a universal λ -controller, which learns from the behavior of the system and automatically adjusts its parameters such that the system tracks a given reference signal $y_{\text{ref}}(\cdot)$ (representing a desired mode of operation) with a prescribed accuracy λ . The value $\lambda > 0$ denotes the size of the feasible tracking error, which means that the error $e(t) := y(t) - y_{\text{ref}}(t)$ is forced, via the adaptive feedback mechanism, towards a ball around zero of arbitrary

small pre-specified radius λ [30]. Choosing $y_{\text{ref}}(\cdot) \equiv 0$, $\lambda = 0$, we arrive at the so-called *adaptive stabilization control objective*.

A preferred control strategy is the following [30]:

$$\left. \begin{aligned} e(t) &:= y(t) - y_{\text{ref}}(t), \\ u(t) &= -\left(k(t)e(t) + \kappa \frac{d}{dt}(k(t)e(t))\right), \\ \dot{k}(t) &= \gamma \left(\max\{0, \|e(t)\| - \lambda\}\right)^2, \end{aligned} \right\} \quad (3)$$

with $k(0) = k_0 \in \mathbb{R}$, $\lambda > 0$, $\kappa = 1$ (just guaranteeing dimensions) and $\gamma \gg 1$.

This controller consists of a very simple feedback mechanism and adaptation law, it is only based on the output of the system and its time derivative - no knowledge of the system parameters is required.

As mentioned in Section I, the biological paradigm vibrissa exhibits two basic modes of operation: a passive and an active mode. Expressing these modes using the presented adaptive control strategies, we conclude that a vibrissa in *passive mode* is a system to be *stabilized* under permanent excitation while enabling to *detect* external extra-perturbations. In an *active mode*, it is to *track* a given oscillatory motion pattern in order to enable the system to recognize, e.g., the surface texture of an external object contacts. Therefore, we can identify these two basic operation modes with

- passive mode: λ -stabilization (see Fig. 8),

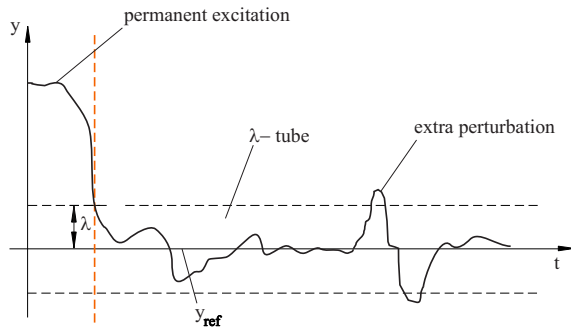


Fig. 8. Vibrissa deflection in passive mode.

- active mode: λ -tracking (see Fig. 9).

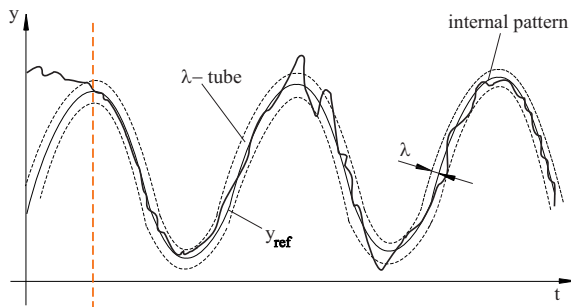


Fig. 9. Vibrissa deflection in active mode.

Note: Because of the randomness of external signals and unknown system parameters, we have to choose the presented adaptive control strategy. The given output of system (1) is $y(t) := \varphi(t)$, hence the equations belong to (2) and the presented controllers achieve their objectives. Now, we apply controller (3) (obviously replacing $u(\cdot)$ by $M_u(\cdot)$) to achieve λ -stabilization ($y_{\text{ref}}(\cdot) \equiv 0$ in passive mode) and λ -tracking (in active mode).

V. SIMULATIONS

We point out that the adaptive nature of the controller is expressed by the *arbitrary choice* of the system parameters. Obviously, numerical simulation needs fixed (and known) system data, but the controller *adjusts* its gain parameter to *each set* of system data. Guided by [25], we choose the following parameters (for all simulations, further data will be given on the spot):

- vibrissa: $m = 0.003 \text{ kg}$, $c = 5.7 \frac{\text{N}}{\text{m}}$, $d = 0.2 \frac{\text{Ns}}{\text{m}}$, $L = 0.04 \text{ m}$, $a = \frac{L}{10} = 0.004 \text{ m}$, $(\varphi(0), \dot{\varphi}(0)) = (0 \text{ rad}, 0 \frac{\text{rad}}{\text{s}})$;
- environment: $t \mapsto F(t) = (0.1 \cos(t) + 2e^{-(t-20)^2}) \text{ N}$ (see Fig. 10), which represents a (small) permanent oscillation with a gust of wind; and $g = 9.81 \frac{\text{m}}{\text{s}^2}$;

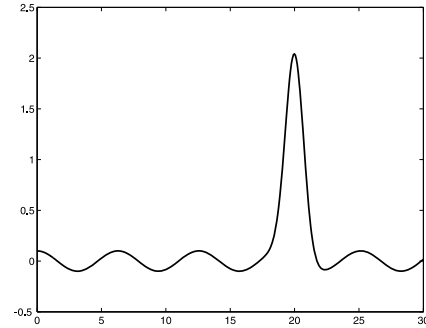


Fig. 10. Excitation F vs. time t .

- λ -tracker: $\lambda = 0.2^\circ \approx 0.064 \pi$, $\gamma = 50$ (additional parameter to increase the convergence of the controller gain [30]) and $k_0 = 0$.

The following reference signals are used for operation in different modes:

- In the passive mode, the rod motion only needs to be stabilized, therefore it can be simulated with the reference signal (4).

$$t \mapsto \varphi_{\text{ref}0}(t) = 0 \quad (4)$$

- The active mode has to be implemented with reference signals performing periodical oscillations enabling the rod to either explore its surroundings or to scan specific objects – and since rodents use two different kinds of oscillations depending on the task, the exploratory and foveal whisking are simulated by two different reference signals. Rodents employ large amplitude sweeps in a low frequency range (5 – 15 Hz) to investigate their

environment. As the range of movement of the biological vibrissa amounts to ca. $100^\circ = 1.74$ rad, the amplitude of the exploratory reference signal (5) can be chosen to $A = \frac{1.74}{2} \approx 0.8$ rad. The frequency of the signal $\varphi_{ref1}(t)$ has been set to $f = 5$ Hz according to the findings in [14]. Foveal whisking has been implemented with the reference signal (6), using an amplitude of $A = 0.2$ rad $\approx 12^\circ$ and a frequency of $f = 25$ Hz, since rodents scan specific objects with small amplitude, high frequency movements (15 – 25 Hz).

$$t \mapsto \varphi_{ref1}(t) = 0.8 \sin(2\pi 5 t) \quad (5)$$

$$t \mapsto \varphi_{ref2}(t) = 0.2 \sin(2\pi 25 t) \quad (6)$$

A. Passive mode: λ -stabilization of $\varphi_{ref0}(\cdot)$

We use controller (3) for stabilization ($y_{ref}(\cdot) \equiv 0$, rest position to be tracked).

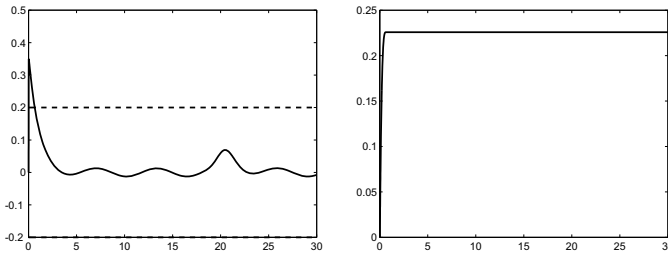


Fig. 11. Output and λ -strip (left), gain parameter (right), all vs. time t .

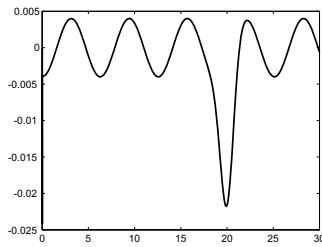


Fig. 12. Control torque M_u vs. time t .

Fig. 11 (left) shows a good stabilization, the output is captured by the tube. Fig. 11 (right) shows the convergence of the gain parameter to a constant value, and Fig. 12 the necessary control torque, which reflects the local disturbance around $t = 20$.

B. Active mode 1: λ -tracking of $\varphi_{ref1}(\cdot)$

Now, we pass to an active mode. Again, we use controller (3) to track reference signal $\varphi_{ref1}(\cdot)$.

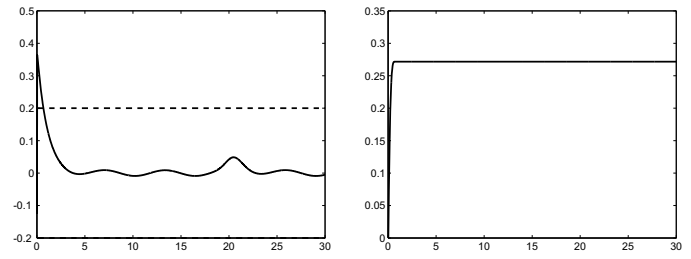


Fig. 13. Error e with λ -strip (left), and gain parameter k (right), all vs. time t .

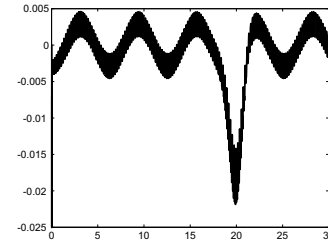


Fig. 14. Control torque M_u vs. time t .

We have a good tracking behavior, the output is captured by the tube. This seems to be true because the error is captured by the tube around zero, see Fig. 13 (left). Let us point out that we omit the figure of the output for reasons of presentation (oscillations with high frequency to be tracked) and focus on the error in the following. The controller gain is given in Fig. 13 (right). Fig. 14 shows the control torque that very weakly responds to the local disturbance.

C. Active mode 2: λ -tracking of $\varphi_{ref2}(\cdot)$

Here, we simulate another active mode in tracking reference signal $\varphi_{ref2}(\cdot)$ using controller (3).

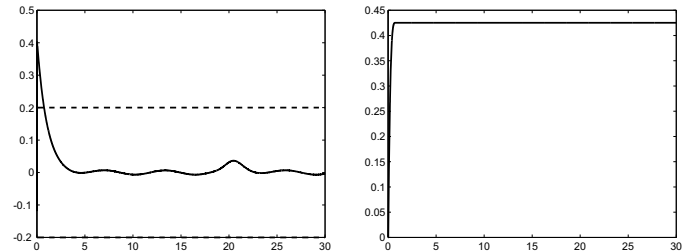


Fig. 15. Error e with λ -strip (left), and gain parameter k (right), all vs. time t .

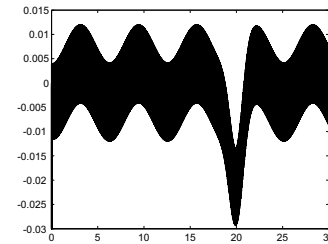


Fig. 16. Control torque M_u vs. time t .

Again, and also in simulation of another active mode (foveal whisking), we have a good tracking behavior because the controller works effectively, see Figs. 15 and 16. But, it is quite hard to detect the gust of wind in the system variable. Only the control torque reflects the “peak” around $t = 20$ s, see Fig. 16. Therefore, we try to detect the additional excitation by means of other observables.

This problem is tackled in the next section.

VI. IMPROVED ADAPTATION LAWS AND CONTROL SCHEMES

The foregoing simulation shows that the system is not really sensitive to notice the excitation peak around $t = 20$, though tracking and stabilization are essentially guaranteed. Moreover, after the control objective is achieved, the gain parameter still stays at its high value. Figs. 11 (right), 13 (right) and 15 (right) show the monotonic increase of $k(\cdot)$ towards a limit k_∞ . But, if some perturbation repeatedly caused the output to leave the λ -strip, then $k(t)$ would take larger values again and again. The aim is now to avoid this drawback.

At first, we introduce some modifications of the control strategy (3) presented in [1]. These show up with an altered feedback law allowing for output disturbances and various adaptors. Let the control system be of class (2). Then, let us consider controllers of the general form:

$$\left. \begin{aligned} e(t) &:= y(t) - y_{\text{ref}}(t) + n(t), \\ u(t) &= -\left(k(t)e(t) + \kappa \frac{d}{dt}(k(t)e(t))\right), \\ \dot{k}(t) &= f_\lambda(k(t), e(t), t), k(t_0) = k_0 \in \mathbb{R}, \end{aligned} \right\} \quad (7)$$

whereby $\lambda > 0$ is the tracking accuracy as in (3). The unknown function $n(\cdot) \in \mathcal{R}$ is a noise corruption of the output, where \mathcal{R} is the set of differentiable functions with absolutely continuous first order derivative and bounded functions and derivatives up to order two, i.e., these functions are elements of \mathcal{L}^∞ . It is very important to claim a bound for the output measurement noise signal $n(\cdot)$. This fact is often neglected in literature concerning adaptive tracking control in the presence of noise, see [31]. Further, one can easily see that λ -tracking only makes sense if the bound of the output measurement noise signal $n(\cdot)$ is smaller than λ :

$$\|n(\cdot)\|_\infty < \lambda, \quad (8)$$

otherwise the controller cannot distinguish between the reference and noise signal, and so it λ -tracks the wrong signal $y_{\text{ref}}(t) - n(t)$.

Secondly, we apply an improved adaptation law, see [32], that makes $k(\cdot)$ decrease as long as further high lever is not necessary. We distinguish three cases:

1. increasing $k(\cdot)$ while e is outside the tube,
2. constant $k(\cdot)$ after e entered the tube - no longer than a pre-specified duration t_d of stay, and
3. decreasing $k(\cdot)$ after this duration has been exceeded.

For instance:

$$\dot{k}(t) = \begin{cases} \gamma \left(\|e(t)\| - \lambda\right)^2, & \text{if } \|e(t)\| \geq \lambda, \\ 0, & \text{if } \left(\|e(t)\| < \lambda\right) \wedge (t - t_E < t_d), \\ -\sigma k(t), & \text{if } \left(\|e(t)\| < \lambda\right) \wedge (t - t_E \geq t_d), \end{cases} \quad (9)$$

with given $\sigma > 0$, $\gamma \gg 1$, and $t_d > 0$, whereas the entry time t_E is an internal variable.

Choosing this new adaptor (9) with $\sigma = 0.2$ (moderate exponential decay rate [22]) and $t_d = 1$ (moderate choice of the duration of stay within the λ -tube [32]), we obtain the following tracking results in an active mode, e.g., λ -tracking of $\varphi_{\text{ref}1}(\cdot)$:

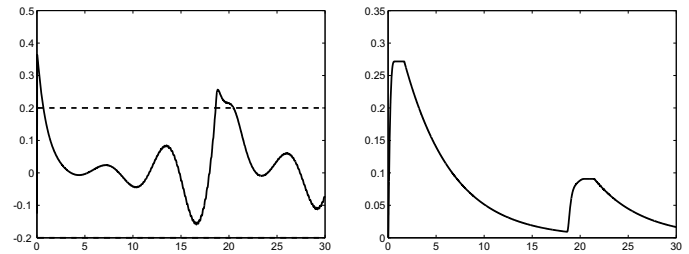


Fig. 17. Error e and λ -strip (left), and gain parameter k (right), all vs. time t .

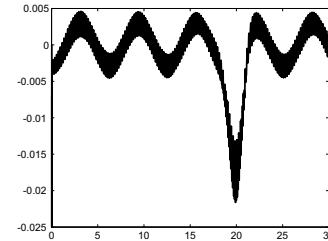


Fig. 18. Control torque M_u vs. time t .

The output is forced into the tube, see Fig. 17 (left). The gain $k(\cdot)$ immediately decreases, see Fig. 17 (right), after a t_d -stay of e in the tube, see Fig. 17 (left). Apparently, the decrease is too fast: e leaves the tube again but, as a consequence of \dot{k} being proportional to the *square* of the (small) deviation from the λ -tube, k increases too slowly as to force e quickly back to the tube. The necessary control input is displayed in Fig. 18.

In order to make the attraction of the tube stronger, we use different exponents for large/small distance from the tube, see [32]. For instance:

$$\dot{k}(t) = \begin{cases} \gamma \left(\|e(t)\| - \lambda\right)^2, & \text{if } \|e(t)\| \geq \lambda + 1, \\ \gamma \left(\|e(t)\| - \lambda\right)^{0.5}, & \text{if } \lambda + 1 > \|e(t)\| \geq \lambda, \\ 0, & \text{if } \left(\|e(t)\| < \lambda\right) \wedge (t - t_E < t_d), \\ -\sigma k(t), & \text{if } \left(\|e(t)\| < \lambda\right) \wedge (t - t_E \geq t_d), \end{cases}$$

with σ, γ, t_d, t_E as before.

Using this adaptor, we obtain the results from Figs. 19 and 20.

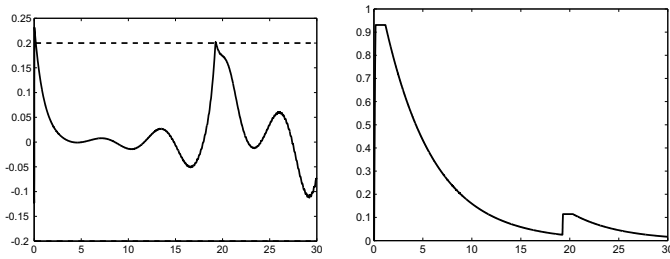


Fig. 19. Error e and λ -strip (left), and gain parameter k , all vs. time t .

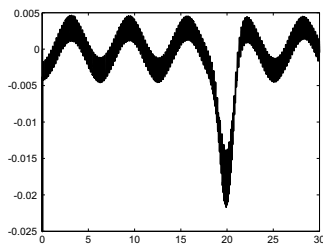


Fig. 20. Control torque M_u vs. time t .

Here, one cannot clearly see the advantage of two alternating exponents. The gain parameter $k(\cdot)$ increases very fast in the beginning of the simulation, see Fig. 19 (right). This is due to the “switching on” of the controller. It forces e faster into the tube at cost of a high k . Then, k decreases if e stays in the tube for a duration larger than t_d , see Fig. 19 (right). The error e is forced back into the λ -tube very fast, see Fig. 19, because the attraction of the tube is stronger for small deviations $\|e(t)\| - \lambda > 0$. This is on the expense of a tolerable overshooting of k at the beginning, mentioned above. But, interestingly, we are also able to detect solitary excitations in observing the gain $k(\cdot)$ instead of $M_u(\cdot)$, see Fig. 20.

VII. CONCLUSIONS

The foregoing considerations have shown that adaptive control is promising in application to vibrissa systems. In particular, it allows, based on the dynamical equations, to describe two main modes of operation of vibrissae: passive and active ones. More precisely, these control strategies allow the artificial system to proceed its scanning procedure / its mode of operation (e.g., to investigate the surface texture of objects as in [35]) despite the existence of external disturbances — as in nature. Hence, the presented controllers can mimic the adaptive nature of this paragon using adaptive control schemes. Further on, improved adaptive controllers are useful to diminish high gain factors to reduce an overload of the scanning device. As mentioned in this paper, the presented controllers are also robust with respect to output measurement noise.

Therefore, this research on improved controllers should be developed further. Simultaneously, the following problems/tasks are under investigation: separation of an extra receptor from vibrissa to hopefully get more insights into this sophisticated biological system and its data processing,

and identification techniques to get knowledge of solitary excitations.

Near future tasks are

- replace the simple model of a circular pendulum by spherical one (to model spatial receptivity),
- tuning of the adaptors (i.e., to find favorable values of γ , σ , t_d), and investigating rates of convergence,
- hardware experiments to validate the theory,
- to develop elastic vibrissae models, e.g., multi-body systems and/or continuum systems,
- consider a tuft of vibrissae (modeling the intrinsic musculature), not only a single vibrissa.

After doing this, one can think about the application of the presented tracking scenario to replace the kinematic drive/kinematic scanning trail in present application for recognition of object contours and/or texture in, e.g., [33], [34].

REFERENCES

- [1] C. Behn, M. Scharff, and L. Merker, “Steps towards the Modeling of Animal Vibrissa Modes Using Adaptive Control,” in INTELLI 2022 - The Eleventh International Conference on Intelligent Systems and Applications, Venice, Italy, May 2022, pp. 43–49.
- [2] M. R. Cutkosky, R. D. Howe, and W. R. Provancher, “Force and Tactile Sensors,” in Springer Handbook of Robotics, B. Siciliano and O. Khatib, Eds. Heidelberg: Springer, 2008, pp. 445–476.
- [3] T. J. Prescott, M. J. Pearson, B. Mitchinson, J. C. W. Sullivan, and A. Pipe, “Whisking with robots: from rat vibrissae to biomimetic technology for active touch,” IEEE Robotics & Automation Magazine, vol. 16, 2009, pp. 42–50.
- [4] A. S. Ahl, “The role of vibrissae in behavior: a status review,” Veterinary Research Communications, vol. 10, 1986, pp. 245–268.
- [5] M. J. Z. Hartmann, “A night in the life of a rat: vibrissal mechanics and tactile exploration,” Annals of the New York Academy of Sciences, vol. 1225, 2011, pp. 110–118.
- [6] Y. S. W. Yu, M. M. Graff, and M. J. Z. Hartmann, “Mechanical responses of rat vibrissae to airflow,” Journal of Experimental Biology, vol. 219, 2016, pp. 937–948.
- [7] S. J. Whiteley, P. M. Knutsen, D. W. Matthews, and D. Kleinfeld, “Deflection of a vibrissa leads to a gradient of strain across mechanoreceptors in a mystacial follicle,” Journal of Neurophysiology, vol. 114, 2015, pp. 138–145.
- [8] M. Brecht, B. Preilowski, and M. M. Merzenich, “Functional architecture of the mystacial vibrissae,” Behavioural Brain Research, vol. 84, 1997, pp. 81–97.
- [9] G. E. Carvell and D. J. Simons, “Biometric analyses of vibrissal tactile discrimination in the rat,” Journal of Neuroscience, vol. 10, 1990, pp. 2638–2648.
- [10] D. Voges et al., “Structural characterization of the whisker system of the rat,” IEEE Sensors Journal, vol. 12(2), 2012, pp. 332–339.
- [11] A. Schierloh, “Neuronal networks and their plasticity within the barrel cortex of a rat,” PhD-Thesis (in German), Technische Universität München, Germany, 2003.
- [12] M. Scharff, “Bio-inspired tactile sensing – Analysis of the inherent characteristics of a vibrissa-like tactile sensor,” PhD-Thesis, Technische Universität Ilmenau, Germany, 2021.
- [13] J. Dörfel, “The musculature of the mystacial vibrissae of the white mouse,” Journal of Anatomy, vol. 135, 1982, pp. 147–154.
- [14] R. W. Berg and D. Kleinfeld, “Rhythmic whisking by rat: retraction as well as protraction of the vibrissae is under active muscular control,” Journal of Neurophysiology, vol. 89, 2003, pp. 104–117.
- [15] M. J. Z. Hartmann and J. H. Solomon, “Robotic whiskers used to sense features: Whiskers mimicking those of seals or rats might be useful for underwater tracking or tactile exploration,” NATURE, vol. 443, 2006, p. 525.
- [16] B. Mitchinson, M. Pearson, C. Melhuish, and T. J. Prescott, “A model of sensorimotor coordination in the rat whisker system,” in From Animals to Animats 9: Proc. 9th. Int. Conf. on Simulation of Adaptive Behaviour, 2006, pp. 77–88.

- [17] B. Mitchinson, C. J. Martin, R. A. Grant, and T. J. Prescott, "Feedback control in active sensing: rat exploratory whisking is modulated by environmental contact," *Proc. R. Soc. B*, vol. 274, 2007, pp. 1035–1041.
- [18] D. Derdikman et al., "Layer-specific touch-dependent facilitation and depression in the somatosensory cortex during active whisking," *The Journal of Neuroscience*, vol. 26(37), 2006, pp. 9358–9547.
- [19] J. C. Curtis and D. Kleinfeld, "Seeing what the mouse sees with its vibrissae: a matter of behavioural state," *Neuron*, vol. 50(4), 2006, pp. 524–526.
- [20] E. E. Fanselow and M. A. L. Nicolelis, "Behavioral modulation of tactile responses in the rat somatosensory system," *The Journal of Neuroscience*, vol. 19(17), 1999, pp. 7603–7616.
- [21] T. A. Schmitz, "Development and analysis of biologically inspired sensor systems with higher degrees of freedom using the example vibrissa," Master thesis (in German), Technische Universität Ilmenau, Germany, 2011.
- [22] C. Behn, "Mathematical modeling and control of biologically inspired uncertain motion systems with adaptive features," Habilitation thesis, Technische Universität Ilmenau, Germany, 2013.
- [23] F. A. Lucianna, A. L. Albarracín, S. M. Vrech, F. D. Farfán, and C. J. Felice, "The mathematical whisker: a review of numerical models of rat's vibrissa biomechanics," *Journal of Biomechanics*, vol. 49, 2016, pp. 2007–2014.
- [24] B. Mitchinson et al., "Empirically inspired simulated electro-mechanical model of the rat mystacial follicle-sinus complex," *Proc. R. Soc. Lond.*, vol. 271, 2004, pp. 2509–2516.
- [25] D. Hill, R. Bermejo, P. Zeigler, and D. Kleinfeld, "Biomechanics of the vibrissa motor plant in rat: rhythmic whisking consists of triphasic neuromuscular activity," *Journal of Neuroscience*, vol. 28, 2008, pp. 3438–3455.
- [26] E. Simony et al., "Temporal and spatial characteristics of vibrissa responses to motor commands," *Journal of Neuroscience*, vol. 30, 2010, pp. 8935–8952.
- [27] S. Haiderliu, E. Simony, D. Golomb, and E. Ahissar, "Muscle architecture in the mystacial pad of the rat," *The Anatomical Record: Advances in Integrative Anatomy and Evolutionary Biology*, vol. 293, 2010, pp. 1192–1206.
- [28] F. G. Barth, "Spider mechanoreceptors," *Current Opinion in Neurobiology*, vol. 14, 2004, pp. 415–422.
- [29] A. N. Kolmogorov and S.V. Fomin, "Elements of the theory of functions and functional analysis," Dover, 1999.
- [30] C. Behn, "Adaptive control of straight worms without derivative measurement," *Multibody System Dynamics*, vol. 26, 2011, pp. 213–243.
- [31] A. Ilchmann and E. P. Ryan, "Universal λ -tracking for nonlinearly-perturbed systems in the presence of noise," *Automatica*, vol. 30(2), 1994, pp. 337–346.
- [32] C. Behn, "Modeling, analysis and control of mechanoreceptors with adaptive features," *Informatics in Control, Automation and Robotics – Lecture Notes in Electrical Engineering (LNEE)*, vol. 325, J.-L. Ferrier et al. Eds., Springer International Publishing Switzerland, 2014, pp. 349–366.
- [33] M. Scharff, J. H. Alencastre, and C. Behn, "Detection of surface texture with an artificial tactile sensor," *Interdisciplinary Applications of Kinematics – Mechanisms and Machine Science*, vol. 71, A. Kecskeméthy et al. Eds., Cham: Springer, 2019, pp. 43–50.
- [34] L. Merker, M. Scharff, K. Zimmermann, and C. Behn, "Surface Sensing of 3D Objects Using Vibrissa-like Intelligent Tactile Sensors," *Proceedings INTELLI 2020: The Ninth International Conference on Intelligent Systems and Applications, Porto (Portugal), IARIA, 2020*, pp. 18–23.
- [35] M. Scharff, "Bio-Inspired Tactile Sensing: Distinction of the Overall Object Contour and Macroscopic Surface Features," *Perspectives in Dynamical Systems I: Mechatronics and Life Sciences, Springer Proceedings in Mathematics & Statistics*, vol 362, J. Awrejcewicz et al. Eds., Cham: Springer, 2022, pp. 107–117.

Designing a Low-Cost Early Diagnosis System Based on Deep Learning

Monitoring the Development of Chronic Venous Disorder with Indirect Augmented Reality

Huseyin A. Erdem

Department of Computer Engineering,
The Graduate School of Natural and
Applied Sciences
Dokuz Eylül University
İzmir, Turkey
e-mail: huseyinaerdem@gmail.com

Hışıl Erdem

Department of Civil Engineering,
The Graduate School
İzmir Institute of Technology
İzmir, Turkey
e-mail: isilerdem@iyte.edu.tr

Semih Utku

Department of Computer Engineering,
Faculty of Engineering
Dokuz Eylül University
İzmir, Turkey
e-mail: semih@cs.deu.edu.tr

Abstract - Today's healthcare industry agrees that early diagnosis is just as important as the treatment of diseases. Academic and commercial studies carried out in this direction within the scope of early diagnosis contribute to a better quality of human life. Thanks to devices that offer early diagnosis, treatments can be started when the diseases are at their initial levels, and thus treatment costs can be reduced. However, most of these devices work with harmful rays and are generally used in hospital environments only by specialized staff. In this study, a low-cost early diagnosis system for home use, developed as part of a doctoral thesis, is introduced. The most important aspect of the proposed system that supports the convenience of home use is that it provides a harmless imaging with near-infrared light for the body. The system can detect both Class-1 (spider/telangiectasias vein) and Class-2 (varicose vein) types of the clinical classification of Chronic Venous Disorder, with 4 different classes (in the form of two separate levels as beginner and advanced). In the system, which will monitor the development of the disorders in the superficial veins, the confidence values and positions of the detections in the images were determined by the You Only Look Once version-3 object detection algorithm used in deep learning applications. Confidence values of 0.90 and above were achieved in the object detection experiments performed with Class-1 and Class-2 type artificial patterns. According to the test results obtained, the system was able to detect Chronic Venous Disorder patterns with the values of Accuracy Rate (1), Misclassification Rate (0), Precision (1), Prevalence (0.5) and F-Score (1). The confidence values and positions of the patterns detected in the study are presented to the user/physician with the help of indirect augmented reality visuals as an e-health application that will support a long-term monitoring system. In this way, the beginner and the advanced levels of venous disorder can be monitored by before and after video visuals.

Keywords - near-infrared light; chronic venous disorder; deep learning; YOLOv3; indirect augmented reality.

I. INTRODUCTION

Especially in the 21st century, in the academic and commercial sector, advances in health technologies have increased at an unstoppable pace. While some of these advances target treatments after the disease occurs, others aim at early diagnosis by making use of various imaging

techniques that are harmful/harmless to the body. This study is an extended version of the study [1] investigating the detection of varicose vein development. In this version, the current system designed for vascular degeneration monitoring within the scope of the doctoral thesis [2] has been restructured in such a way that it can detect 2 different types (spider_vein and varicose_vein) of vein enlargement at 2 levels (beginner and advanced) in more detail. The current system [2] consists of 6-phases. In the Imaging Technique Phase, video recordings of superficial veins are obtained using a low-cost (65 dollars) near-infrared camera. With the Digital Image Pre-Processing Phase, these recordings are converted into images and enhancements are made on the raw images. These first two phases are detailed in the study [3]. In the enhanced images, the discontinuous vascular structures caused by illumination are removed to a certain level in the Digital Image Post-Processing Phase. In the Classification Phase, the classes of vascular degeneration are determined by using Convolutional Neural Networks and Hybrid Decision-Making Algorithm (first introduced in the study [4]), and the positions of these degenerations are determined in the Object Detection Phase. In the last phase, the Augmented Reality Phase, the object detection results obtained are superimposed on the raw images, and the video visuals are created and presented to the user and his/her physician. All phases of this system are described in the study [4] specifically for vascular narrowing (stenosis_vein class).

Medical imaging devices are one of the primary auxiliary methods used in hospitals to diagnose different diseases. The devices used in this context work on the basis of visualizing the area to be viewed with light or sound waves. Imaging with light is carried out by utilizing different wavelengths in the electromagnetic spectrum. Medical imaging devices currently in use are classified according to “the body tissue they can monitor” and “the effects of the light used to illuminate the area of interest on the body”. While the X-Ray device, which emits harmful rays (ionizing radiation) to the body, is predominantly used in the imaging of bone tissue and abdominal diseases, Computed Tomography is used for imaging both bone tissue and internal organs [5]-[7]. In addition, Magnetic Resonance Imaging provides imaging of tissues with magnetic waves, whereas Ultrasound uses high-

frequency sound waves for imaging [5][6]. Computed Tomography or Magnetic Resonance Imaging techniques can be used for vascular imaging [6]. However, both the negative effects of these devices on human health and their high costs limit their use to hospital environments only. Furthermore, even if the ultrasound device, which provides visualization of blood flow [5][6], is harmless to the body, it has a high cost and is generally used and interpreted by radiologists in hospitals.

Although technology advances at a dizzying pace, many lives are still lost due to late detection of diseases that can be easily cured if detected earlier. Despite efforts to raise awareness of early diagnosis of all kinds of diseases, today's people do not give up the habit of going to the doctor after the onset of the disease and often neglect routine checkups. In these omissions, the concern of triggering other diseases by imaging devices working with harmful rays to the body during controls has a large share. However, technological techniques currently under development offer the possibility of producing safe alternatives for the early detection of some diseases. Among them, we can include, the detection of varicose veins, which is one of the most common venous disorders and caused by the enlargement of veins close to the surface of the skin (i.e., superficial veins), can be counted. Near-infrared light, which is a type of light that is harmless to the body, is used in hospitals within the scope of superficial vein imaging, especially during vascular access procedures.

The main advantage of near-infrared light in the scope of vein imaging is that photons of this type of light can be absorbed by Hemoglobin molecules in the veins [8]-[10]. The Hemoglobin (Hb) molecule is a blood protein [11] that is found in the vascular system and is in charge of carrying Oxygen to the tissues. While the molecule carries Oxygen to the tissues and organs by passing through the arteries in the form of oxygenated Hb (HbO_2), it returns to the heart through the veins as de-oxygenated Hb (Hb) after leaving its Oxygen. These molecules transported in a recirculation system are more sensitive to near-infrared light in the range of 800-900 nanometers (nm) as HbO_2 and in the range of 700-800 nm as Hb [12]. One of the tricks in near-infrared imaging is to choose the wavelength of the near-infrared light that illuminates the tissue and the wavelength of the camera that will take the image in harmony. In this way, the veins in the tissue area illuminated with near-infrared light of a certain wavelength (in the studies carried out in [9]-[13], a wavelength of 850 nm was used, which usually gives optimum results) can be viewed in a better quality with a camera having the same wavelength filter. Superficial veins (thanks to the Hb molecules inside) absorb the near-infrared light (700-900 nm range of the electromagnetic spectrum) that penetrates 3-5 millimeters, passing through the skin and fat layer in the illuminated tissue area, and creates dark areas in the images. These dark areas in the images represent the veins, while the bright areas represent the surrounding tissues. In this way, the visualization of the superficial veins can be easily performed with only the light source and the camera (even an ordinary camera can be turned into a simple near-infrared camera by changing the filter on it). This

imaging method is evaluated within the scope of Spectroscopy (acquiring knowledge of the structure of matter interacting with a particular type of light [14]). Although the dark areas in near-infrared spectroscopy images more or less allow the visualization of veins, they are not of sufficient quality for further analysis. For this, by applying digital image processing filters on the obtained near-infrared image, some improvements can be made on the image. The 6-phase system used in the study performs image enhancement processes in two separate phases. In the Digital Image Pre-Processing Phase, two-coloured binary images consisting of black (vein) and white (surrounding tissues) are obtained from raw videos (video recordings are taken during tissue imaging) with image processing filters and methods. In this way, it is ensured that the edges of the veins are sharpened, only the relevant vein patterns are revealed by eliminating the surrounding tissues and the noise in the images is removed. In the veins of these images, the discontinuous structures caused by the illumination have been eliminated up to a certain level with the Digital Image Post-Processing Phase (Speeded Up Robust Features (SURF) Local Feature Detector Algorithm [15] is used). Processed near-infrared vascular images can be used for many different purposes from disease pre-diagnosis to biometric recognition [3][4][16][17]. For these purposes, deep learning techniques (such as classification or object detection/recognition) are applied on images. The Classification Phase of the 6-phase system makes it possible to determine to which class the observed tissue belongs. At this phase, video recordings of the first viewing period are used to introduce the classes to be used in the system. Within the scope of monitoring, the system checks the belongingness of the images obtained in the following periods (can be set as day, week, month) to one of the defined classes (as many as the number of different tissue regions the user views in the first period). If the classes of new images can be determined, the Object Detection Phase is used to detect vascular degenerations from these images. In this study, the vein enlargement patterns in the images are detected by the object detection algorithm, too.

The system, which was prepared within the scope of the doctoral study (near-infrared images of the right and left forearms were used) and which enables the superficial veins (in the near-infrared images) to be visualized as an e-health application in the home environment, was re-trained in the study [1] to monitor the vein enlargement. In order to increase the low confidence values encountered in object detection in the study [1] and to perform a more sensitive detection, the system was re-trained with 4 different classes in this study. In addition, in the study [1], two artificial datasets (representing vein enlargements) created to be used in the training and testing processes of the You Only Look Once version-3 (YOLOv3) object detection algorithm were re-arranged. In this study, in addition to the processes described in the study [1], the Augmented Reality Phase, which is the 6th phase of the system, was also included in the study. In this way, it has been ensured that the detections and developments of vein enlargement can be visually presented to the user and his/her physician within the scope of Indirect Augmented Reality.

In Section II, both object detection studies within the scope of the YOLOv3 object detection algorithm and the virtual environment literature within the scope of Indirect Augmented Reality were examined. In Section III, Chronic Venous Disorder (CVD) types were introduced and the re-trained YOLOv3 object detection algorithm was explained so that the system can detect vein enlargement in the Object Detection Phase. How the datasets were created, which classes were defined and the results obtained as a result of the experiments were also stated in this section. In Section IV, how video-based images are arranged for the Augmented Reality Phase is detailed. In the last section, the study is discussed in general terms.

II. RELATED WORK

Classification processes are used to determine the class to which an image belongs. Traditional Convolutional Neural Networks can detect the belongingness of the inputs in the form of images, audio or video to defined classes. However, these networks do not give the position information of the objects they detect in the image. For this, object detection algorithms (Single Shot Detector SSD [18], Fast/Faster Region-based Convolutional Neural Networks [19]-[21], You Only Look Once YOLO [22]) are used. The YOLO algorithm is frequently preferred in studies especially because it can perform real-time object detection faster. In this context, YOLO version-3 [23] is included in this study because it can detect small objects as well [24].

In the study [25], which provides recognition of human movements and classification with location detection, the YOLO algorithm was trained using a total of 10 classes, including actions such as conversation between two people, exiting/entering the room, and handshaking. Images were processed as video streams and action recognition was performed with a small number of images (even a single image was sufficient in some cases).

In the study [26], which aims to provide real-time social distance detection in public areas within the scope of the Covid-19 pandemic, close proximity of more than 2 meters was detected by using the YOLOv3 object detection algorithm and marked with a red bounding box.

In the study [27], which performed fire detection as a real-time video-based tracking application, the tiny-YOLOv3 algorithm [28], a lighter version of the YOLOv3 object detection algorithm, was used. Experimental results obtained using 5000 training images and 5000 test images in the study confirmed the effectiveness of the proposed system.

In the study [29] investigating water consumption monitoring, the consumption indicator on the water meter counter images were determined by using the YOLOv4 algorithm [30], and the image was processed through the image processing stage and digit recognition was performed by converting it to black and white format. In addition, within the scope of the system developed in the study, a mobile application was made available. The study had an object detection accuracy of 98%.

In the study [31], which aimed to detect suspicious breast lesions on digital mammography images, early diagnosis and classification was performed using the YOLO algorithm. In

the study, 4 different classes were used as mass, calcification, architectural distortion and normal.

In the study [32], in which the YOLO algorithm was used for the detection of Diabetic retinopathy, which manifests with fundus lesions at its early level, fundus lesions were defined in 4 different classes as microaneurysms, hemorrhages, hard exudates and soft exudates.

In the study [33], which aims to detect Pediatric Pneumonia, Convolutional Neural Networks, which use X-Ray images as input, were used and it was aimed to accelerate the diagnosis decision process in this way. It was stated that the classification accuracy of the study for 3 different classes as normal, viral pneumonia, and bacterial pneumonia was 90.71%.

In the study [34], which aims to detect chest abnormality with deep learning, it had been underlined that doctors could be provided with a faster decision-making opportunity in diagnosing. In the study, Computed Tomography scan image inputs, a dataset of 18000 images (15000 train / 3000 test) labelled by radiologists, 14 different classes (Atelectasis, Calcification, Cardiomegaly, Consolidation, ILD, Infiltration, Lung Opacity, Nodule/Mass, Other lesions, Pleural effusion, Pleural thickening, Pneumothorax, Pulmonary fibrosis, No finding observation) and the YOLOv5 algorithm [35] were used.

In the system used in this study, Indirect Augmented Reality was used to present the CVD detection results obtained with the YOLOv3 object detection algorithm and their position in the image to the user/physician. Indirect Augmented Reality is a video-based virtual technology that has two separate modes, offline (creation of video visuals where virtual material is superimposed on real material) and online (displaying the superimposed video to the user in its real-world location). Studies in the literature on the concept are very limited.

In the study [36], which introduced the concept of Indirect Augmented Reality to the literature, previously recorded panoramic video images were used in two separate case studies within the scope of location finding and it was emphasized that the concept was useful for outdoor use.

In the study [37], in which it was stated that the alignment problems between virtual and real material could be solved with Indirect Augmented Reality, the participants gave positive feedback according to the results of the trials of virtual applications introducing Rome.

In the study [38], which combines both traditional Augmented Reality and Indirect Augmented Reality within the scope of the Casa Batllo museum promotion application in Spain, it was underlined that Indirect Augmented Reality could also be used as an indoor application. The application was also covered under the mobile-based Augmented Reality title. The application automatically switches between traditional and Indirect Augmented Reality according to the user's location. According to the results obtained in the study, the application can easily reflect the life of the beginning of the 20th century to the user.

In the study [39], that aims to eliminate temporal discrepancies (e.g., if online registration is performed at night while offline images are created with daytime images),

which are the negative aspects of Indirect Augmented Reality applications especially in outdoor use, samples taken from different environmental conditions at different times were added to the dataset. For online registration, a selection was made among the images in the dataset according to the histogram similarity.

In the study [40], which presents the Omaha Beach landing in an Indirect Augmented Reality environment, an environment was prepared in such a way that panoramic video images containing war scenes and narrations would be activated when the user was within 200 meters of the relevant region.

III. VEIN ENLARGEMENT DETECTION: DEEP LEARNING AND THE YOLOV3 OBJECT DETECTION ALGORITHM

Near-infrared imaging system is basically examined in two parts as hardware and software. While the hardware part is about the wavelength of the light source, Light Emitting Diode (LED) placements and camera features, the software part covers the extraction of vein patterns by making the veins in the obtained near-infrared images more prominent via digital image processing techniques. In this way, superficial veins can be visualized. The hardware part and digital image processing steps of the doctoral study were introduced in [3]. Also, the presentation of narrowing detections in processed images (using the YOLOv3 object detection algorithm with a single-class as *stenosis_vein*) to patient and his/her physician as a video-based Indirect Augmented Reality environment was explained in [4]. The 2-class vein enlargement patterns (*spider_vein* and *varicose_vein*) in the superficial vein images discussed in the study [1] were detailed as a total of 4 classes, with each 2 class represented by 2 levels (beginner and advanced) in this study.

When the superficial vein valves do not work properly, blood accumulations occur, and as a result, the veins expand, elongate, and form twisted folds, resulting in varicose veins [41][42]. Although varicose veins are most commonly observed in leg veins (which are under more pressure than other veins [41]), varicose veins can be encountered in any part of the body [43]. In general, however, the development of venous disorder in hand veins does not give results as dramatic as in leg veins. Chronic Venous Disorders (CVDs) affecting millions of people worldwide are caused by morphological and functional abnormalities of the venous system [44][45]. Risk factors such as heredity (family history, height), lifestyle (long term standing/sitting, occupation, smoking), gain (age, pregnancy, obesity, deep vein thrombosis) or hormones (female gender, progesterone) can lead to venous disorders, such as vein enlargement [46][47]. CVD clinical types are defined by the CEAP (Clinical, Etiological, Anatomical and Pathophysiological [44]) classification system (letter C represents "Class"): C0 (no visible signs of venous disease), C1 (visible veins, spider/telangiectasias veins), C2 (varicose veins), C3 (swelling/edema), C4 (changes to skin quality), C5 (healed ulceration), and C6 (active ulceration) [45][48]. CVD is often overlooked at its early levels [44]. In case of early diagnosis, advanced symptoms such as edema, skin changes

or leg ulcers can be alleviated with the support of lifestyle changes [45][47]. It was determined that the incidence of venous disorders in adults in urban and rural areas of Bonn in Germany was 59% for telangiectasias vein and 14% for varicose vein, respectively [45].

As most superficial veins, varicose veins are also not easily visible to the naked eye, so near-infrared light is used to visualize these veins [49]. In this study, the hand vein dataset (an example image from the dataset and its processed version are given in Fig. 1) obtained in the study [1] by using the superficial vein monitoring system was used for the experiments of the YOLOv3 object detection algorithm, which was re-trained to detect the beginner and advanced levels of CVD in the C1 (spider/telangiectasias veins) and C2 (varicose veins) types.

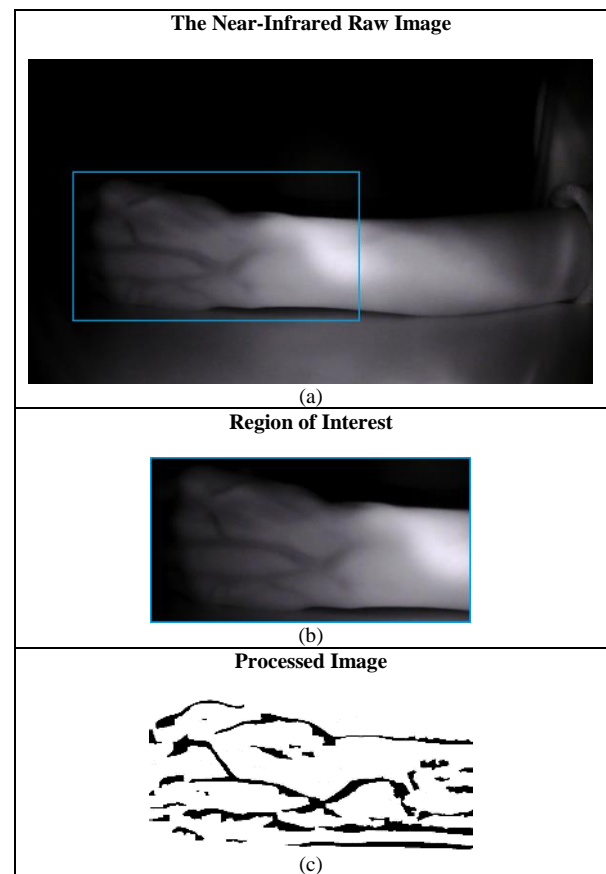


Figure 1. The near-infrared vein image. (a) The near-infrared raw image of hand dorsum. (b) Region of interest, containing only the veins to be examined. (c) Vein patterns obtained by digital image processing. [1]

The ability of the computer to make a determination (i.e., classification) on similar new data by using previously learned data is a decision-making process. Decision making is unique to biological creatures. However, nowadays computers can also "imitate" this process in various ways. This imitation is provided by Artificial Intelligence (the ability to imitate human-specific abilities such as recognition, classification, problem solving and learning by machines using various inputs such as image, sound and

signal [50]). In Machine Learning, which is a sub-branch of Artificial Intelligence, rule sets defined with expert knowledge (human factor) are needed to provide learning or to determine the distinctive features of the patterns [51]. In this way, various classification, regression or clustering operations (disease classification [52], stock forecasting [53] or airport passenger forecasting [54]) can be performed [51]. In Deep Learning, a sub-branch of Machine Learning, with the help of Artificial Neural Networks, features that cannot be detected by humans can be detected without any human intervention. In this way, learning is carried out via Deep Learning Algorithms by itself when only training and test data are given to the system as input. With Deep Learning, operations such as object recognition, speech recognition or object detection can be provided [55].

The YOLOv3 is a Deep Learning Algorithm that performs object detection. With Object Detection Algorithms, training can be performed for multiple objects (up to 80 classes [23] placed at certain positions on the image) that can represent different classes. The YOLOv3 object detection algorithm marks the positions of the objects detected onto the image with bounding boxes. In addition, the name and detection rate (confidence value is shown between 0.00 and 1.00 in the study) of the class with the highest probability to which the object may belong are printed on the box.

In this study, the YOLOv3 object detection algorithm was used for CVD detection in vein patterns obtained by image processing steps. The developed near-infrared imaging system was re-trained in this study to detect 2 different CVD types (C1 and C2) as 4 classes (spider_beginner, spider_advanced, varicose_beginner and varicose_advanced).

There is currently no venous disorder dataset consisting of near-infrared images, available to the public. For this, in this study, a new 4-class (to detect vascular degenerations in more detail) training dataset was prepared by adding artificial patterns on to near-infrared images (the dataset, which is also used in the study [1], was created by the method of obtaining images from video recordings described in the study [4]). The new dataset used in this study was prepared with images that each contain 10 spider_beginner and 10 spider_advanced artificial patterns, and each 5 varicose_beginner and 5 varicose_advanced artificial patterns (the dataset in the study [1] contains 150 near-infrared images, each containing 5 spider_vein and 5 varicose_vein patterns). Furthermore, 50 additional images were created (as in the study [1]) from the existing images by data augmentation methods (10-degree rotation, 30-degree rotation, mirroring, noise addition and downscaling). In this way, a (4-class) training dataset with 6000 artificial patterns was obtained (in the study [1], a (2-class) dataset with 2000 artifacts including 1000 spider_vein and 1000 varicose_vein patterns was used). The patterns in the images were labelled with the free (under General Public License version 3) makesense [56] web-based application.

A second dataset consisting of 600 images containing artificial vein enlargement patterns was prepared for the test

process to be carried out after the trainings (in the study [1] the test dataset consists of 300 images). The test dataset was created by adding only a single pattern (artificial patterns not used in the training) to each image in random rotations and positions (preserving a certain figural format, 150 patterns for each class) (the dataset used in [1] was created by adding only one spider_vein or varicose_vein pattern). In this way, a test dataset of 600 images with 4 classes containing 150 patterns was obtained (in the study [1], a test dataset of 300 images in total was obtained, with 150 test images containing spider_vein class and 150 test images containing varicose_vein class). The confusion matrix of the object detection results of the YOLOv3 object detection algorithm, obtained by using the test dataset is given in Table I for the study [1] (for comparison purposes) and in Table II for this study. As can be seen from the matrix, all of the searched objects (spider_beginner, spider_advanced, varicose_beginner and varicose_advanced patterns) in the test images were detected correctly (for the study [1], all of the spider_vein and varicose_vein patterns were detected correctly). The developed system can detect CVD patterns in C1 and C2 types with Accuracy Rate (1), Misclassification Rate (0), Precision (1), Prevalence (0.5) and F-Score (1) values (similar to the study [1]). 10 sample patterns for each class with the YOLOv3 object detection algorithm confidence values marked are given in Table III.








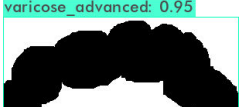






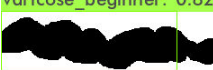



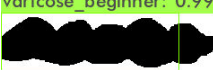




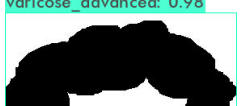


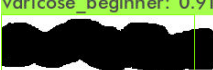

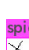

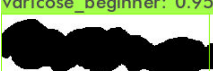







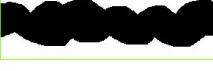

TABLE I. THE CONFUSION MATRIX OF THE YOLOV3 OBJECT DETECTION ALGORITHM RESULTS OBTAINED WITH SPIDER_VEIN AND VARICOSE_VEIN CLASSES [1]

		Predicted Class	
		<i>spider_vein</i> (Positive)	<i>varicose_vein</i> (Negative)
Actual Class	<i>spider_vein</i> (Positive)	True Positive=150	False Negative=0
	<i>varicose_vein</i> (Negative)	False Positive=0	True Negative=150

TABLE II. THE CONFUSION MATRIX OF THE YOLOV3 OBJECT DETECTION ALGORITHM RESULTS OBTAINED WITH SPIDER_BEGINNER, SPIDER_ADVANCED, VARICOSE_BEGINNER AND VARICOSE_ADVANCED CLASSES

		Predicted Class				
		<i>spider beginner</i>	<i>spider advanced</i>	<i>varicose beginner</i>	<i>varicose advanced</i>	<i>unclassified</i>
Actual Class	<i>spider beginner</i>	150	0	0	0	0
	<i>spider advanced</i>	0	150	0	0	0
	<i>varicose beginner</i>	0	0	150	0	0
	<i>varicose advanced</i>	0	0	0	150	0

TABLE III. CONFIDENCE VALUE RESULTS OF THE YOLOV3 OBJECT DETECTION ALGORITHM FOR SPIDER_BEGINNER, SPIDER_ADVANCED, VARICOSE_BEGINNER AND VARICOSE_ADVANCED CLASS PATTERNS

#	spider_beginner	spider_advanced	varicose_beginner	varicose_advanced
1	spider_beginner: 0.86 	spider_advanced: 0.88 	varicose_beginner: 0.99 	varicose_advanced: 0.99 
2	spider_beginner: 0.94 	spider_advanced: 0.91 	varicose_beginner: 0.98 	varicose_advanced: 0.95 
3	spider_beginner: 0.55 	spider_advanced: 0.92 	varicose_beginner: 0.99 	varicose_advanced: 1.00 
4	spider_beginner: 0.85 	spider_advanced: 0.80 	varicose_beginner: 0.82 	varicose_advanced: 1.00 
5	spider_beginner: 0.97 	spider_advanced: 0.90 	varicose_beginner: 0.99 	varicose_advanced: 0.98 
6	spider_beginner: 0.75 	spider_advanced: 0.91 	varicose_beginner: 0.91 	varicose_advanced: 0.98 
7	spider_beginner: 1.00 	spider_advanced: 0.98 	varicose_beginner: 0.91 	varicose_advanced: 0.99 
8	spider_beginner: 0.95 	spider_advanced: 0.98 	varicose_beginner: 0.95 	varicose_advanced: 1.00 
9	spider_beginner: 0.87 	spider_advanced: 0.83 	varicose_beginner: 0.93 	varicose_advanced: 1.00 
10	spider_beginner: 0.83 	spider_advanced: 0.98 	varicose_beginner: 0.98 	varicose_advanced: 1.00 

The venous disorder detection confidence values of the YOLOv3 object detection algorithm performed with sample images of the C1 type of CVD are shown in Fig. 2 (a, b, c) for spider_vein (0.99) [1], spider_beginner (0.99) and spider_advanced (1.00). Also, confidence values for C2 type are shown in Fig. 3 (a, b, c) for varicose_vein (0.90) [1], varicose_beginner (0.98) and varicose_advanced (0.98). Although all classes in the test images were predicted correctly in the study [1], the YOLOv3 object detection algorithm had a lower confidence value for some patterns. As stated in Table IV, in the study [1], among 150 images

containing spider_vein patterns, 130 had a confidence value in the range of 0.95-1.00, 13 in the range of 0.90-0.94, 6 in the range of 0.80-0.89, and 1 of them was determined as 0.32. When the pattern with the confidence value of 0.32 is examined, it is determined that it is not much different from the patterns in the training dataset (mostly large-sized patterns were used) or other test patterns, but it is smaller in size, as can be seen in Fig. 4 (a). It was evaluated that this situation may result in a low confidence value.

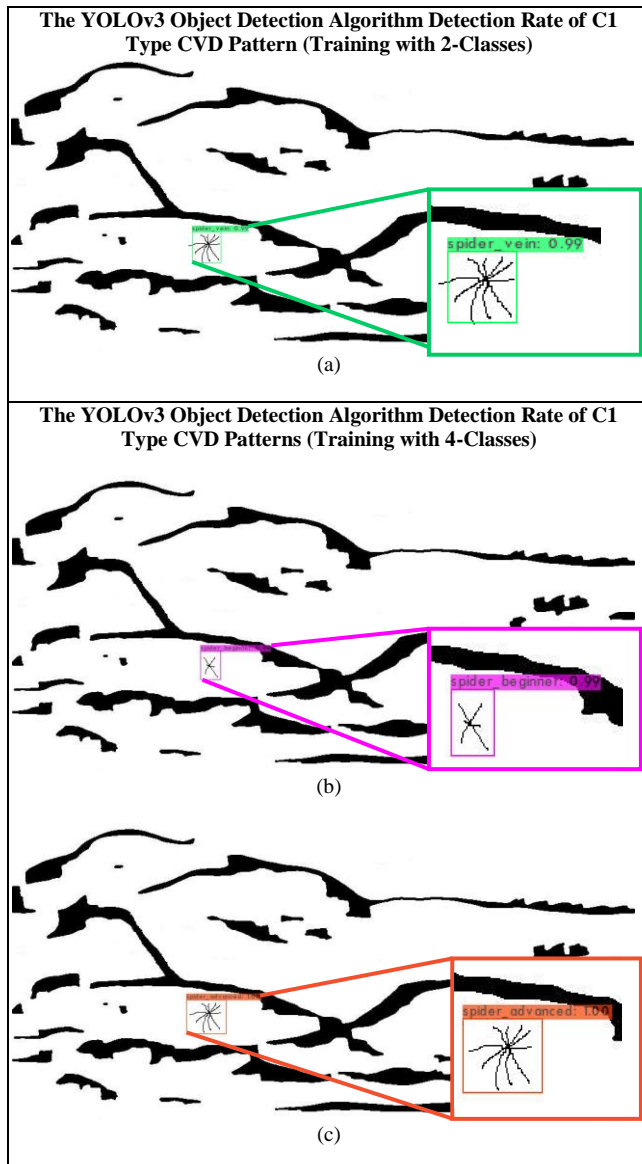


Figure 2. The YOLOv3 object detection algorithm test process result image samples for C1 type CVD patterns. (a) 0.99 confidence valued result for spider_vein class [1]. (b) 0.99 confidence valued result for spider_beginner class. (c) 1.00 confidence valued result for spider_advanced class.

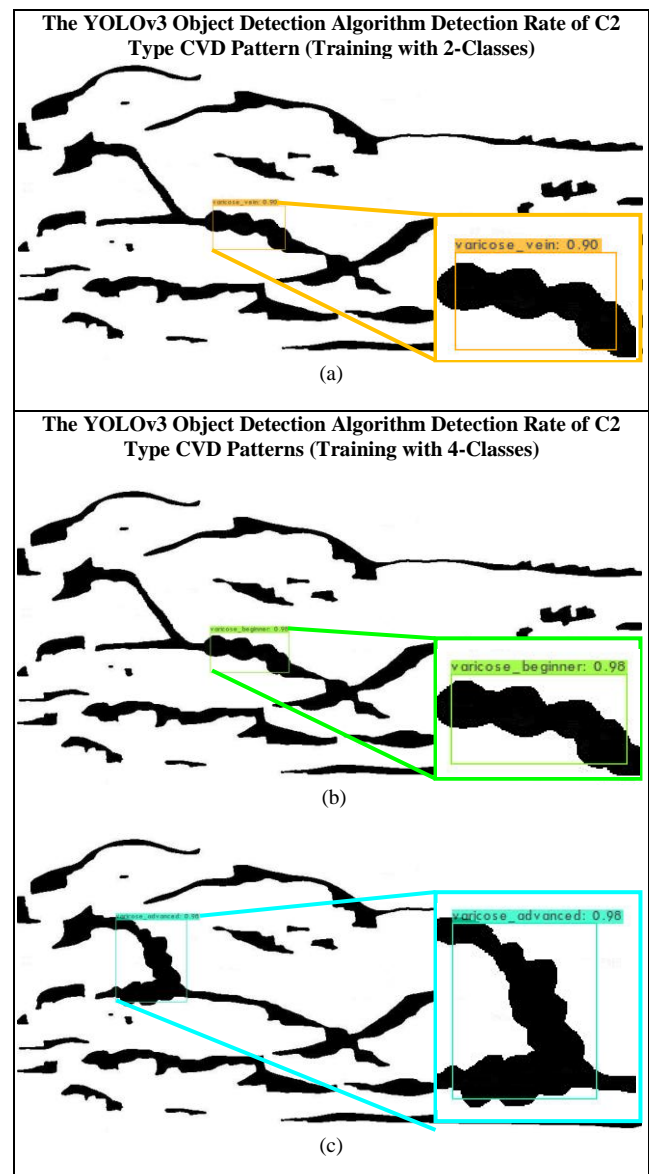


Figure 3. The YOLOv3 object detection algorithm test process result image samples for C2 type CVD patterns. (a) 0.90 confidence valued result for varicose_vein class [1]. (b) 0.98 confidence valued result for varicose_beginner class. (c) 0.98 confidence valued result for varicose_advanced class.

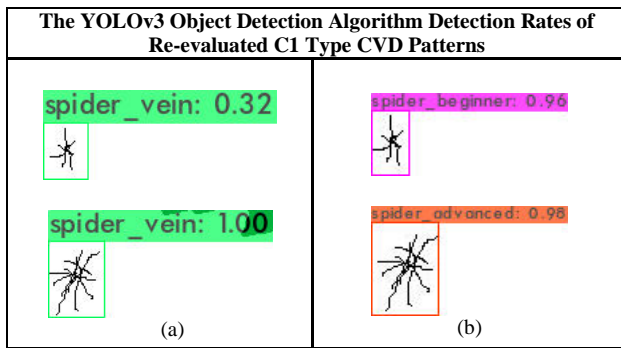


Figure 4. C1 type CVD patterns shown in accordance with their actual dimensions. (a) Patterns with confidence values of 0.32 and 1.00 belonging to the spider_vein class [1]. (b) Patterns with confidence values of 0.96 and 0.98 belonging to the spider_beginner and spider_advanced classes, respectively.

In this study, for control purposes, the CVD artificial patterns that were detected with low confidence values in the study [1] were re-examined. For this reason, spider_beginner patterns (smaller sized and less branched spider_vein patterns to represent the beginner level of C1) were added to the dataset in this study. Spider_vein detection with a confidence value of 0.32 obtained in [1] was determined as a spider_beginner with a confidence value of 0.96 according to the results of the YOLOv3 object detection algorithm trained with 4 classes, as in Fig. 4 (b). This shows that the system can also detect vascular degenerations in smaller sizes (at the beginner level).

As shown in Table IV, again in the study [1], among the 150 images containing varicose_vein pattern, 126 had a confidence value in the range of 0.95-1.00, 6 had a range of 0.90-0.94, 11 had a range of 0.80-0.89, and 7 had a range of 0.79-0.30. When the 7 patterns with the lowest confidence values are examined, it is determined that these patterns are slightly different (U-shaped, twisted) from the patterns in the training dataset or other test patterns (mostly linear line patterns were used) which can be seen in Fig. 5 (a). It was evaluated that this condition may lead to a low confidence value. Therefore, in this study, varicose_advanced patterns (U-shaped and twisted patterns of varicose_veins to represent the advanced level of C2) were added to the dataset. According to the results of the YOLOv3 object detection algorithm trained with 4 classes, the varicose_vein pattern with a confidence value of 0.30 obtained in the study [1] was determined as the varicose_advanced pattern with a confidence value of 0.94 as in Fig. 5 (b). This indicates that the system can also detect vascular degenerations when the patterns become more twisted (for monitoring progress at advanced levels).

Since small-sized spider_vein patterns represent the early levels of CVD (spider_beginner) and varicose_vein patterns can also twist and fold (may not follow a linear line) over time (varicose_advanced), such patterns are important in the scope of detection system. Therefore, in order to overcome the low confidence values of spider_vein and varicose_vein classes described in the study [1], new smaller-sized patterns and also new U-shaped patterns were added to the training dataset with different rotations.

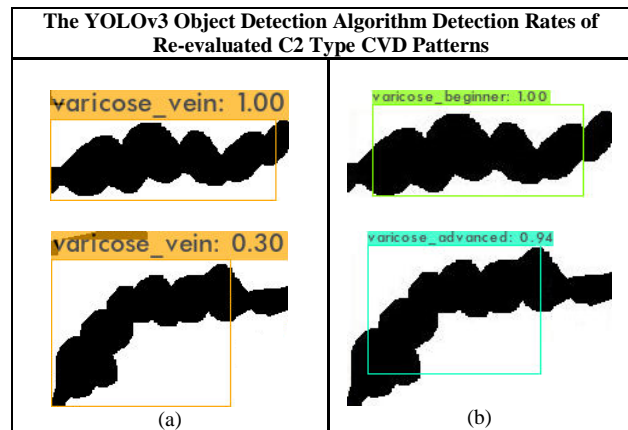


Figure 5. C2 type CVD patterns shown in accordance with their actual dimensions. (a) Patterns with confidence values of 1.00 and 0.30 belonging to the varicose_vein class [1]. (b) Patterns with confidence values of 1.00 and 0.94 belonging to the varicose_beginner and varicose_advanced classes, respectively.

Examining Table V showing the results obtained, it can be seen that out of 150 images containing spider_beginner pattern, 68 of them had confidence values in the range of 0.95-1.00, 28 of them in the range of 0.90-0.94, 43 of them in the range of 0.80-0.89, and 11 of them in the range of 0.79-0.55. For the spider_advanced pattern, the confidence values for 113 images were found to be in the range of 0.95-1.00, 16 of them between 0.90-0.94, 12 of them between 0.80-0.89, and 9 of them between 0.79-0.63. Looking at Table V for the varicose_beginner pattern, 135 confidence values were found between 0.95-1.00, 10 between 0.90-0.94, 3 between 0.80-0.89, and 2 confidence values between 0.79-0.63. For the varicose_advanced pattern, 145 confidence values were found between 0.95-1.00, 3 between 0.90-0.94, 1 between 0.80-0.89, and 1 between 0.79-0.63. The number of CVD types' confidence results obtained in this study, especially in the range of 0.95-1.00, is greater for the C2 (varicose_vein) type (280 confidence values) than for the C1 (spider_vein) type (181 confidence values). This shows that the system can detect varicose levels with higher confidence. In addition, as it can be seen from Table II, the fact that no misclassification has been made in the system proves that the system works extremely effectively in the detection of both CVD types and progress.

The confidence value arithmetic mean (0.973) of the single-class C1 type (spider_vein) in Table IV is slightly higher than the arithmetic mean (0.912 and 0.953) of the two-class C1 type (spider_beginner and spider_advanced) in Table V. Since, the patterns of spider_vein and varicose_vein are very different from each other in shape, it provides an easier distinction (130 spider_vein patterns were correctly classified with a confidence value in the range of 0.95-1.00, which increased the arithmetic mean). This less significant decrease in the test results of the system in this study is a result of the distribution of the confidence values to different detection intervals (0.95-1.00, 0.90-0.94, 0.80-0.89 and 0.79-0.00) when the C1 type is divided into two separate classes with basically similar pattern formats. On the other hand, the fact that the minimum confidence values (0.55 and 0.63) in

Table V for C1 type are higher than those in Table IV (0.32), it draws attention to the fact that a more precise classification decision can be made.

TABLE IV. RESULTS OF CONFIDENCE VALUES FOR THE YOLOV3 OBJECT DETECTION ALGORITHM TRAINED WITH TWO CLASSES [1]

n=300 (150 for each class)	C1: spider vein	C2: varicose vein
Arithmetic Mean	0.973	0.955
Minimum	0.32	0.30
Maximum	1.00	1.00
[0.95-1.00] Range	130	126
[0.90-0.94] Range	13	6
[0.80-0.89] Range	6	11
[0.79-0.00] Range	1	7

TABLE V. RESULTS OF CONFIDENCE VALUES FOR THE YOLOV3 OBJECT DETECTION ALGORITHM TRAINED WITH FOUR CLASSES

n=600 (150 for each class)	C1: spider beginner	C1: spider advanced	C2: varicose beginner	C2: varicose advanced
Arithmetic Mean	0.912	0.953	0.982	0.993
Minimum	0.55	0.63	0.67	0.79
Maximum	1.00	1.00	1.00	1.00
[0.95-1.00] Range	68	113	135	145
[0.90-0.94] Range	28	16	10	3
[0.80-0.89] Range	43	12	3	1
[0.79-0.00] Range	11	9	2	1

Looking at Table IV and Table V for C2 type CVD (varicose_vein), it can be seen that the two-class arithmetic mean results (0.982 and 0.993) are higher than the one-class result (0.955). It was evaluated that the introduction of U-shaped patterns to the system (due to the use of flat shaped patterns for training, twists are detected with lower confidence values in Table IV) contributed to this situation. In addition, as can be seen from Table V, the confidence value determinations for both levels of the C2 type are especially concentrated in the range of 0.95-1.00. In addition, the minimum confidence values (0.67 and 0.79) in Table V for C2 type were higher than those in Table IV (0.30). These cases also reinforce that the system can make a classification decision with higher precision.

IV. INDIRECT AUGMENTED REALITY

Virtual technologies are used in every imaginable field, especially health, education, construction, agriculture, tourism and entertainment. Although these technologies are known as virtual reality with the most popular definition among the public, they are called virtual environments in academic context [57]. The goal of virtual environments is to create a perception of reality in the user. The degree of perception of reality can be determined by criteria such as sense of presence, immersion, real-time and interaction [58]-[61]. While the user's mental feeling in the virtual environment expresses the "sense of presence" criterion, the coverage of the user's field of view with the physical hardware expresses the "immersion" criterion, and the manipulation of the environment in "real-time" expresses the

"interaction" criterion. The more these criteria can be supported, the more the environment is perceived as real by the user. The perception of reality is application-specific. For example, while the main goal in computer games is to create a feeling of reality, in some educational applications, only the visualization of 3-D concepts can be aimed. The type of virtual environment to be designed according to the target and the devices to be used are determined. Milgram's Reality-Virtuality Continuum [62] is one of the most basic classifications used for virtual environments. In this Continuum, there are Virtual Environment (containing completely virtual material) and Real Environment (containing completely real material) under the main heading of Mixed (Hybrid) Reality. In the case of a mixture of these two environments, the concepts of Augmented Virtuality (contains virtual material more than real ones) and Augmented Reality (contains real material more than virtual ones) are defined.

The aim of this study is to present the confidence values and positions (virtual material) of CVD development to the user and his/her physician as a low-cost early diagnosis system within the scope of e-health service. For this reason, the method of providing access to these contents from mobile device screens has been preferred instead of high-cost devices. Although, monitoring the virtual content from a small screen minimizes the perception of reality (due to lack of immersion), it is considered useful within the scope of the study. However, the computing capacity and hardware features of a mobile device are insufficient for the operations to be performed in the 6-phase system used. For this, all operations in the system (except the Imaging Technique Phase) are carried out on the server and processed video visuals (containing only virtual-real material with calculation results) are returned to the user/physician.

Although one of the important criteria in Augmented Reality applications is real-time, there is a visualization spread over a long time interval (to support monitoring at certain periods) in this study. For this reason, real-time of visuals is supported only when the region where the relevant tissue is displayed and the class of the images stored on the server match (requires Classification Phase to be used for a second test). Displaying videos of the matched class on the screen in this way is examined under Indirect Augmented Reality [36]. Indirect augmented reality is especially suited for outdoor use [36]. Its basis is the superimposition (overlay of virtual and real material) of virtual models of structures/places in their real locations while displaying them in their real environment. Two separate registration (spatial alignment of virtual and real material) methods (offline and online registration) are used in Indirect Augmented Reality [39]. Offline registration is combining the pre-recorded video of the relevant tissue with the virtual model. In the offline registration in this study, the YOLOv3 object detection algorithm confidence values and positions of the CVD detected in the digitally processed image are superimposed on the near-infrared raw video recordings. Online registration, on the other hand, is the real-time superimposition of the superimposed video prepared in offline registration on the relevant tissue viewed in the real

world. In the online registration of this study, offline video visuals are presented to the user in real-time when the tissue region to which they belong is displayed.

Among the advantages of using Indirect Augmented Reality within the scope of this study, having low-cost and low computational/processing load requirements (effective for use on mobile devices as no additional hardware is required), tight matching of virtual and real material with offline registration (effective for displaying the vein position on the relevant tissue), and offering a time-independent visualization as before/after (effective for tracking CVD development process from images obtained at certain periods) can be counted [36][40][63].

In the offline registration of this study, on near-infrared raw image(s) (it is the real material captured in the Imaging Technique Phase and shown in Fig. 6 (a)), processed image(s) (it is virtual material processed by the Digital Image Post-Processing Phase and shown in Fig. 6 (b)) and their YOLOv3 object detection algorithm results (it is the virtual material obtained from the Object Detection Phase and shown in Fig. 6 (c)) were superimposed, as depicted in Fig. 6 (d) and video visuals of the relevant period were created. As online registration, these superimposed video visuals are presented to the user/physician via the mobile device (smartphone) screen when the relevant tissue is displayed, as shown in Fig. 6 (e).

V. CONCLUSION AND FUTURE WORK

Visualization of superficial veins by using near-infrared light is among the applications currently used in the healthcare industry. This imaging technique, which is especially useful for vascular access and is harmless to the body, was used in this study within the scope of early diagnosis. The superficial vein monitoring system, which was prepared within the scope of the doctoral study, was re-trained in this study to detect Chronic Venous Disorder with 4 different classes (spider_beginner, spider_advanced, varicose_beginner and varicose_advanced). In this study, all of the artificial vein enlargement patterns in the test images could be accurately detected by using the You Only Look Once version-3 object detection algorithm and no misclassification was encountered. The absence of misclassification can show that the proposed system is particularly useful for the health sector. The classes and their detection rates of the tested patterns are marked on the resulting image as the class name and the confidence value. The developed system was able to detect the classes of objects with the values of Accuracy Rate (1), Misclassification Rate (0), Precision (1), Prevalence (0.5) and F-Score (1). In addition to the class detection, the pattern positions are also determined with the help of this algorithm and marked on the images. Also, a video-based indirect augmented reality environment was integrated into the study for the monitoring of 4 classes of superficial vein enlargement, thus informing the patient and the physician.

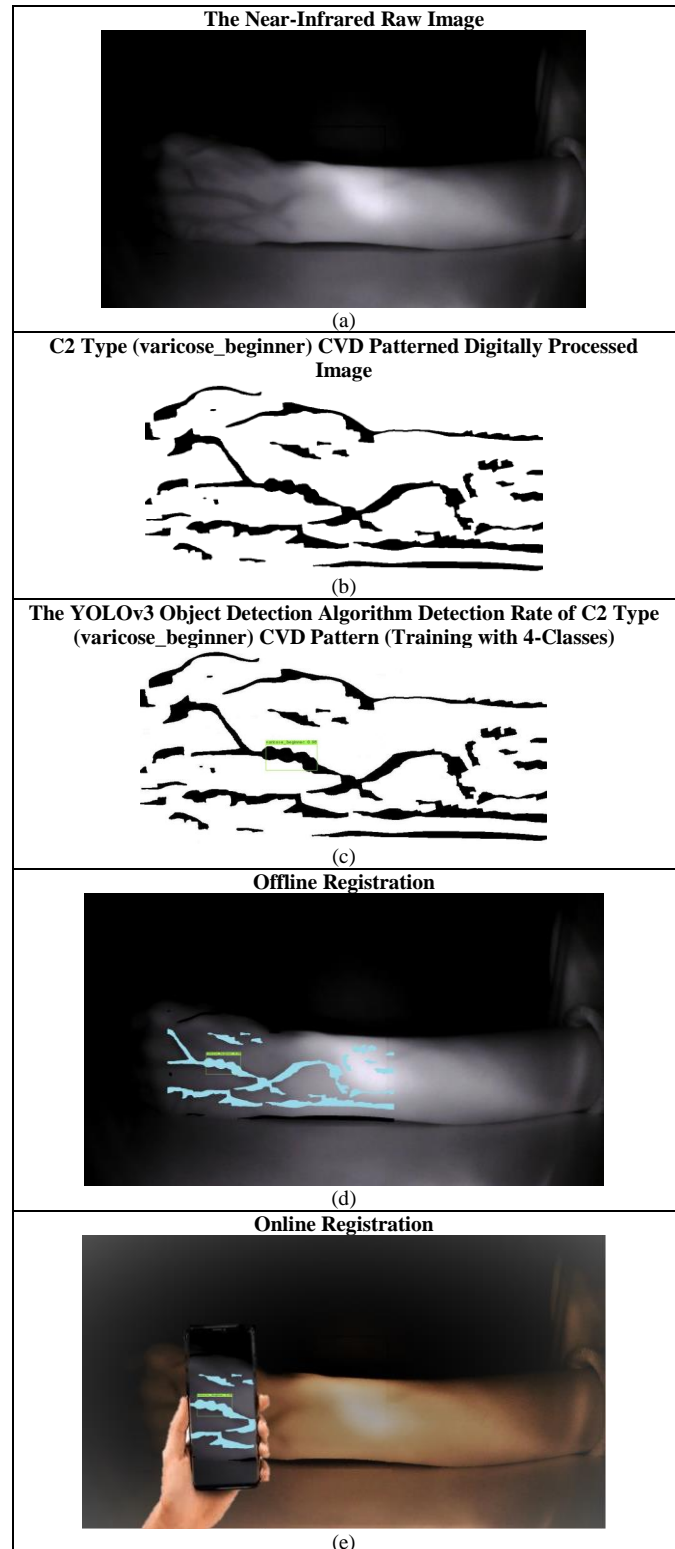


Figure 6. Indirect augmented reality offline registration and online registration for C2 type CVD pattern (varicose_beginner). (a) The near-infrared raw image. (b) Digitally processed image with artificial varicose_beginner pattern added. (c) The YOLOv3 object detection algorithm confidence value obtained with the 4-class training. (d) Offline registration. (e) Online registration.

On the other hand, black pixels that may occur on the image due to the illumination or imaging can have a negative effect on the detection process. In the experiments, this situation was encountered in a few images. It was observed that the dense accumulation of these pixels in a certain region makes detections of the spider_beginner type (due to its small size), which does not actually exist, albeit with low confidence values (0.25, 0.30). However, when considered within the scope of video visuals, these determinations in one or more images were not taken into account, since there are 100 or more image combinations.

Detection of Class-1 type (spider/telangiectasias vein) of Chronic Venous Disorder is of very critical importance especially in determining the transition process to Class-2 type (varicose vein) and the treatment process. In this respect, the most important benefit of the indirect augmented reality environment within the scope of this system and early diagnosis is that it allows visualization in the form of before and after presentation. In this way, treatment can be started and directed without delay. Although the system has been tested with near-infrared data and artificial patterns, it is planned to test the system on real patients within the scope of future studies. In addition, it is considered that the proposed system can shed light on researchers who want to make similar determinations on images obtained with different imaging techniques.

REFERENCES

- [1] H. A. Erdem and S. Utku, "Detecting Venous Disorders via Near-infrared Imaging: Observation of Varicose Vein Development", The IARIA Annual Congress on Frontiers in Science, Technology, Services, and Applications (IARIA Congress 2022), IARIA, Jul. 2022, pp. 65-68, Nice, France. https://www.thinkmind.org/index.php?view=article&articleid=iaria_congress_2022_I_130_50088
- [2] H. A. Erdem, "Integrating Detection of Vascular Degeneration into Augmented Reality Environment: An E-Health Application Based on Near-Infrared Spectroscopy and Deep Learning", Doctoral Dissertation, Dokuz Eylül University, İzmir, Turkey, Aug. 2022. https://tez.yok.gov.tr/UlusalTezMerkezi/TezGoster?key=kIrlFdtdJ31bRgjb6fHvMUaznxXZ9naUDrsvd_v_8KDNe7rlBiHk9Ti8ryVaaMRGz
- [3] H. A. Erdem, I. Erdem, and S. Utku, "Near-Infrared Mobile Imaging Systems for E-Health: Lighting the Veins". The Twelfth International Conference on eHealth, Telemedicine, and Social Medicine (eTELEMED), Nov. 2020, IARIA, pp. 80-84, Valencia, Spain. https://www.thinkmind.org/index.php?view=article&articleid=etelemed_2020_3_90_40039
- [4] H. A. Erdem and S. Utku, "Augmented Reality Aided Pre-Diagnosis Environment for Telemedicine: Superficial Vein Surveillance System". European Journal of Science and Technology, vol. 38, pp. 376-385, Aug. 2022. <https://doi.org/10.31590/ejosat.1107531>
- [5] M. Y. M. Chen, T. L. Pope, and D. J. Ott, Basic Radiology, 2nd ed., McGraw Hill: Lange Clinical Medicine, 2011.
- [6] Inside View: A Blog For Our Patients, From UVA Radiology and Medical Imaging. *Different Imaging Tests, Explained*. 17.Sep.2017. [Online]. Available from: <https://blog.radiology.virginia.edu/different-imaging-tests-explained/> [retrieved: May, 2023]
- [7] Bravo Imaging. *Medical Imaging Modality Options and Their Uses*. 20.Jul.2008. [Online]. Available from: <https://www.bravoimaging.com/medical-imaging-equipment-miami/medical-imaging-modality-options-and-their-uses/> [retrieved: May, 2023]
- [8] V. P. Zharov et al., "Infrared Imaging of Subcutaneous Veins", *Lasers in Surgery and Medicine: The Official Journal of the American Society for Laser Medicine and Surgery*, 34(1), pp. 56-61, 2004. <https://doi.org/10.1002/lsm.10248>
- [9] R. Fuksis, M. Greitans, O. Nikisins, and M. Pudzs, "Infrared Imaging System for Analysis of Blood Vessel Structure", *Electronics and Electrical Engineering, System Engineering, Computer Technology*, 97(1), pp. 45-48, 2010. <https://eejournal.ktu.lt/index.php/elt/article/view/9943>
- [10] N. Bouzida, A. H. Bendada, and X. P. Maldague, "Near-Infrared Image Formation and Processing for the Extraction of Hand Veins", *Journal of Modern Optics*, 57(18), pp. 1731-1737, 2010. <https://doi.org/10.1080/09500341003725763>
- [11] Enclopedia Britannica, *Hemoglobin*. [Online]. Available from: <https://www.britannica.com/science/hemoglobin> [retrieved: May, 2023]
- [12] S. Crisan, "A novel perspective on hand vein patterns for biometric recognition: Problems, challenges, and implementations", in *Biometric security and privacy. Signal Processing for Security Technologies*, R. Jiang, S. Al-Maadeed, A. Bouridane, P. Crookes, and A. Beghdadi, Eds. Springer International Publishing, Cham., pp. 21-49, 2017. https://doi.org/10.1007/978-3-319-47301-7_2
- [13] Y. Ayoub et al., "Diagnostic Superficial Vein Scanner", International Conference on Computer and Applications (ICCA 2018), Aug. 2018, IEEE, pp. 321-325. <https://doi.org/10.1109/COMAPP.2018.8460229>
- [14] Royal Society of Chemistry, *Introduction to Spectroscopy*. [Online]. Available from: <https://edu.rsc.org/download?ac=11384> [retrieved: May, 2023]
- [15] H. Bay, T. Tuytelaars, and L. Van Gool, "SURF: Speeded up robust features", in *Computer vision-European Conference on Computer Vision Lecture Notes in Computer Science*, vol 3951. A. Leonardis, H. Bischof, and A. Pinz, Eds. Springer, Berlin, Heidelberg, pp. 404-417, 2006. https://doi.org/10.1007/11744023_32
- [16] C. L. Lin and K. C. Fan, "Biometric Verification Using Thermal Images of Palm-Dorsa Vein Patterns", *IEEE Transactions on Circuits and Systems for Video Technology*, 14(2), pp. 199-213, 2004. <https://doi.org/10.1109/TCSVT.2003.821975>
- [17] R. Garcia-Martin and R. Sanchez-Reillo, "Vein Biometric Recognition on a Smartphone", *IEEE Access*, 8, pp. 104801-104813, 2020. <https://doi.org/10.1109/ACCESS.2020.3000044>
- [18] W. Liu et al., "SSD: Single Shot Multibox Detector", *Computer Vision-ECCV 14th European Conference, Amsterdam, The Netherlands, Part I 14 Springer International Publishing, October 2016*, pp. 21-37. <https://arxiv.org/abs/1512.02325>
- [19] R. Girshick, J. Donahue, T. Darrell, and J. Malik, "Rich Feature Hierarchies for Accurate Object Detection and Semantic Segmentation", In: *Proceedings of the IEEE conference on computer vision and pattern recognition*, 2014, IEEE, pp. 580-587. <https://arxiv.org/abs/1311.2524>
- [20] R. Girshick, "Fast R-CNN", In: *Proceedings of the IEEE International Conference on Computer Vision*, 2015, pp. 1440-1448. <https://arxiv.org/abs/1504.08083>
- [21] S. Ren, K. He, R. Girshick, and J. Sun, "Faster R-CNN: Towards Realtime Object Detection with Region Proposal Networks", *Advances in Neural Information Processing Systems (NIPS)*, 2015, pp. 91-99. <https://arxiv.org/abs/1506.01497>

- [22] J. Redmon, S. Divvala, R. Girshick, and A. Farhadi, "You Only Look Once: Unified, Real-Time Object Detection", In: Proceedings of the IEEE Conference on Computer Vision and Pattern Recognition (CVPR), 2016, pp. 779-788.
- [23] J. Redmon and A. Farhadi, "YOLOv3: An Incremental Improvement", Arxiv preprint, 2018. <https://doi.org/10.48550/arXiv.1804.02767>
- [24] H. Bandyopadhyay, *YOLO: Real-Time Object Detection Explained*. [Online]. Available from: <https://www.v7labs.com/blog/yolo-object-detection> [retrieved: May, 2023]
- [25] S. Shinde, A. Kothari, and V. Gupta, "YOLO Based Human Action Recognition and Localization", *Procedia Computer Science*, 2018, 133, pp. 831-838. <https://doi.org/10.1016/j.procs.2018.07.112>
- [26] K. S. Babulal et al., "Real-Time Surveillance System for Detection of Social Distancing", *International Journal of E-Health and Medical Communications (IJEHMC)*, vol. 13(4), pp. 1-13, 2022. <https://doi.org/10.4018/IJEHMC.309930>
- [27] L. W. Kang, I. S. Wang, K. L. Chou, S. Y. Chen, and C. Y. Chang, "Image-Based Real-Time Fire Detection Using Deep Learning with Data Augmentation for Vision-Based Surveillance Applications", *The 16th IEEE International Conference on Advanced Video and Signal Based Surveillance (AVSS 2019)*, IEEE, Sept. 2019, pp. 1-4. <https://doi.org/10.1109/AVSS.2019.8909899>
- [28] R. Huang, J. Pedoeem, and C. Chen, "YOLO-LITE: A Real-Time Object Detection Algorithm Optimized for Non-GPU Computers", In: 2018 IEEE International Conference on Big Data (Big Data). IEEE, 2018. pp. 2503-2510. <https://doi.org/10.48550/arXiv.1811.05588>
- [29] J. Ktari, T. Frikha, M. Hamdi, H. Elmannai, and H. Hmam, "Lightweight AI Framework for Industry 4.0 Case Study: Water Meter Recognition", *Big Data and Cognitive Computing*, 2022, vol. 6(3), 72, July 2022. <https://doi.org/10.3390/bdcc6030072>
- [30] A. Bochkovskiy, C. Y. Wang, and H. Y. M. Liao, "YOLOv4: Optimal Speed and Accuracy of Object Detection", ArXiv preprint, 2020. <https://doi.org/10.48550/arXiv.2004.10934>
- [31] A. Baccouche, B. Garcia-Zapirain, Y. Zheng, and A. S. Elmaghaby, "Early Detection and Classification of Abnormality in Prior Mammograms Using Image-to-Image Translation and YOLO Techniques", *Computer Methods and Programs in Biomedicine*, vol. 221, Jun. 2022. <https://doi.org/10.1016/j.cmpb.2022.106884>
- [32] C. Santos, M. Aguiar, D. Welfer, and B. Belloni, "A New Approach for Detecting Fundus Lesions Using Image Processing and Deep Neural Network Architecture Based on YOLO Model", *Sensors*, vol. 22 (17), Aug. 2022. <https://doi.org/10.3390/s22176441>
- [33] E. Ayan, B. Karabulut, and H. M. Ünver, "Diagnosis of Pediatric Pneumonia with Ensemble of Deep Convolutional Neural Networks in Chest X-Ray Images", *Arabian Journal for Science and Engineering*, vol. 47, pp. 2123-2139, Sept. 2022. <https://doi.org/10.1007/s13369-021-06127-z>
- [34] Y. Luo, Y. Zhang, X. Sun, H. Dai, and X. Chen, "Intelligent Solutions in Chest Abnormality Detection Based on YOLOv5 and ResNet50", *Journal of Healthcare Engineering*, vol. 2021, Oct. 2021. <https://doi.org/10.1155/2021/2267635>
- [35] R. Couturier, H. N. Noura, O. Salman, and A. Sider, "A Deep Learning Object Detection Method for an Efficient Clusters Initialization", Arxiv preprint, 2021. <https://doi.org/10.48550/arXiv.2104.13634>
- [36] J. Wither, Y. T. Tsai, and R. Azuma, "Indirect Augmented Reality", *Computers and Graphics*, vol. 35(4), pp. 810-822, Aug. 2011. <https://doi.org/10.1016/j.cag.2011.04.010>
- [37] G. Liestol and A. Morrison, "Views, Alignment and Incongruity In Indirect Augmented Reality", 2013 IEEE International Symposium on Mixed and Augmented Reality - Arts, Media, and Humanities (ISMAR-AMH), Adelaide, SA, Australia, pp. 23-28, 2013. <https://doi.org/10.1109/ISMAR-AMH.2013.6671263>
- [38] J. Gimeno, C. Portales, I. Coma, M. Fernandez, and B. Martinez, "Combining Traditional and Indirect Augmented Reality for Indoor Crowded Environments: A Case Study on the Casa Batllo Museum", *Computers and Graphics*, vol. 69, pp. 92-103, Dec. 2017. <https://doi.org/10.1016/j.cag.2017.09.001>
- [39] F. Okura, T. Akaguma, T. Sato, and N. Yokoya, "Indirect Augmented Reality Considering Real-World Illumination Change", In Proceedings of the IEEE International Symposium on Mixed and Augmented Reality (ISMAR), IEEE, Sept. 2014, pp. 287-288, Munich, Germany. <https://doi.org/10.1109/ISMAR.2014.6948453>
- [40] G. Liestoel, "Augmented Reality Storytelling: Narrative Design And Reconstruction Of A Historical Event In Situ", *International Journal of Interactive Mobile Technologies*, vol. 13(12), pp. 96-209, 2019. <https://doi.org/10.3991/ijim.v13i12.11560>
- [41] N. Özbayrak, "Varis Çoraplarının Performans Özelliklerinin İncelenmesi (An Investigation About Performance Properties of Compression Stockings)", Master's Thesis, Uludağ University, Bursa, Turkey, Jul. 2009. Thesis in Turkish with an abstract in English. <http://hdl.handle.net/11452/3321>
- [42] A. E. Gabbey and J. Marcin (reviewed by), Healthline. *Varicose Veins*. 8.Mar.2019. [Online]. Available from: <https://www.healthline.com/health/varicose-veins> [retrieved: May, 2023]
- [43] Health. Johns Hopkins Medicine. *Varicose Veins*. [Online]. Available from: <https://www.hopkinsmedicine.org/health/conditions-and-diseases/varicose-veins> [retrieved: May, 2023]
- [44] T. Feodor, S. Baila, I. A. Mitea, D. E. Branisteanu, and O. Vittos, "Epidemiology and Clinical Characteristics of Chronic Venous Disease in Romania", *Experimental and Therapeutic Medicine*, vol. 17(2), pp. 1097-1105, Dec. 2019. <https://doi.org/10.3892/etm.2018.7059>
- [45] H. Partsch, "Varicose Veins and Chronic Venous Insufficiency", *Vasa: European Journal of Vascular Medicine*, 38(4), pp. 293-301, Jan. 2009. <https://doi.org/10.1024/0301-1526.38.4.293>
- [46] G. Piazza, "Varicose Veins", *Circulation*, vol. 130(7), pp. 582-587, Aug. 2014. <https://doi.org/10.1161/CIRCULATIONAHA.113.008331>
- [47] N. Labropoulos, "How Does Chronic Venous Disease Progress from the First Symptoms to the Advanced Stages? A Review". *Advances in Therapy*, vol. 36(1), pp. 13-19, Feb. 2019. <https://doi.org/10.1007/s12325-019-0885-3>
- [48] S. Behring and A. Gonzalez (reviewed by), Healthline. *What Are the Stages of Chronic Venous Insufficiency?* 10.Jun.2021. [Online]. Available from: <https://www.healthline.com/health/chronic-venous-insufficiency-stages> [retrieved: May, 2023]
- [49] N. Kahraman et al., "Detection of Residual Varicose Veins with Near Infrared Light in the Early Period After Varicose Surgery and Near Infrared Light Assisted Sclerotherapy", *Vascular*, vol. 30(6), Oct. 2021. <https://doi.org/10.1177/17085381211051489>
- [50] Cambridge Dictionary. *Artificial Intelligence*. [Online]. Available from: <https://dictionary.cambridge.org/dictionary/english/artificial-intelligence> [retrieved: May, 2023]
- [51] O. Campesato, *Artificial Intelligence, Machine Learning, and Deep Learning*. Mercury Learning and Information, 2020.

- [52] A. Govindu and S. Palwe, "Early Detection of Parkinson's Disease Using Machine Learning", *Procedia Computer Science*, vol. 218, pp. 249-261, Jan. 2023. <https://doi.org/10.1016/j.procs.2023.01.007>
- [53] N. N. Sakhare, I. S. Shaik, and S. Saha, "Prediction of Stock Market Movement via Technical Analysis of Stock Data Stored on Blockchain Using Novel History Bits Based Machine Learning Algorithm", *The Institution of Engineering and Technology IET Software*, Jan. 2023. <https://doi.org/10.1049/sfw2.12092>
- [54] I. Erdem, "Ülkemizdeki Havalimanlarının Yolcu ve Uçak Taleplerinin Çok Yönlü Değerlendirilmesi (Multivariate Analysis of Passenger and Aircraft Demands of Airports in Turkey)", Master's Degree Thesis, Dokuz Eylül University, İzmir, Turkey, Aug. 2012. Thesis in Turkish with an abstract in English. https://tez.yok.gov.tr/UlusalTezMerkezi/tezDetay.jsp?id=beo_mkTrj0BSyzbqajYaYpQ&no=WHgKOWHTcFfbOi8a3PerJA
- [55] Y. LeCun, Y. Bengio, and G. Hinton, "Deep Learning", *Nature*, vol. 521, pp. 436-444, May 2015. <https://doi.org/10.1038/nature14539>
- [56] P. Skalski, Makesense, Alpha. *Free To Use Online Tool For Labelling Photos*. [Online] Available from: <https://www.makesense.ai/> [retrieved: May, 2023]
- [57] T. Mazuryk and M. Gervautz, "History, Applications, Technology And Future", *Virtual Reality Vienna: Vienna University of Technology*, vol.72, 1996. https://www.researchgate.net/publication/2617390_Virtual_Reality_-_History_Applications_Technology_and_Future
- [58] M. A. Gutiérrez, F. Vexo, and D. Thalmann, *Stepping Into Virtual Reality*, England: Springer-Verlag London, 2008. <https://doi.org/10.1007/978-1-84800-117-6>
- [59] W. R. Sherman and A. B. Craig, *Understanding Virtual Reality-Interface, Application and Design*, The United States of America: Morgan Kaufmann Publishers, 2003. <https://doi.org/10.1016/C2013-0-18583-2>
- [60] C. C. Ko and C. D. Cheng, *Interactive web-based virtual reality with Java 3D*. The United States of America: Information Science Reference, 2009.
- [61] H. A. Erdem, "Utilization of Virtual Reality Environment as an Interactive Visual Learning Tool in Primary School Education System", Master's Degree Thesis, Dokuz Eylül University, İzmir, Turkey, Aug. 2013. https://tez.yok.gov.tr/UlusalTezMerkezi/tezDetay.jsp?id=iofm_MFGdK7U1KPrXLYjzQ&no=L77dJQmcOK5zBMOxhpMcUw
- [62] P. Milgram, H. Takemura, A. Utsumi, and F. Kishino, "Augmented Reality: A Class of Displays on the Reality-Virtuality Continuum", *Telemanipulator and Telepresence Technologies. Society of Photo-Optical Instrumentation Engineers (SPIE) Digital Library*, vol. 2351, pp. 282-292, Dec. 1995. <https://doi.org/10.1117/12.197321>
- [63] J. B. Alves, B. Marques, C. Ferreira, P. Dias, and B. S. Santos, "Comparing Augmented Reality Visualization Methods for Assembly Procedures", *Virtual Reality*, vol. 26, pp. 235-248, Jul. 2022. <https://doi.org/10.1007/s10055-021-00557-8>

Step Measurement Using a Household Floor Mat and Shoe Sensors

Tomoko Funayama

Dept. of Occupational therapy
Teikyo University of Science
Yamanashi, Japan
e-mail: funayama@ntu.ac.jp

Yasutaka Uchida

Dept. of Life Science
Teikyo University of Science
Tokyo, Japan
e-mail: uchida@ntu.ac.jp

Yoshiaki Kogure

Professor Emeritus
Teikyo University of Science
Tokyo, Japan
e-mail: kogure@ntu.ac.jp

Abstract—Recently, many healthcare devices have been developed to monitor the health conditions of older people and others with health problems. To detect even the slightest changes in physical condition, it is crucial to carry out assessments during long periods of time while people are engaged in their normal daily activities, which do not change from usual. However, while devices to assess health conditions are beneficial, they also present challenges, such as invasion of privacy by monitoring systems, difficulty in operation, and handling of large amounts of data. Walking is sometimes referred to as the sixth vital sign, and is used to assess various diseases, including central nervous system, orthopedic, cardiovascular and respiratory diseases. Research on the development of smart insoles that can acquire digital data is increasing. However, smart insoles cannot be used at home in cultures in which shoes are not worn at home. To overcome these challenges, we have developed a gait assessment device that integrates pressure sensors into a floor mat for daily use. The purpose of developing this device is not to analyze gait improvement, but to capture changes in physical condition in daily living activities through changes in walking. The equipment comprises a grid of eight pressure sensors, each perpendicular and parallel to the walking direction. Because this floor mat is intended for use in homes, the measurement distance is shorter compared to conventional gait assessments. Therefore, we study the possibility of floor mats via the timed up and go (TUG) test, a conventional walking assessment method, and shoes fitted with pressure and acceleration sensors. Three subjects performed free walking, walking with an older people experience set, and walking with ankle and knee joints restricted by supporters. In addition to simulated motions and visual limitations, comfort walking and fast walking were also performed and examined. The obtained results indicate a high correlation between insoles with pressure sensors and floor mats relative to step time, thereby suggesting the usefulness of floor mats.

Keywords—Walking Assessment; Floor Sensors; Smart Shoes; Activities of Daily Living; Health Care.

I. INTRODUCTION

We have been performing studies to capture changes in health conditions during daily life activities with digital measuring instruments [1]. These studies are conducted by an interdisciplinary team consisting of occupational therapists, physical therapists, human-machine interface experts, physicists, medical doctors, and others [2]. We have been suggesting the importance of assessments of everyday life [2]–[4]. However, it is not easy to make a routine health assessment actions on your own. Activities of daily living such as eating, changing, dressing, toileting, and bathing involve the use of various items, such as dishes, clothes, toothbrushes, and toilet seats. By incorporating sensors that can measure these activities, rehabilitation assessments can be made easier. Optical, acceleration, and pressure sensors are useful tools for rehabilitation assessment of activities of daily living. Floor mats are frequently used every day, making it easy to detect changes in activity. Walking is sometimes referred to as the sixth vital sign [5], and assessments of soles and walking have a high potential for understanding health status. Gait measurements using smart insoles with pressure and acceleration sensors have high accuracy; however, in areas where there is no culture of wearing shoes indoors, measurements cannot be taken indoors.

The population of the world is aging, which has led to an increase in the number of people facing health problems [6]. Therefore, having a healthy body and being active are important for as long as possible. For this purpose, an assessment of the activities will be useful. Gait assessment can be an indicator of overall health as well as lower extremity disease. Walking assessment is used for various patients, including older people [7]–[16], and to assess various disabilities, central nervous system diseases such as cerebrovascular disease, Parkinson's disease, multiple sclerosis [17]–[24], cardiovascular and respiratory diseases [25]–[27], orthopedic diseases such as back pain [28],

cognitive dysfunctions [29,30], and others [31]. Recently, several monitoring support equipment and systems for older adults and those with health problems have been researched, developed, and marketed [32]–[38]. The use of this type of equipment is becoming an important method of health support. Wearable devices for assessing health conditions are becoming increasingly popular in the healthcare field. Digital devices are also being used to evaluate gait, [39]–[45] and the research and development of smart insoles for aging, disease assessment, and fall prevention is increasing [45]–[48]. While beneficial, these types of equipment also present problems, such as invasion of privacy by the monitoring system, difficulty in operation, and handling large amounts of data. Health conditions are often detected through vital sign measurement and movement monitoring. The sensors used in these devices include infrared, acceleration, temperature, and pressure sensors [40].

Long-term assessments during normal daily activities are important for monitoring even slight changes in health. The assessment of walking during dual tasks, when attention is focused on activities other than walking, is considered important for understanding life risks. The environment and comfort level vary between a laboratory or hospital and their homes, and their health conditions can change throughout the day. Therefore, it is crucial to conduct ongoing and long-term assessments in the home environment, where people spend their everyday lives, rather than relying solely on evaluations conducted in hospitals or medical facilities. By incorporating sensors into items used in daily life, assessments can be performed for extended periods at home. However, because a large amount of data is collected over a long period, it is important to focus on which data is effective and how it is needed to determine an individual's health conditions [46]. In addition, to eliminate invasion of privacy, it is useful to turn measurements on and off at one's will; however, this requires the operation of the device. Older people or disabled users are required to be able to use the device in their daily lives. However, it is not easy to habituate device operation for healthcare in daily life. Self-care equipment should be beneficial, easy to operate, convenient, and practical for older people and those with disabilities who face health challenges. In addition, it is important that healthcare professional supporters are able to understand and utilize the meaning of the data.

Therefore, we developed gait assessment equipment that incorporates a pressure sensor in a floor mat used in daily life [49]. The floor mat is expected to measure a person's movement speed in their daily life without being turned on or off. The two key points of this equipment are privacy protection through a floor mat and the ability to understand health conditions without measuring vital signs. We previously used this device to study hemodialysis patients [40]. The conventional assessment methods used in rehabilitation, including the timed up and go (TUG) test, do not assess activities of daily living that are repeated daily. Digital measuring devices for daily activities can increase the measurement interval and amount of measurement data. The measurement accuracy was also improved, making it easy to compare the data we obtained with past data. This is not just a

digitalization of the conventional rehabilitation assessment methods. This floor mat is designed for daily household use and is shorter than conventional gait assessments, such as TUG test; however, it can increase the measurement interval. The time per step can also be measured. Gait measurement is highly accurate with smart insoles with built-in pressure and acceleration sensors; however, in areas where there is no culture of wearing shoes inside the home, it is not possible to measure gait inside the home.

This report studies step measurement on a floor mat with built-in sensors that can be used in daily life and examines the potential use of the floor mat by comparing it with the TUG test, a gait assessment method, and smart shoes. Three subjects wore an older people experience set that simulated motor impairment and performed fast and comfortable walking on the TUG test and floor mats to determine the usefulness of the floor mats and speed calculation formula [1]. The same three subjects then walked and took measurements on the floor mat wearing shoes with acceleration and pressure sensors attached, with the knee and ankle joints restricted by the supporters. The step time, step length, and speed were compared between the floor mat and shoe-worn sensors. The characteristics used by occupational therapists to judge gait measurement in activities of daily living were also examined.

This study was approved by the Ethics Committee on Research with Humans as Subjects of Teikyo University of Science. Section II describes the experimental method, Section III describes the results, Section IV presents a discussion, and Section V presents the conclusion.

II. EXPERIMENTAL METHOD

A. Devices and Measurement Systems

1) Floor mat

The study used a floor mat with a grid array of 16 pressure sensors. Eight sensors (P0–P7) were perpendicular to the walking direction, and eight sensors (Q0–Q7) were parallel to the walking direction (see Figure 1). The perpendicular sensors were 10 cm apart only at the initial P0–P1 sensor interval and 15 cm apart at the other sensor intervals.

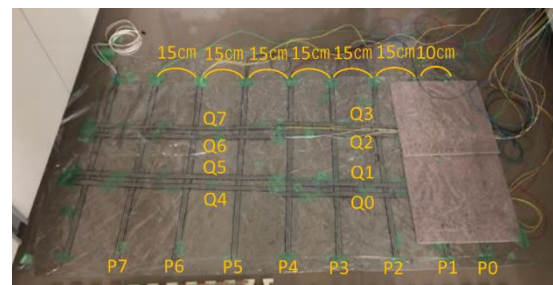


Figure 1. Floor mat-type equipment with pressure sensor array.

The parallel Q sensors were in pairs, two pairs in the front and two pairs in the rear, with each pair approximately 15 cm apart. The length of the sensor was

62 cm, and it measured approximately 120 cm in the direction of walking. The equipment size allows its use and placement at home. A clear plastic sheet protects the surface so that the sensor position can be checked. The sampling frequency of the equipment was 100 Hz. The approximate cost required for the creation of this floor mat is approximately 215 US dollars, with 16 sensors costing 180 dollars at 11 dollars each and one Arduino costing 35 dollars.

2) Insole with Pressure sensors

The smart insoles used were of a wireless type (FEELSOLE®) that measured four parts per foot and eight parts in total on both sides (see Figure 2). The insoles must be calibrated before they can be used. Calibration was performed four times: no pressure with no feet in the shoes, standing on both feet, and standing on one foot on each side. A 10 s operation was possible. The colors of the four parts (toe, heel, inside, and outside) changed according to the applied weight. The video was also recorded, and the video and pressure sensor data from the smart insole were synchronized. The data were saved on an iPad Air (Apple) and could be viewed on a screen. They were transferred from the tablet to a PC via email and made available for analysis. The sampling frequency was 50 Hz, and the data were output in CSV format.

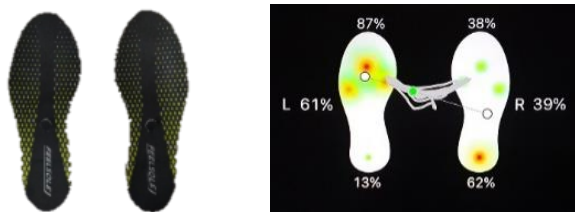


Figure 2. Exterior of FEELSOLE and tablet screen.

3) Accelerometer with Shoe Adhesion

The accelerometer used was the ORPHE CORE® (see Figure 3). It was measured using the iPhone application ORPHE TRACK®. The ORPHE TRACK® app and ORPHE CORE® connect wirelessly via Bluetooth. The data were uploaded to the cloud through the app and could be confirmed in CSV format every minute with ORPHE TRACK®, analyzing steps, distance, stride, step speed, pronation, impact angle, cadence, landing force, and contact time. The sampling frequency was set to 200 Hz. The video was not synchronized; therefore, comparison with the data of each step on the floor mat was impossible. The assessments were carried out with the device attached to the outside of the shoe and with it installed in the insole.



Figure 3. Accelerometer ORPHE CORE.

B. Walking measurements and Analysis Methods

1) TUG test and walking on floor mat

a) Walking measurements

Three subjects in their 50s to 70s (Cases A, B, and C) performed the TUG test and walked on the sensor array floor mat under a simulated restricted motion while wearing the older person experience set (see Figure 4).

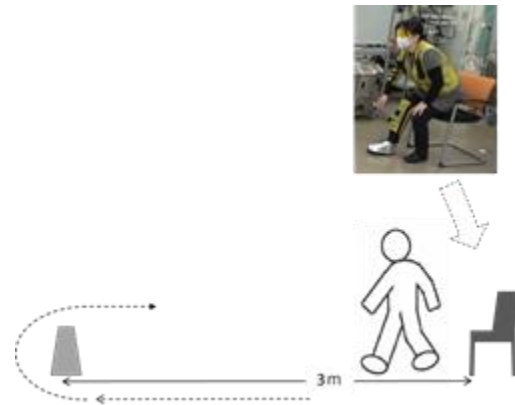


Figure 4. Timed Up and Go test.

The TUG test measures the time it takes to get up from a chair, go around a cone 3 m away, walk back to the chair, and sit down. The time taken was measured. The TUG test is often used in walking assessment during rehabilitation. Walking assessment is important for maximal walking speed (MWS) and self-selected walking speed (SSWS). Thus, we performed the test not only with comfortable walking, which is a standard practice, but also with fast walking. The motion restrictions varied by the subject. Participant A wore tinted eyeglasses in addition to (1) trunk-weighted and left upper and lower limb restrictions, followed by (2) trunk-weighted and right upper and lower limb restrictions. Subject B was (3) weighted on the trunk and had both legs restricted. Subject C was (4) weighted on the trunk. The subjects then walked on the sensor array floor mat without any motion restrictions. Videotaping and ankle joint range of motion (ROM) measurements were

also conducted by an occupational therapist. The ROM of the ankle joint with plantar flexion and dorsiflexion is shown in Table I. R and L represent the right and left sides, respectively.

TABLE I. RANGE OF MOTION FOR CASES A, B, AND C

Direction of Motions	R / L Side	Subjects		
		Case A	Case B	Case C
plantar flexion	R	50	60	45
	L	55	50	50
dorsi flexion	R	20	10	20
	L	20	5	-5

b) Analysis

Figures 5 and 6 show examples of graphical representations of the output data for P0–P7 and Q0–Q7, respectively. For the least-Squares Method (LSM) calculation, data over half the height of the highest signal were used. In addition, data with very few continuous signals were judged to be noisy and were not used.

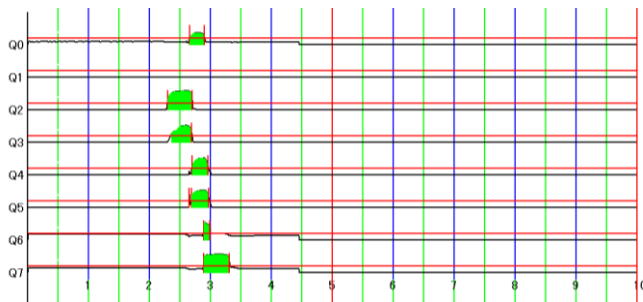


Figure 5. Q sensor output data.

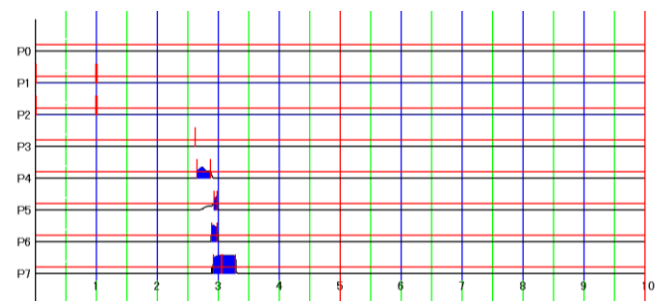


Figure 6. P sensor output data.

Speed was calculated by programming using the LSM. LSM was used so that the relationship between the distance

of each sensor corresponding to the time the sensor was stepped on was a linear function (see Figure 7). The slope was obtained as the velocity.

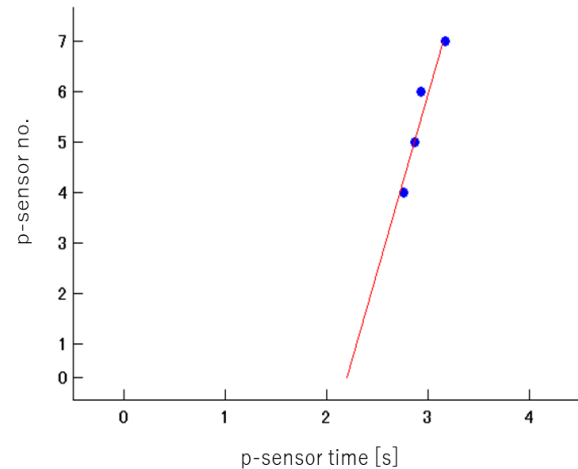


Figure 7. Speed by the least-Squares Method.

Figure 7 shows the time (s) and distance (sensor position), where the inclination of the red line is the speed. The least-squares method was used, assuming a linear function.

Subsequently, a footprint diagram was drawn by examining the raw data from the P and Q sensors, plantar ground contact was determined, and the speed was calculated. When two sensors were stepped on simultaneously at the same time by a single sole, it was assumed to be a single ground contact, and the position and time in the middle of the two sensors were used to determine the speed. It was calculated directly by a manual process (Direct calculations regarding floor mats: DCF1).

The judgment terms in DCF1 were as follows: (1) If there was an output that appeared to be noise that was not understood for a short time, the plantar ground contacts were judged to be grounded when ten consecutive pieces of data were obtained. (2) Data with <2.0% of the maximum value ten times in a row were excluded from sole grounding. (3) When the front and rear sensor data responded simultaneously, the same plantar contact was assumed when >70% of the front sensor data overlapped the rear data. (4) When adjacent P-sensors did not respond consecutively, that is, there was one or more unresponsive P sensors in between, we assumed a different plantar ground contact. Two major differences were noted between LSM and DCF1 for speed using footprint diagrams. First, LSM calculates the speed based on the position and time of each sensor, regardless of whether the

two sensors are stepped on simultaneously. The speed by DCF1 is calculated by judging when two sensors are outputting simultaneously, whether they are one footprint or two footprints, that is, the same grounding. Second, it determines whether to use data with small values or responses in the calculation, or to exclude them and treat them as noise. In addition, we compared the TUG test results with sensor array data. An occupational therapist evaluated and validated the videos. On the sensor array, subjects walked straight ahead, whereas on TUG test, subjects walked straight ahead and then U-turn. The speeds on the TUG test were converted and compared with the LSM and DCF1 results from the sensor array data.

2) Walking on a floor mat wearing shoes with sensors

a) Walking measurements

Three subjects walked on a floor mat wearing shoes equipped with pressure and acceleration sensors (see Figure 8).

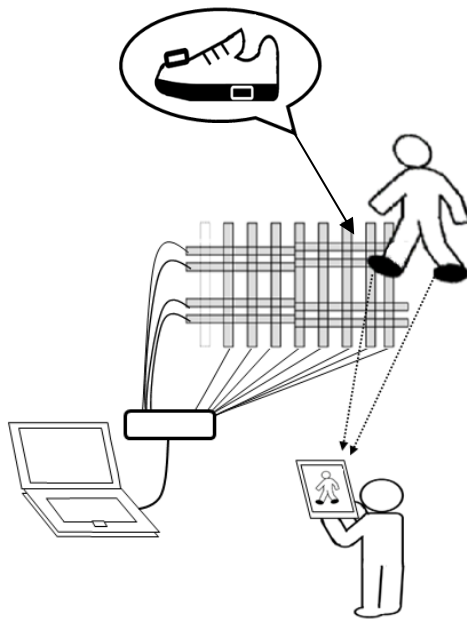


Figure 8. Walking on floor mats with sensor-equipped shoes.

They walked normally without intentional restriction of movement and with the right knee and right ankle joints restricted with supporters. Pressure sensors were placed in the insoles. The acceleration sensors were placed in two locations: one attached to the top of the shoes and one was integrated into the insoles. The video was also recorded while the subjects were walking with the pressure sensor insoles, and the sensor reaction time and video time were synchronized. However, the accelerometer was not synchronized with the video.

b) Analysis

Step times were compared between the floor mats and insoles. Step length and speed were examined between the floor mats, and stride length and speed data were calculated using the analysis application ORPHE TRACK®, which corresponds to the accelerometer ORPHE CORE®. Because the accelerometer was not synchronized with the video, we compared the left and right instead of each step. The judgment terms for plantar grounding were DCF2 in addition to DCF1, the method used for TUG test comparisons. In DCF2, both the P sensor and Q sensor were used. The data with the fastest response among the P and Q sensors were used to determine the time. Although the P sensor does not respond to plantar contact after the P7 sensor, the plantar contact of only the Q sensor, which is not responded to by the P7 sensor, was used in the determination. The determination of the plantar contact position used for calculating the distance was based on only one sensor that responded the earliest using the P sensor.

The judgment terms for DCF2 are as follows: (2) and (3) are the same as those for DCF1. (1) The consecutive data of "Q0Q1 and Q4Q5" on the left side and "Q2Q3 and Q6Q7" on the right side of the floor mat were judged to be the same ground, while those of the left side "Q0Q1, Q4Q5" and the right side "Q2Q3, Q6Q7" were judged to be different grounds. This term was prioritized in determining whether one identical or two grounds were made. (2) When adjacent P-sensors did not respond consecutively, that is, when there was one or more unresponsive P-sensors in between, they were assumed to have different plantar groundings. (3) When two sensor data points (front and rear) responded simultaneously, the same plantar ground contact was assumed when more than 70% of the front sensor data overlapped the rear sensor data. (4) In addition to excluding the calculation when the noise processing was 2% or less of the maximum value, the calculation was also excluded if the same numerical data with a maximum value of 90% or less were continuously repeated five times. However, even if it was 90% or more of the maximum value, the data were considered noise and excluded if 30 consecutive values or 50 intermittently identical values were connected.

Step times were compared between floor mats and insoles by measuring the time taken for one step. An example of insole data is shown in the graph below (see Figure 9). To calculate the distance of the step using the floor mat, the stride length was calculated as the position of the plantar contact when the P sensor first responded. The calculation of step distance using the accelerometer ORPHE CORE® relied on the stride calculated using the analysis application ORPHE TRACK®.

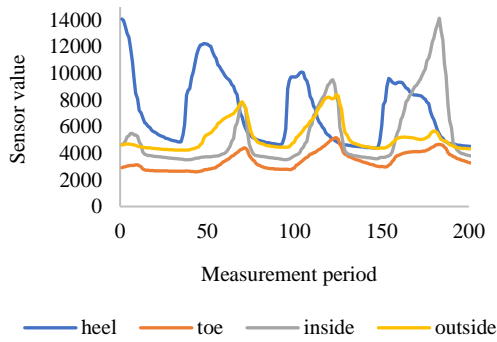


Figure 9. Right insole with normal walking in Case C.

One stride is equal to two steps (see Figure 10). The accelerometer was not synchronized with the video. Hence, a comparison between the data for each step on the floor mat could not be made. Instead of comparing floor mats and acceleration regarding stride length and speed for each step, we made a left-right comparison for step and stride for each floor mat and acceleration. We used the maximum stride length data from the accelerometers for two minutes before and after the measurement. From the floor mats, we only used data that had left and right data, that is, data with more than two steps.

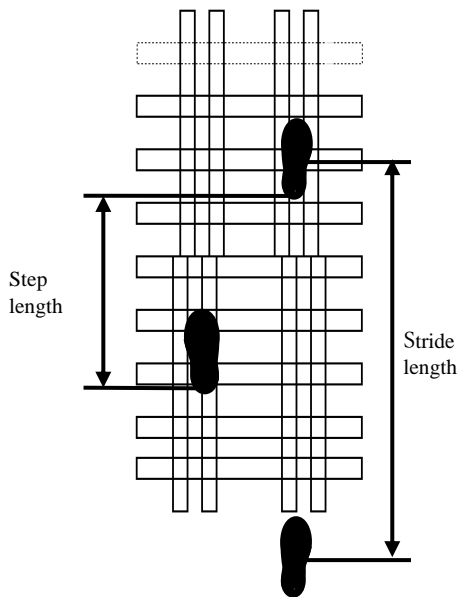


Figure 10. Gait Parameters including step length, and stride length.

The stride length from the accelerometer is the distance from the foot-flat to the foot-flat of one foot. The step length from the floor mat is the distance from one foot to

another during a step. The stride and step lengths are not the same (see Figure 10).

III. RESULTS

A. TUG test and Walking on Floor Mat

1) Floor Mat and TUG test Comparison

The speed of the TUG test was compared with that of the subjects walking on a sensor array floor mat. Walking speed on the sensor-placed floor mat was calculated using LSM and DCF1. The mean speeds of Subjects A, B, and C were calculated when they walked comfortably and fast with restricted motion. Figure 11 shows the results for TUG test, LMS, and DCF1. The figure is graphed in ascending order of TUG test speed. In the graph, the first letter corresponds to subjects A, B, and C. The following letter indicates “Rr” for right upper and lower limb restriction, “Lr” for left upper and lower limb restriction, “W” for weight loading, “E” for wearing tinted eye glasses, “c” for comfortable walking, and “f” for fast walking.

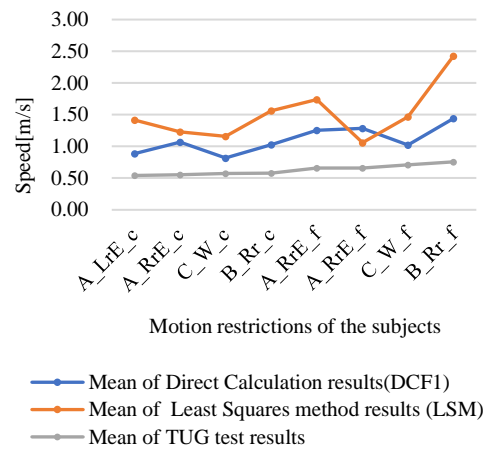


Figure 11. Speed comparison between TUG test and sensor array walking.

The calculation results from the pressure sensor array differed according to the two calculation methods, i.e., LSM by programming and DCF1 by manual calculation using a footprint diagram. In LSM, the calculation result revealed that the speed was slower by three of seven times than the slowest speed in the “left upper and lower limbs and eye limits (A_LrE_c)” TUG test in Case A. In DCF1, the calculation result revealed that only one of the seven times the speed was slower than the slowest speed in the “A_LrE_c” TUG test in Case A. The relationship between TUG test and DCF1, which is a manual calculation using footprint diagrams, is stronger than that between TUG test and LSM using programming. This shows that LSM tends to be faster than DCF1. In the sensor array, walking was measured only straight ahead, whereas in the TUG test,

walking was measured both straight ahead and in U-turns. Therefore, the speed of TUG test walking would be slower than that of sensor array walking. The two discrepancies between TUG test and DCF1 were C_W_c and C_W_f for Subject C. Subject C's walking was assessed on video by an occupational therapist, and a left-right difference was judged. Both C_W_c and C_W_f were observed during plantar grounding of the left foot. The ankle joint ROM in Case C was R20/45 and L-5/50, with a left-right difference.

2) *Detection of the Speed of the Left and Right Foot*

The results of the speeds calculated by DCF1 for the simulated left and right upper and lower limb movements when restricted are shown in Figures 12 and 13, respectively. Figure 12 shows the right motion restrictions, and Figure 13 shows the left motion restrictions. The X-axis shows comfortable or fast gait with the left or right plantar-grounded foot. The initial letter C in the graph X-axis labels stands for "comfortable" and "F" stands for fast walking. The numbers following the letters C or F denote the number of times performed. The right upper limb lower limb is then indicated by R and the left upper limb lower limb restriction by L. The right and left upper and lower limbs were restricted only in Case A. The color of the bars in the graph is blue when the right plantar is grounded, that is, when the right foot is in the stance phase and the left foot is in the swing phase. Yellow indicates the left plantar-grounded foot, that is, the left foot is in the stance phase and the right foot is in the swing phase. The results when walking faster are indicated by the lines around the bars. Right-side walking, that is, the blue one in the bar graph, tended to be faster than that of the left side, regardless of whether the motions were restricted to the left or right side. The fastest walking was observed when the right foot was grounded, regardless of the left or right side of the upper or lower limb restrictions.

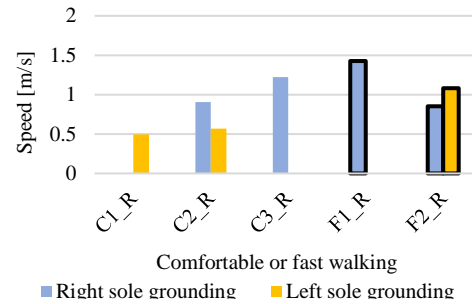


Figure 12. Right upper and lower limb restrictions.

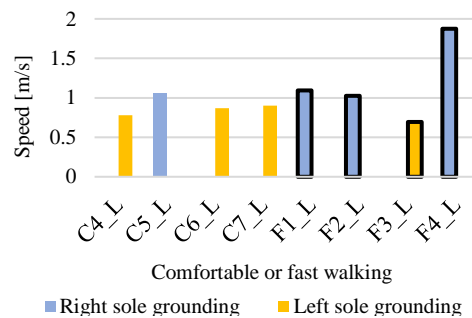


Figure 13. Left upper and lower limb restrictions.

B. *Walking on a Floor mat Wearing Shoes with Sensors*

1) *Step Time*

The step times were calculated from the floor mats and insoles. The floor mat data were calculated in two ways: using the same method DCF1 as TUG test and a new method DCF2 with some modifications. The walking performance of three subjects was conducted 13 times, with the number of steps taken on a floor mat ranging from 1 to 3 per performance, and the total number of steps was 30.

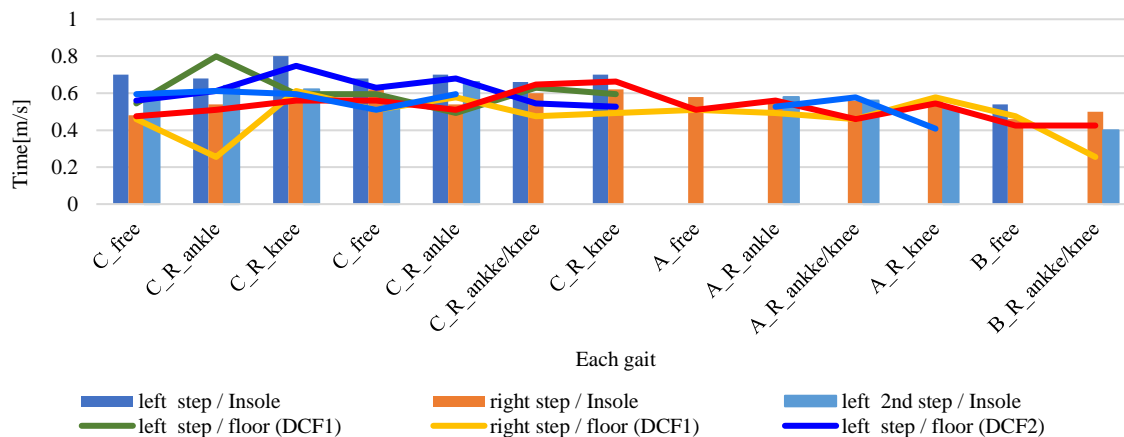


Figure 14. Step time detected from floor mats and pressure sensor insoles.

Of the four parts of the insole (toe, heel, inside, and outside), the heel with a clear sensor response to ground contact was used. We measured the time from when the heel was on to when the other heel was on. The results for 30 data points are shown in the graph (see Figure 14).

The bar graph indicates the step time determined from the insole, and the line graph indicates the step time determined from the floor mat. In the graph, three bar graphs in one walking sequence indicate that three steps were performed on the floor mat. The two-bar graphs represent the two steps and a single step taken on the floor mat in one bar. Left foot grounding after the right foot was labeled as the left second step. The left foot is blue, light blue, and green in the bar graph, and navy and blue in the line graph. The right foot is orange on the insole, and red and yellow on the floor mat. The letters after the numbers indicate that “R_ankle” represents the restriction of the right ankle and “R_knee” represents the restriction of the right knee.

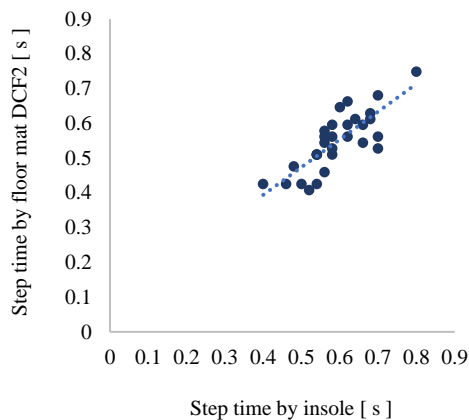


Figure 15. Step time by floor mat DCF2 and insole.

We observed that DCF2 had a higher correlation with the insole data than DCF1. Therefore, we performed a correlation analysis between 30 pairs of data from the insole and the DCF2. The Pearson correlation coefficient was 0.80 (see Figure 15).

2) *Left-right Comparison of Step and Stride*

The step and stride lengths of the left and right sides were compared. The number of steps taken per walk ranged from 1 to 3, allowing for four trials in which the left and right sides could be compared for two or more steps. The total number of data points was eight. The graph shows the stride length calculated from the floor mat and the maximum stride length in 2 min calculated from the accelerometer (see Figures 16 and 17).

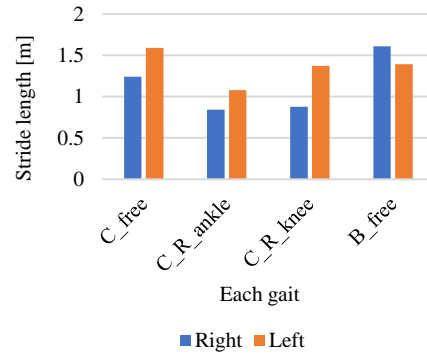


Figure 16. Maximum stride length from the accelerometer.

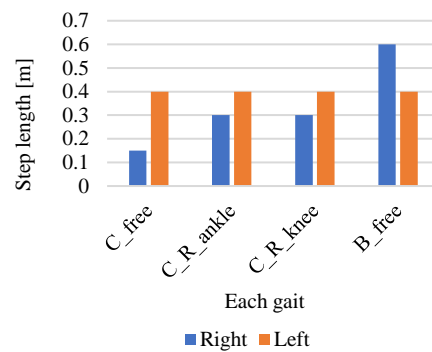


Figure 17. Step length from the floor mat.

The graph shows a similar trend in the left - right comparison of stride length calculated by the accelerometer and step length calculated by the floor mat. As for C_free, the left - right balance of the floor mats and accelerometers is very different. Upon checking the video, it was confirmed that the left sole makes plantar contact slightly farther away from the P2 sensor and closer to P3. The subject stepped on the P3 sensor with the toes and not on the P2 sensor. Then, only the right heel stepped on P4. This pattern of slightly stepping on or not stepping on the sensor was repeated twice.

3) *Left-right comparison of speed*

Using the same method as for the aforementioned steps and strides, the speed was calculated four times over two steps and eight times for the left and right sides combined. Speeds were calculated from the times and distances obtained from the previous items 2) and 3), and compared to the left and right. The speed calculation using the floor mat used the time of the foot that was not in contact with the ground. For example, the time from right foot contact to left foot contact was calculated as the speed during the left foot swing.

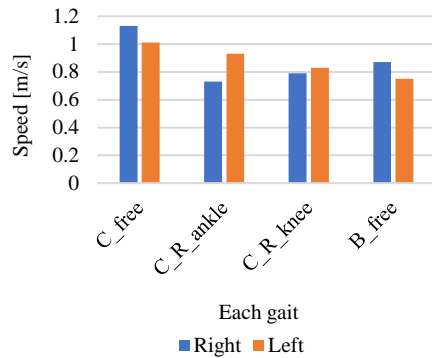


Figure 18. Speed from the accelerometer.

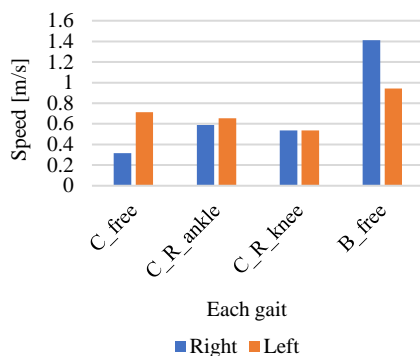


Figure 19. Speed from the floor mat.

The relationship between the speed of the floor mats and acceleration could not be considered as high (see Figures 18 and 19).

IV. DISCUSSION

This floor mat is shorter than conventional gait assessments such as the TUG test. However, because the equipment can be placed at home at all times, considering its size, anything larger than this is not considered practical. The equipment is based on the premise that the detection accuracy will improve as the number of data points increases with daily repetition. Conventional gait assessments are based on a single measurement; therefore, the use of this floor mat differs from conventional assessment methods.

Even with this approximately 120 cm equipment, a high correlation was observed between the insole and the floor mat regarding step time. The correlation was higher in DCF2 than in DCF1 because of the P sensor and also because the Q sensor was included in the calculation. It is important to determine whether the left and right soles are in contact and to increase the accuracy of determining the time of sole contact with the parallel Q sensor while walking. Although the Q sensor parallel to the walking gait is considered useful for measuring steps, video observation revealed plantar ground contact that did not step on the parallel sensor on one side.

There were some walks on which one of the longitudinal sensors was not stepped on owing to the narrow stride width. To further improve the accuracy of the mat, it may be necessary to slightly narrow the distance between the longitudinal sensors. Regarding the measuring equipment, it is necessary to thoroughly examine it, including the distance between the sensors, in the future, as it may change slightly in noise and sensor position because of its movement to the survey facility and its possible slight changes from one implementation to another.

Regarding speed, there seemed to be a relationship between the speed of the TUG tests, but no strong relationship was found in the left-right comparison with the insoles. This may be because the accelerometer was not synchronized with the video and could not investigate each step individually. It could also be attributed to the floor mat's low accuracy in step length determination. In the gait where there was a large difference in the left-right balance of step and stride length from the floor mat and accelerometer, the left sole made plantar contact slightly farther away from the P2 sensor but closer to P3. The P3 sensor was stepped on with the toes, but the P2 sensor was not stepped on. Subsequently, only the right heel stepped on P4. This pattern of slightly stepping on or not stepping on the sensor was repeated twice. A solution to this problem would be to slightly narrow the distance between the P sensors. Although it depends on the body size of the subject and gait distance, narrowing the vertical sensor installed in parallel with the gait and the horizontal sensor at right angles by approximately 2 cm is thought to improve the accuracy.

This study was experimentally conducted using a floor mat sensor intended for repeated use in activities of daily living. Although the data sample size is small and generalization is not possible, the high correlation with accurate insole data suggests a high potential for usefulness. The ability to measure gait daily at home would be useful not only for the early detection of disease and disability, but also for the treatment of those with fluctuating physical conditions such as rheumatism, those whose activity capacity changes under the influence of medications such as the on-off phenomenon of Parkinson's disease, and those with rhythm disorders. Reports have shown that walking speed assessment at home differs from that in a laboratory setting [5]. Walking during dual tasking is slower than walking alone. In daily life, walking is often used as a means of transportation to perform activities. Walking during dual tasking is slower than walking alone. Attention must also be paid to environmental factors, such as flooring and objects, and sudden stimuli, such as someone approaching. Attention may also be low in a low-awareness state. Occupational and physical therapists routinely assess walking conditions but do not always use measuring devices or quantify them. They observe and assess their interactions with the patients, and health conditions are determined based on the patients' gait. If walking conditions could be measured naturally in daily life, it would be possible to assess walking ability without a therapist. This also leads to objective data showing the therapist's tacit knowledge and experience [2].

Measuring walking ability in daily life at home can help provide information that cannot be obtained from laboratory or hospital measurements.

V. CONCLUSION AND FUTURE WORK

Regarding the floor mat used, the usefulness of step time was suggested, although challenges were associated with step length. The floor mat has the potential to predict health changes. The ability to measure walking ability during daily activities at home is thought to be useful in providing life support, self-care, and diagnostic assistance to older people and the disabled, as well as in understanding what is unknown from measurements taken in the hospital. Although the amount of data is small, there seems to be a strong correlation with high-accuracy smart insoles, suggesting that they may be useful. In the future, we plan to increase the amount of data and conduct further investigations to generalize our findings. Studies have already been conducted on synchronizing acceleration and pressure sensors attached to shoes.

ACKNOWLEDGMENT

This work was supported by the JAPS KANENHI Grant Number JP20K11924.

REFERENCES

- [1] T. Funayama, Y. Uchida, and Y. Kogure, "Assessment of Walking Condition Using Pressure Sensors in the Floor Mat," *Global Health* 2022, pp. 7-12, 2022.
- [2] T. Funayama, Y. Kogure, R. Kimura, N. Homma, and Y. Uchida, "Application of the human-machine interface technology to occupational therapy", *Proceedings of 16th International Congress of the World Federation of Occupational Therapists*, No. PCI-19-21, Yokohama, Japan, June, 2014.
- [3] T. Funayama, Y. Uchida, and Y. Kogure, "Detection of motion restriction with smart insoles," *Sensors & Transducers Journal*, Vol. 259, Issue 5, pp. 61-68, 2022.
- [4] T. Funayama, Y. Kogure, K. Hori, and Y. Uchida, "A pilot study on the relationship between daily life and biological information," *Human Interface Society in Japanese*, vol. 22, No. 2, pp. 31-34, 2020, ISSN 2188-6652.
- [5] A. Middleton, G. D. Fulk, M. W. Beets, T. M. Herter, and S. L. Fritz, "Self-selected walking speed is predictive of daily ambulatory activity in older adults," *Journal of Aging and Physical Activity*, vol. 24, Issue 2, pp. 214 -222, 2016. doi: 10.1123/japa.2015-0104
- [6] World Health Organization, "World health statistics 2022 monitoring health for the SDGs," *Sustainable development goals*, 2022.
- [7] N. Takayanagi, M. Sudo, Y. Yamashiro, I. Chiba, S. Lee, Y. Niki, and H. Shimada, "Predictivity of daily gait speed using tri-axial accelerometers for two-year incident disability among Japanese older adults," *Scientific Reports*, vol. 12, No. 10067, 2022.
- [8] F. Ayoubi, C. P. Launay, A. Kabeshova, B. Fantino, C. Annweiler, and O. Beauchet, "The influence of fear of falling on gait variability: results from a large elderly population-based cross-sectional study," *Journal of NeuroEngineering and Rehabilitation*, vol. 11, No. 128, 2014.
- [9] O. Beauchet, G. Allali, C. Annweiler, S. Bridenbaugh, F. Assal, R. W. Kressigi, and F.R. Herrmann, "Gait variability among healthy adults: low and high stride-to-stride variability are both a reflection of gait stability," *Gerontology*, vol. 55, pp. 702-706, 2009.
- [10] J. M. Leach, S. Mellone, P. Palumbo, S. Bandinelli, and L. Chiari, "Natural turn measures predict recurrent falls in community dwelling older adults: a longitudinal cohort study," *Scientific Reports*, vol.8, No. 4316, pp. 1-9, 2018. doi: 10.1038/s41598-018-22492-6
- [11] J. S Brach, J. E Berlin, J. M. VanSwearingen, A. B. Newmani, and S. A Studenski, "Too much or too little step width variability is associated with a fall history in older persons who walk at or near normal gait speed," *Journal of NeuroEngineering and Rehabilitation*, vol. 2, Issue 21, pp. 1-8, 2005. doi: 10.1186/1743-0003-2-21
- [12] X. Zeng, H. S. L. Bárusoni, and A. Sundvall, "Walking step monitoring with a millimeter-wave radar in real-life environment for disease and fall prevention for the elderly," *Sensors*, vol. 22, Issue 24, pp. 1-15, 2022.
- [13] K. T. Kall, A. Peters, B. Thorand, E. Grill, C. Autenrieth, A. Horschi, and C. Meisinger, "Description of spatio-temporal gait parameters in elderly people and their association with history of falls: results of the population-based cross-sectional KORA-Age study," *BMC Geriatrics*, vol. 15, No. 32, 2015. doi: 10.1186/s12877-015-0032-1
- [14] A. R. Molinero, A. H. Larrea, A. Miñarro, L. Narvaiza, C.G. Barrón, N. G. León, et al., "The spatial parameters of gait and their association with falls, functional decline and death in older adults: a prospective study," *Scientific Reports*, vol. 9, No. 8813, 2019. doi: 10.1038/s41598-019-45113-2
- [15] M. Y. Osoba, A. K. Rao, S. K. Agrawali, and A. K. Lalwani, "Balance and gait in the elderly: a contemporary review," *Laryngoscope Investigative Otolaryngology*, vol. 4, Issue 1, pp. 143-153, 2019.
- [16] I. Bytyçi, and M. Y Henein, "Stride length predicts adverse clinical events in older adults: a systematic review and meta-analysis," *Journal of Clinical Medicine*, vol. 10, No.2670, No.2670, 2021. doi: 10.3390/jcm10122670
- [17] L. Comber, R. Galvini, and S. Coote, "Gait deficits in people with multiple sclerosis: A systematic review and meta-analysis," *Gait & Posture*, vol. 51, pp. 25-35, 2017.
- [18] L. Angelini, W. Hodgkinson, C. Smith, J. M. Dodd, B. Sharrack, C. Mazzà, and D. Paling, "Wearable sensors can reliably quantify gait alterations associated with disability in people with progressive multiple sclerosis in a clinical setting," *Journal of Neurology*, vol. 267, pp. 2897-2909, 2020.
- [19] M. Pau, S. Mandaresu, G. Pilloni, M. Porta, G. Coghe, M. G. Marrosui, and E. Cocco, "Smoothness of gait detects early alterations of walking in persons with multiple sclerosis without disability," *Gait & Posture*, vol. 58, pp. 307-309, 2017.
- [20] C. J Hass, P. Malczak, J. R. Nocera, and E. L. Stegemöller, "Quantitative normative gait data in a large cohort of ambulatory persons with parkinson's disease," *Plos One*, vol. 7, 2012. doi: 10.1371/journal.pone.0042337
- [21] R. Sharma, L. Pillaia, A. Gloverai, and T. Virmani, "Objective impairment of tandem gait in Parkinson's disease patients increases with disease severity," *Parkinsonism & Related Disorders*, vol. 68, pp. 33-39, 2019. doi: 10.1016/j.parkreldis.2019.09.023
- [22] G. Chen, C. Patten, D. H. Kothari, and F. E. Zajac, "Gait differences between individuals with post-stroke hemiparesis and non-disabled controls at matched speeds," *Gait & Posture*, vol. 22, pp. 51-56, 2005.
- [23] D. M. Mohan, A. H. Khandoker, S. A. Wasti, S. I. I. Alali, H. F. Jelineki, and K. Khalaf, "Assessment methods of post-stroke gait: a scoping review of technology-driven approaches to gait characterization and analysis," *Frontiers in Neurology*, vol. 12, No. 650024, 2021. doi: 10.3389/fneur.2021.650024

- [24] A. Dever, D. Powell, L. Graham, R. Mason, J. Das, S. J. Marshall, R. Vitorio, A. Godfrey, and S. Stuart, "Gait impairment in traumatic brain injury: A systematic review," *Sensors* 2022, 22, 1480, 2022. doi: 10.3390/s22041480
- [25] K. Kamiya, N. Hamazaki, Y. Matsue, A. Mezzani, U. Corra, R. Matsuzawa, et al., "Gait speed has comparable prognostic capability to six-minute walk distance in older patients with cardiovascular disease," *European Journal of Preventive Cardiology*, vol. 25, Issue 2, pp. 212–219, 2018. doi: 10.1177/2047487317735715
- [26] J. Afilalo, "Frailty in Patients with Cardiovascular Disease: why, when, and how to measure," *Current Cardiovascular Risk Reports*, vol. 5, pp. 467–472, 2011. doi: 10.1007/s12170-011-0186-0
- [27] G. Fischer, F. B. Queiroz, D. C. Berton, P. Schons, H. B. Oliveira, M. Coertjens, M. Gruet, and L. A. P. Tartaruga, "Factors influencing self-selected walking speed in fibrotic interstitial lung disease," *Scientific Reports*, No. 12459, 2021. doi: 10.1038/s41598-021-91734
- [28] A. Demirel, D. Onan, M. Oz, Y. O. Ashyuce, and O. Ulger, "Moderate disability has negative effect on spatiotemporal parameters in patients with chronic low back pain," *Gait & Posture*, vol. 79, pp. 251–255, 2020.
- [29] Y. C. Kuan, L. K. Huang, Y. H. Wang, C. J. Hu, I. J. Tseng, H. C. Chen, and L. F. Lin, "Balance and gait performance in older adults with early-stage cognitive impairment," *European Journal of Physical and Rehabilitation Medicine*, vol. 57, Issue 4, pp. 560–567, 2021. doi: 10.23736/S1973-9087.20.06550-8
- [30] M. Pau, I. Mulas, V. Putzu, G. Asoni, D. Viale, I. Mameli, B. Leban, and G. Allali, "Smoothness of gait in healthy and cognitively impaired individuals: A study on italian elderly using wearable inertial sensor," *Sensors* 2020, 3577, 2020.
- [31] O. A. Donoghue, S. Leahy, and R. A. Kenny, "Longitudinal associations between gait, falls, and disability in community-dwelling older adults with type ii diabetes mellitus: Findings From The Irish longitudinal study on ageing (TILDA)," *The Journals of Gerontology*, vol. 76, No. 5, pp. 906–913, 2021.
- [32] B. Marques, J. McIntosh, A. Valera, and A. Gaddam, "Innovative and assistive ehealth technologies for smart therapeutic and rehabilitation outdoor spaces for the elderly demographic," *Multimodal Technol. Interact.*, vol. 4, Issue 76, pp. 2020. doi: 10.3390/mti4040076
- [33] N. Davoody, and M. Hägglund, "Care professionals' perceived usefulness of ehealth for post-discharge stroke patients," *Exploring Complexity in Health*, pp. 589–593, 2016. doi: 10.3233/978-1-61499-678-1-589
- [34] S. Díaz, J. B. Stephenson, and M. A. Labrador, "Use of wearable sensor technology in gait, balance, and range of motion analysis," *Applied Sciences*, vol. 10, Issue 1, 234, 2020. doi: 10.3390/app10010234
- [35] F. Muheidat, and L. Tawalbeh, "In-home floor based sensor system-smart carpet- to facilitate healthy aging in place (AIP)," *IEEE Access*, vol. 8, pp. 178627–178638, 2020. doi: 10.1109/ACCESS.2020.3027535
- [36] A. Torqu, A. P. C. Chan, E. H. K. Yung, J. Seo, and M. F. A. Afari, "Wearable sensing and mining of the informativeness of older adults' physiological, behavioral, and cognitive responses to detect demanding environmental conditions," *Environment and Behavior*, vol. 54, Issue 6, pp. 1005–1057, 2022. doi: 10.1177/00139165221114894
- [37] J. O. O. Aguirre, J. R. Campos, G. A. Hernández, I. M. Cano, L. R. Mazahua, and J. L. S. Cervantes, "Remote healthcare for elderly people using wearables: A Review," *Biosensors*, vol. 12, Issue 73, pp. 2022. doi : 10.3390/bios12020073
- [38] F. J. S. Thilo, S. Hahn, R. J. G. Halfens, and J. M. G. A. Schols, "Usability of a wearable fall detection prototype from the perspective of older people-A real field testing approach," *Journal of Clinical Nursing*, vol. 28, Issue 1-2, pp. 310–320, 2018. doi: 10.1111/jocn.14599
- [39] Y. Uchida, T. Funayama, and Y. Kogure, "Classification accuracy of support vector machine, decision tree and random forest modules when applied to a health monitoring with flexible sensors", *Sensors & Transducers*, vol. 245, pp.83-89, 2020.
- [40] Y. Uchida, T. Funayama, K. Hori, Y. Yuge, N. Shinozuka, and Y. Kogure, "Feature value extraction for body condition change measurement system using pressure sensor array," *Human Interface Society in Japanese*, vol. 24, No. 1, pp. 79-82, 2022, ISSN 2188-6652.
- [41] J. Beyea, C. A. McGibbon, A. Sexton, J. Noble, and C. O'Connell, "Convergent validity of a wearable sensor system for measuring sub-task performance during the timed up-and-go test," *Sensors*, 17, 934, 2017, doi: 10.3390/s17040934.
- [42] L. Tran, and D. Choi, "Data augmentation for inertial sensor-based gait deep neural network," *IEEE Access*, vol. 8, pp. 12364-12378, 2020. doi: 10.1109/ACCESS.2020.2966142
- [43] A. M. Herran, B. G. Zapirain, and A. M. Zorrilla, "Gait Analysis Methods: An overview of wearable and non-wearable systems, highlighting clinical applications," *Sensors* 2014, vol. 14, pp. 3362-3394, 2014. doi: 10.3390/s140203362
- [44] S. U. Yunas, and K. B. Ozanyan, "Gait Activity Classification Using Multi-Modality sensor fusion: A deep learning approach," *IEEE Sensors Journal*, vol. 21, No. 15, pp. 16870-16879, 2021.
- [45] A. S. Alharthi, S. U. Yunas, and K. B. Ozanyan, "Deep learning for monitoring of human gait: a review," *IEEE sensors JOURNAL*, vol. 19, No. 21, pp. 9575-9591, 2019.
- [46] V. Bucinskas, A. Dzedzickis, J. Rozene, J. S. Zemaitiene, I. Satkauskas, V. Uvarovas, et al., "Wearable feet pressure sensor for human gait and falling diagnosis," *Sensors* 2021, pp. 5240, 2021.
- [47] S. Yoo, H. Gil, J. Kim, J. Ryu, S. Yoon, and S. K. Park, "The optimization of the number and positions of foot pressure sensors to develop smart shoes," *Ergonomics Society of Korea*, Vol. 36, Issue 5, 2017, pp. 395-409.
- [48] S. Subramaniam, S. Majumder, A. I. Faisal, and M. J. Deen, "Insole-based systems for health monitoring: current solutions and research challenges," *Sensors* 2022, 22, 438, 2022. doi: 10.3390/s22020438.
- [49] T. Funayama, Japanese Patent 7150321, 2022-10-11.

Possibility of Gait Analysis with MediaPipe and Its Application in Evaluating the Effects of Gait-assist Devices

Yasutaka Uchida

Dept. of Life Science
Teikyo University of Science
Adachi-ku, Tokyo, Japan
e-mail: uchida@ntu.ac.jp

Tomoko Funayama

Dept. of Occupational therapy
Teikyo University of Science
Uenohara-shi, Yamanashi, Japan
e-mail: funayama@ntu.ac.jp

Yoshiaki Kogure

Professor Emeritus
Teikyo University of Science
Adachi-ku, Tokyo, Japan
e-mail: kogure@ntu.ac.jp

Abstract—The use of free software in motion analyses in the medical and healthcare fields could contribute to the collection of improved data through rehabilitation and daily health management. The possibility of gait analyses using moving images is examined using the free software, MediaPipe. As a preliminary experiment for applying this software in the rehabilitation field, we attempt a timed up-and-go test and obtain detailed ankle trajectories. Additionally, considering the limitations of the camera installation during measurement, we examine the differences in the camera position when capturing the gait characteristics. Consequently, the characteristics captured were almost similar, although some discrepancies were observed between the data from the front and oblique directions. The detection of the ankle angle was possible. However, a motion analysis using the gait velocity will be required for the correct placement of objects. We analyzed the data obtained from the application of the Orthobot, a gait aid device, for the measurement of gait. The detection of the differences in gait before and after the application of the Orthobot would significantly contribute to the gait assessment. The data were compared with those obtained using ORPHE ANALYTICS. Because MediaPipe only provides relative coordinate values for 33 different target body parts, data interpretation requires correction. However, it proved to be a tool that provided a lot of information by allowing researchers to incorporate the necessary formulas.

Keywords—Gait analysis; MediaPipe; detection of ankle angle; health care; walking aid device.

I. INTRODUCTION

The measurement of the lower limb function is useful in assisting the prevention of falls. To date, medical and welfare professionals such as rehabilitation and nursing care staff have been responsible for providing support to prevent

falls. In recent years, devices for measuring the lower limb function have become widespread. However, the equipment used in rehabilitation medicine and sports requires detailed data and specialized knowledge of the equipment operations. Decisions related to health conditions in daily life are difficult to make. Lower limb dysfunction can lead to serious accidents, such as falls. Stumbling and falling accidents are common social issues [1]–[8].

Wearable devices are now applied in daily life. They can collect various information, such as a runner's running route and speed, as well as their pulse rate. This information can be used as management records by connecting it to the Internet. Daily health-related data managed by servers can be very useful for the elderly. Internet of Things (IoT) devices have been developed for many applications. An IoT device can help prevent falls and stumbling by measuring the ankle joint data. Previously, we measured the gait of hemodialysis patients; however, the analysis required specialized knowledge of machine learning [9]–[12].

MediaPipe is a free software from Google. Numerical data related to faces can be obtained using this software, which specializes in facial data and poses corresponding to the entire body. It is also possible to display three-dimensional (3D) skeletons from two-dimensional (2D) detection on a screen. The ability to see images of the skeleton as it is projected onto the physique can be easily implemented in rehabilitation facilities [13]–[17].

This software provides 3D coordinates that increase its effectiveness. Specifically, if the ankle angles can be obtained from images, it could be a promising alternative for determining physical condition changes based on the experience of physical and occupational therapists. Long-term ankle angle data would also be useful for the early

detection of physical condition changes due to illness or other causes.

Image-based video analyses have long been used in rehabilitation and other medical and healthcare fields, such as the joint research field. Despite the ongoing research, it is impossible to state that image analysis is applied in daily rehabilitation support for patients. The demonstration of the application of video analysis in rehabilitation at a low cost, would cause many people to use it [18]–[22].

Therefore, we examined the possibility of gait analysis by video using MediaPipe. Motion analysis using free software could lead to the rapid spread of video analysis in the medical and healthcare fields.

We adopted this software to conduct a basic analysis of how gait changes using Orthobot®, an assistive device for walking that was not considered previously, to determine the extent to which it can be applied in the field of rehabilitation [23].

If the range of motion of the ankle joint is narrow, even in the lower limbs, the toes do not rise, making it is easy to stumble and fall. We inferred that walking involved not only the lower limb functions but also the entire body.

Considering the gait from an inverted pendulum model, an initial experiment was conducted to determine how the effect of wearing the assistive device would manifest and whether the effect would be sustained by examining the change in the neck angle from the direction perpendicular to the center of the body [24][25].

This research was approved by the Ethics Committee of Teikyo University of Science.

II. EXPERIMENTS

The subjects were two men in their 60s and 70s, respectively. The two gait events differed in terms of the ankle restrictions. The supporter restricted the ankle joint motion. For the elderly patient experience set, the subject wore glasses that did not restrict the ankle joint motion.

The corresponding locations of the 33 landmark data locations on the body output by MediaPipe are listed in Table I.

We used arrays with previously reported pressure sensors to compare the accuracy of the comma-separated value (CSV) data obtained from MediaPipe skeletal certification. The resistance of the pressure sensors changed depending on the pressure, ranging from 100 to 1 M Ω . A 1 k Ω resistor was connected in series with this sensor, and the voltage change of the resistor was used as the input signal. Each sensor measured the voltage at 1 kHz. Eight sensors were arranged parallel to the travel direction. The pressure sensor data were transferred to an Arduino Mega 2560 R3 connected to a personal computer. The connection between the sensors and the Arduino is shown in Figure 1.

TABLE I. Pose Landmark of MediaPipe.

Pose Landmark	
0. nose	
1. left_eye_inner	4. right_eye_inner
2. left_eye	5. right_eye
3. left_eye_outer	6. right_eye_outer
7. left_ear	8. right_ear
9. mouth_left	10. mouth_right
11. left_shoulder	12. right_shoulder
13. left_elbow	14. right_elbow
15. left_wrist	16. right_wrist
17. left_pinky	18. right_pinky
19. left_index	20. right_index
21. left_thumb	22. right_thumb
23. left_hip	24. right_hip
25. left_knee	26. right_knee
27. left_ankle	28. right_ankle
29. left_heel	30. right_heel
31. left_foot_index	32. right_foot_index

The output signals of sensor numbers A0–A7 and the distance between each sensor were used to calculate the walking speed.

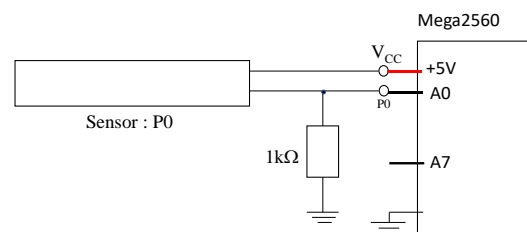


Figure 1. Connection of sensors and Arduino.

A Accuracy check of CSV data outputted by MediaPipe

We evaluated the possibility of using CSV data output by MediaPipe to perform gait analysis considering the elderly patient experience set. This measurement indicates the accuracy of the quantification of the ankle position. Because the assessment was performed during gait, we used

images from the timed up-and-go measurement, which is used as a basis for the evaluation of falls experienced by the elderly, to conduct the analysis in MediaPipe.

Figure 2 shows the trajectory of the timed up-and-go measurements. The trajectory was similar to that of the left ankle movement, which was assumed from being seated in the chair to approximately 3 m away and being seated in the chair again. A detailed ankle trajectory was obtained. The video analysis of the timed up-and-go test confirmed the maintenance of the integrity of the specifications [24]–[28].

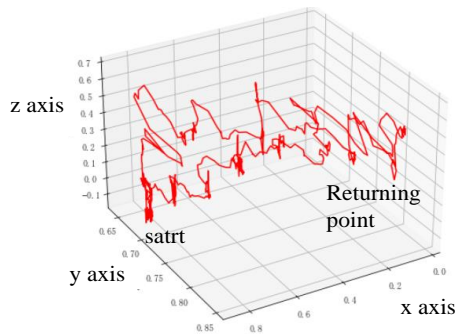


Figure 2. Trajectory of timed up-and-go analyzed by MediaPipe.

B Results from the front angle

Gait videos taken from the front under two different conditions, without motion restriction and with motion restricted by a knee supporter, were analyzed using MediaPipe. Figure 3 shows the skeleton analysis of the motion without/with restrictions using a video from the front.



Figure 3. Skeleton analysis of motion (a) without and (b) with restrictions using video from front.

The values of z in Figure 4, which represent the heights of the left and right ankle joints, were plotted against the presence and absence of motion restriction, respectively.

It can be deduced that the time that the heel is on the floor is short because the average of the integrated values of the z values of the foot that applies the restriction is large.

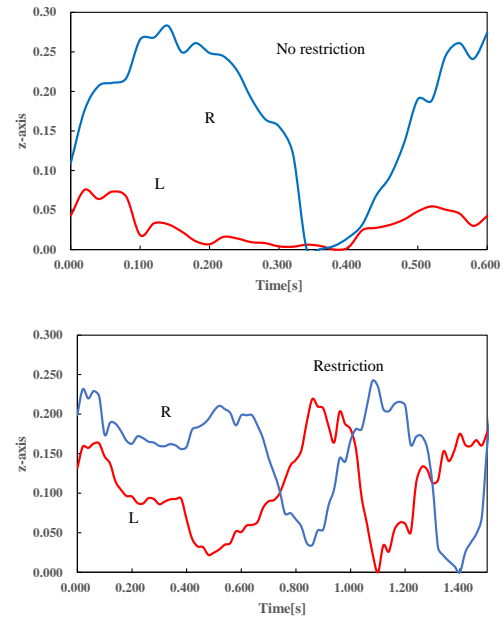


Figure 4. Values of z that represent the ankle height.

C Results from an oblique upward angle

In this analysis, the image was obtained from an oblique upward angle to enhance the z -axis length ratio. Peaks corresponding to the left and right toes were also observed. Differences owing to the angle of filming were analyzed from the images obtained from the front and diagonally above the angles.

Figure 5 shows the image without/with restrictions using the video from an oblique angle. The sheet on the floor consisted of the pressure sensors described in Figure 1.

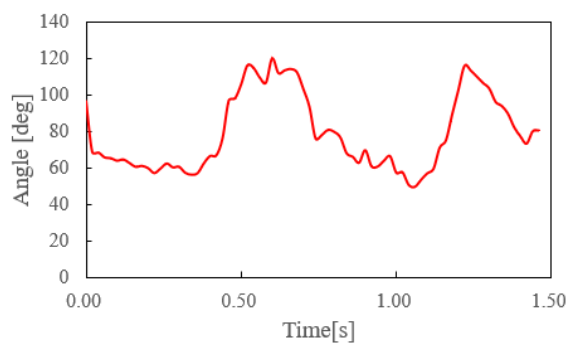
The separately conducted results of the ankle angle measurements indicate that the subjects' left and right feet have different flexibilities. The results are presented in Table II. The left ankle joint was more restricted than the right ankle joint, but there was no significant left-right difference. Therefore, we considered the ankle-to-knee and ankle-to-toe lines as vectors and obtained the angle between them from the inner product. The images were captured in two different ways while the subjects were walking and then analyzed.



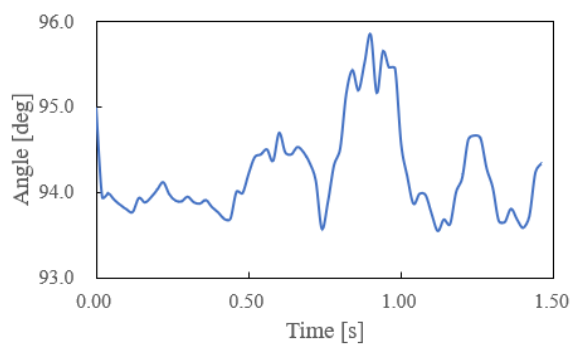
Figure 5. Skeleton analysis of motion (a) without and (b) with restrictions using video from oblique upward angle.

TABLE II. Range of Motion.

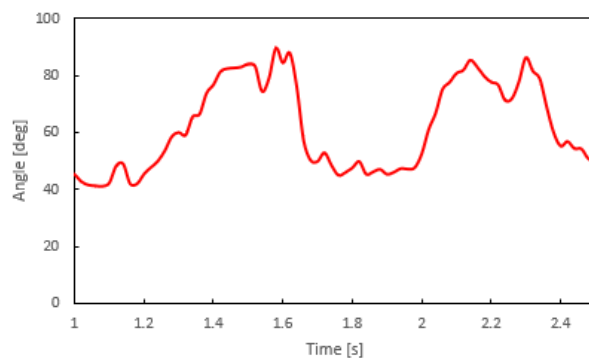
Direction of motions	R / L Side	Joint angle [deg]
Plantar flexion	R	60
	L	50
Dorsi flexion	R	10
	L	5



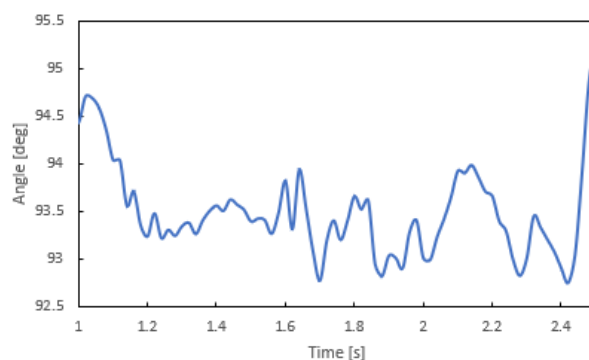
(a)



(b)



(c)



(d)

Figure 6. Results of ankle angle from the front and oblique upward angle

Based on these results, the ankle angles that significantly affected gait were determined. The results of this analysis are shown in Figure 6. The changes in the left and right ankle angles were almost identical with and without motion restriction. However, in both cases, the change in the right ankle angle was smaller. It is unclear whether this was a feature of the subject's gait or a software problem. Further studies with different subjects are necessary to determine the cause.

D Gait speed

The gait speed was examined. Because the coordinates are those of the projection from the camera, correction was required [31]–[34]. Although it is best to correct the coordinates from a 3D viewpoint, in this case, the correction is based on the walking trajectory. Therefore, we compared the walking speeds based on measurements for which specific lengths were known.

For the gait speed, we compared the data from the camera with the data from the pressure sensor and determined the points that should be analyzed to obtain accurate results based on the software. We inferred that it would be difficult to determine the walking speed when shooting from an oblique direction because the screen was moved in an oblique direction. However, data could be

obtained for comparison if the same conditions were used. The problem with the images captured from the front was that the size of the subject varied depending on the measurement data point.

Therefore, we considered the part of the image that moved as slightly as possible on the screen, which was the shoulder area, because it was close to the central part. Figure 7 shows the plot of the right shoulder, which had the largest slope. The obtained value was approximately 0.17, and this value was equal to 0.67 km/h.

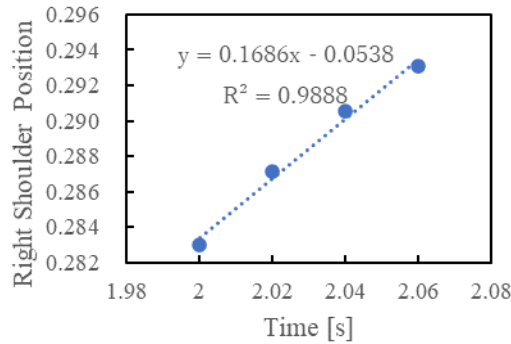


Figure 7. Right shoulder position as a function of time.

Figure 8 shows a 3D display of the trajectory of the right shoulder position. Because the slope of the change in the right shoulder position is approximately 45°, it was deduced that using the correction value for the direction of motion on the screen, a walking speed of 1.4 km/h, which is almost the same as the 1.3 km/h obtained from the mat, could be obtained.

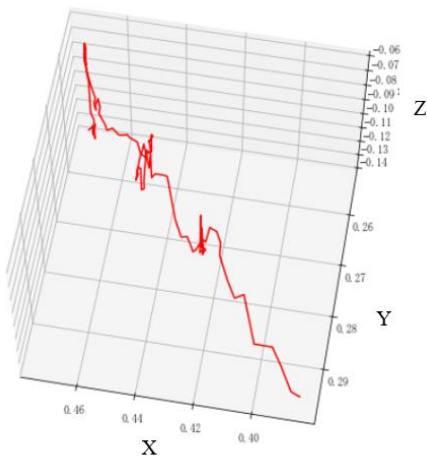


Figure 8. 3D display of the trajectory of the right shoulder position.

E Orthobot

The Orthobot employed in this study is a gait-assist device that supports walking by estimating the gait phase from the thigh posture and generating torque. The Orthobot can be attached to a conventional knee-ankle-foot orthosis to control an individual's knee.

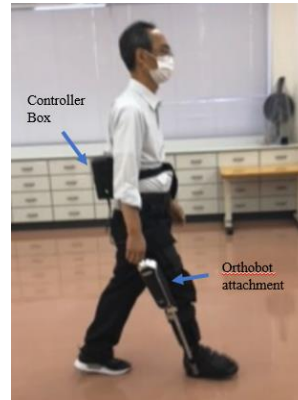
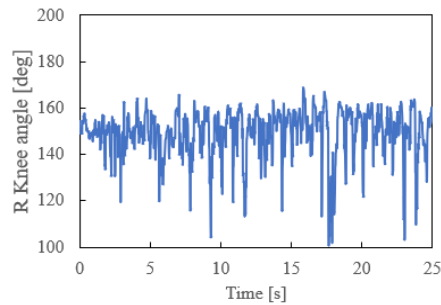
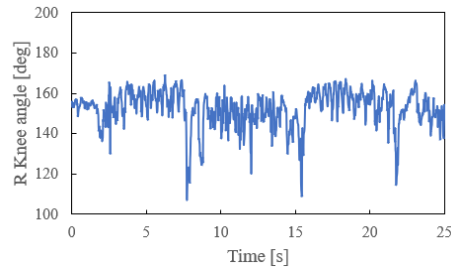


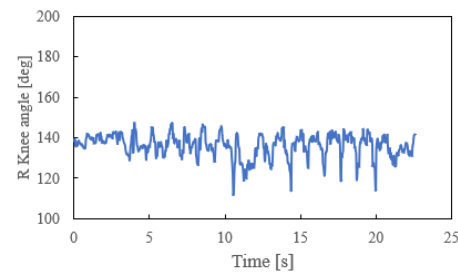
Figure 9. Photograph of the Orthobot attached.



(a)



(b)



(c)

Figure 10. Results of calculated knee angle from MediaPipe.

It automatically assists in the flexion and extension of the knee joint at the appropriate time. The motion state of the leg wearing the aid was measured using drone measurement technology by considering the wearer's swing phase as a pendulum. The torque generated was calculated by estimating the gait phase from the thigh posture to assist walking. Figure 9 shows a photograph of the attached Orthobot.

Orthobots can be attached to general walking aids and are considered highly versatile. The driving device is located in the knee portion, and signals from a controller attached to the back portion of the device move the assistive device, allowing the paralyzed person to experience walking motion, thereby restoring the function.

Figures 10(a)–(c) show the changes in the knee joint during walking before, during, and 5 min after wearing the Orthobot, respectively. The change in the angle of nearly 100° is due to the change in direction. The view of the knee joint angle is not significant during walking, and the machine assists with the swing of the knee. Five minutes after use, the change in the knee joint decreases.

F Neck tilt angle for the subject wearing the walking assist device

Walking affects the entire body and not just the lower extremities. In this section, we focus on the head and neck parts of the body. We used an inverted pendulum model for walking. We calculated how much the neck part was tilted from the axis of the center of the torso during walking, based on the coordinate information obtained from MediaPipe. As shown in Figure 11, the angle of the neck was defined as the angle between the line connecting the coordinates of the midpoints of the left and right shoulders and the line connecting the coordinates of the midpoints of the left and right shoulders and the tip of the nose, calculated using the formula for the interior angle of a vector.

The analysis software ORPHE ANALYTICS® manufactured by ORPHE was also used to obtain the neck tilt angle, which was used for confirmation. The neck angle obtained from this software depends on the direction of gait; therefore, absolute values are used because they are positive or negative depending on the gait.



Figure 11. Neck angle definition.

Figure 12 shows the results of the analysis when walking without an aid. It also shows changes in the left and right ankles. The angle of the neck corresponds to the left-side axis, whereas the angles of the left and right heels correspond to the right axis. The measurement started before the movement from the starting point; hence, the walk began facing left approximately 2 s later. At approximately 10 s, the direction changed 180° to a rightward walk. The data started with a leftward walk. At approximately 10 s, the data shows a 180° turn around and a rightward walk. Neck movement during walking is in the form of a slowly changing wave with a higher-frequency component. The orange line in the figure shows the left heel change, whereas the gray line shows the right heel. The values are larger at farther distances from the camera. The vertical movement of the heel changed in response to the neck tilt angle signal.

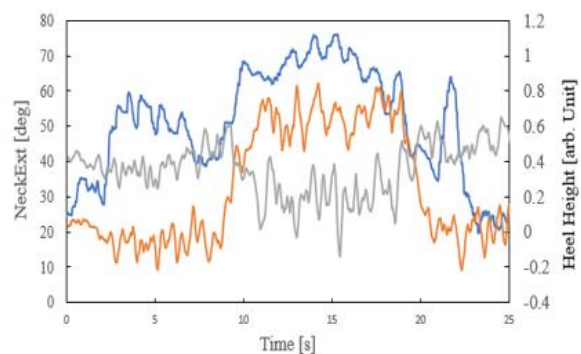


Figure 12. Results of the analysis when walking without aid.

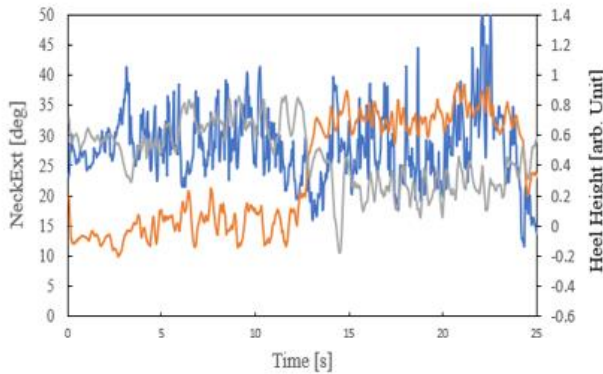


Figure 13. Results obtained when a walking aid was used.

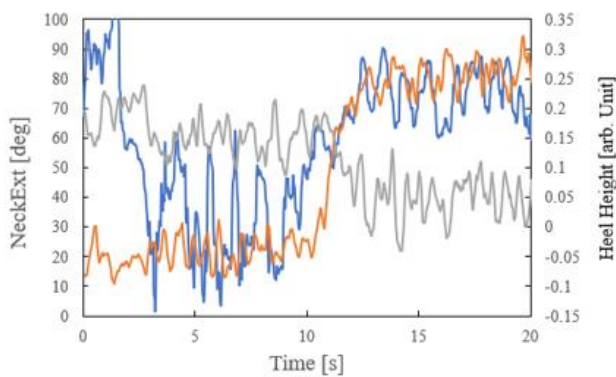


Figure 14. Results obtained approximately 5 min after using aid.

Figure 13 shows the results obtained when a walking aid was used. The tilt angle of the neck is also indicated by the blue line.

Figure 14 shows the measurement taken approximately 5 min after the aids were removed. This is a short time measurement because MediaPipe could not continuously capture the arm movements during this measurement, and the data stopped at 20 s.

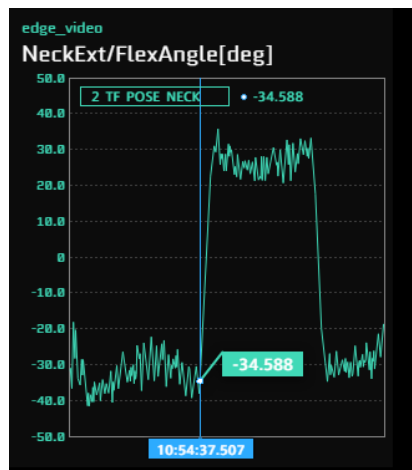


Figure 15. Change in neck tilt obtained using ORPHE ANALYTICS.

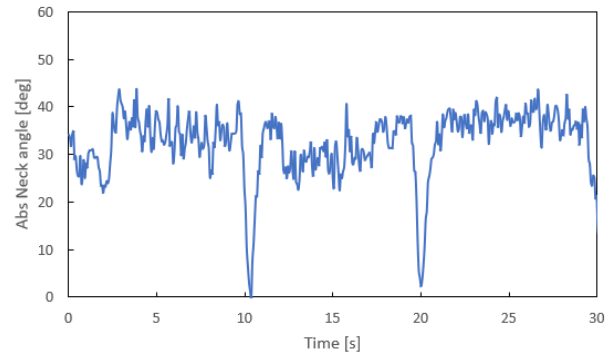


Figure 16. Absolute values of neck tilt before Orthobot use.

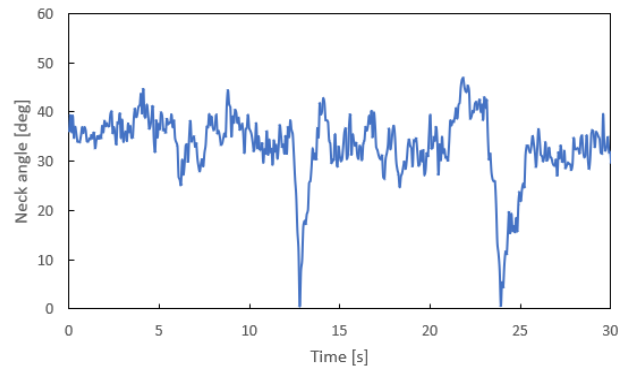


Figure 17. Absolute values of neck tilt during Orthobot use.

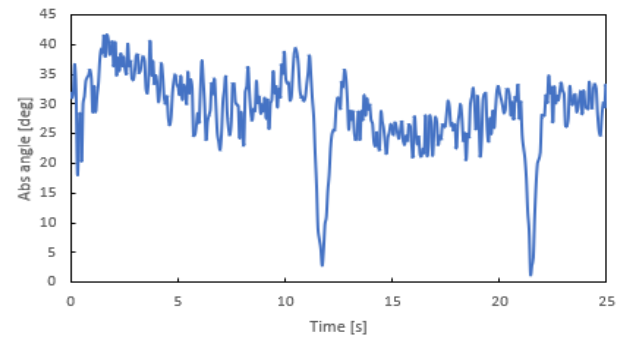


Figure 18. Absolute values of neck tilt 5 min after Orthobot use.

Figure 15 shows the change in the neck tilt obtained using the ORPHE ANALYTICS. This measurement was performed before the use of the Orthobot.

Figure 16 plots the absolute values for comparison with MediaPipe. This measurement was also conducted before the use of the Orthobot. Figure 17 shows the tilt of the neck while using the Orthobot. Figure 18 shows the measured neck tilt approximately 5 min after using the Orthobot. In Figure 16, the high-frequency signal with a relatively small amplitude is superimposed on the low-frequency signal as in the calculation with MediaPipe. For assisted aids, the high frequencies with large amplitudes have a noticeable number component. This trend is also observed in Figure 18, which

shows results of approximately 5 min after the supplementation with the Orthobot, with large amplitude high-frequency components.

G Discrete Fourier-transformation analysis for stride variability

The risk of falling is closely related to stride variability. Therefore, we focused on the variability and examined the frequency intensity using discrete Fourier-transformation (DFT) analysis. Figures 19-22 show the analysis results from the MediaPipe software, and Figures 23-25 show those from the ORPHE ANALYTICS. The DFT spectra were measured before, during, and 5 min after wearing the Orthobot walking assist device. Only 22 s of signal were used for the DFT evaluation, until the MediaPipe lost sight of a landmark point and stopped working properly when measured 5 min after removing the Orthobot.

The spectra of the neck angle changes before, during, and after using the assistive device obtained from ORPHE ANALYTICS are shown in Figures 23-25, with large peaks obtained in the low-frequency region below 0.5 Hz. The low-frequency peaks were particularly strong in the case of Figure 23 without the assistive device. The peak at approximately 1.6

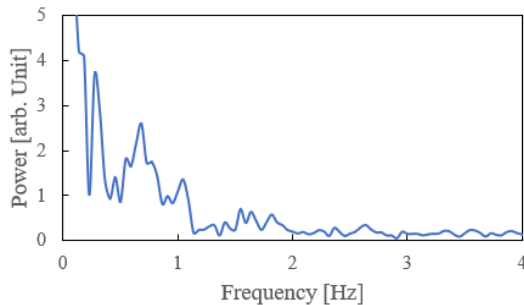


Figure 19. Spectrum before using Orthobot.

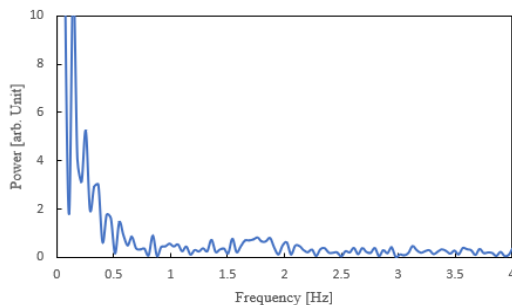


Figure 20. Spectrum when using Orthobot.

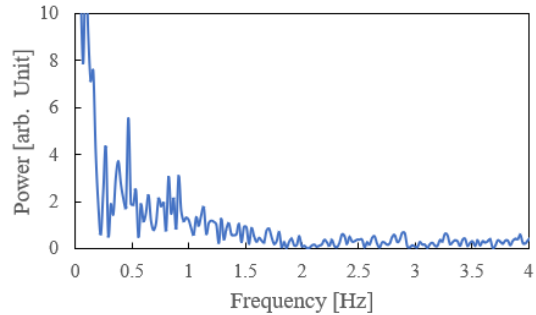


Figure 21. Spectrum after using Orthobot

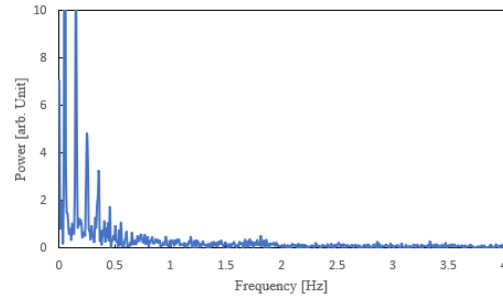


Figure 22. Sepctrum of heel using Orthobot.

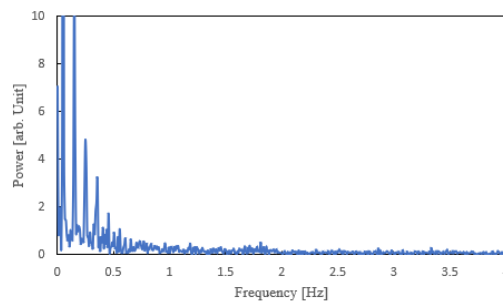


Figure 23. Spectrum before using Orthobot analyzed data obtained by ORPHE ANALYTICS.

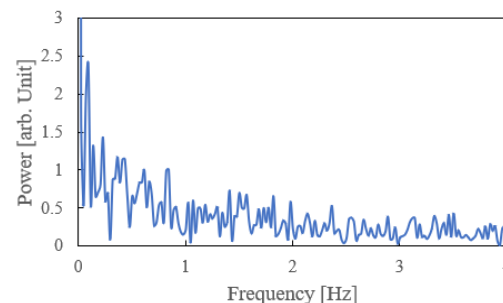


Figure 24. Spectrum when using Orthobot analyzed data obtained by ORPHE ANALYTICS.

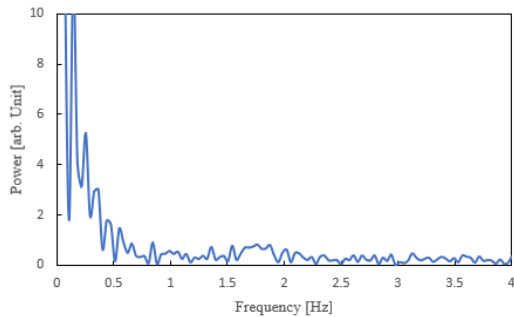


Figure 25. Spectrum of heel using the Orthobot analyzed data obtained by ORPHE ANALYTICS.

Hz decreased after the use of the assistive device, which may be due to the characteristics of the subject's gait.

III. DISCUSSION

A Accuracy check of CSV data outputed by MediaPipe

The analysis using MediaPipe reproduced the left ankle trajectory in the timed up-and-go measurements, as shown in Figure 2. The z-axis values corresponding to the vertical motion are small owing to the screen settings; therefore, the z-axis values are emphasized. Consequently, it is necessary to make a prior reference measurement and correction for an accurate evaluation. Detailed ankle trajectories were obtained. Video analysis of the timed up-and-go test confirmed that the specifications remained consistent.

B Skeleton analysis of without/with restrictions using video from front and oblique upward angle

As shown in Figures 4 and 6, it was possible to determine the ankle angle as gait condition data, although we did not calculate this timed up-and-go measurement. Comparing the independently measured range-of-motion angle data of the ankle joint and comparative ankle joint range-of-motion angles obtained from the video, slight differences were observed owing to the camera angles. The angular change in the right foot was almost the same, regardless of the camera angle. In contrast, the angular change in the left leg tended to be smaller. For the subject's gait, another measurement showed that the joint change in the left foot was smaller than that in the right foot. Further investigation is required in another experiment with a different subject.

C Gait speed

We considered the parts of the image that were considered to move as slightly as possible on the screen. In this image, the shoulders were close to the center of the image, so this was considered. In the walking speeds obtained by walking on the mat, differences of approximately 2.1 km/h and 1.3 km/h were obtained with

and without the motion restriction, respectively. The values obtained from MediaPipe, however, were approximately an order of magnitude lower.

Although it is desirable to correct the coordinates from a three-dimensional perspective, in this case, the correction was based on the gait trajectory. Therefore, we compared the walking speeds based on measurements with known specific lengths. We examined the points that could be analyzed to obtain accurate results based on software principles. We inferred that it would be difficult to determine the gait speed when shooting from an oblique direction because the screen is moved in an oblique direction. However, we believe that, under the same conditions, we could obtain data for comparison. Obviously, the images taken from the front had a problem in that the size of the subject differed from one measurement data point to another.

Figure 8 shows a three-dimensional display of the trajectory of the right shoulder position. Because the slope of the change in the right shoulder position is approximately 45°, it was found that using the correction value for the direction of motion on the screen, a walking speed of 1.4 km/h was obtained, which was almost the same as the 1.3 km/h obtained from the mat.

Because the walking speed can be corrected by the choice of the detection point, it is necessary to be creative when capturing videos, for example, by shooting parallel to the direction of motion.

D Tilt angle of neck calculated by Mediapipe and ORPHE ANALYTICS

As shown in Figure 12, the tilt angle of the neck, indicated by the blue line, does not show a gradual change compared to the case without the aid, and a higher-frequency component can be observed. The change in the heel shape corresponded to the change in the vertical movement of the heel.

As shown in Figure 13, the tilt angle of the neck does not exhibit a gradual change compared with the case without the aid. A higher-frequency component can be observed in the change in the shape of the heel corresponding to the vertical movement of the heel.

Figure 14 shows a measurement taken approximately 5 min after the aids were removed. Although long-period waves were observed, high-frequency waves corresponding to the same up-and-down heel movements as when the assistive device was used were also observed, suggesting that the effect of the assistive device was still present.

In Figure 16, a high-frequency signal of a relatively small amplitude is superimposed on a low-frequency signal, as in the calculations with MediaPipe. In the assisted case, high species with large amplitudes have a noticeable number of components. This trend is also observed in Figure 19, which shows approximately 5 min after Orthobot replenishment and includes a high-frequency component of a large amplitude.

E DFT analysis for stride variability

In the spectrum before mounting shown in Figure 19, the peak change was gradual, as observed in the waveform, and the peak spectra were observed at 0.3, 0.6, and approximately 1 Hz. A small peak was also observed at approximately 1.7 Hz. Many fine peaks were observed in the knee joint flexion and extension movements when the subject wore the walking assist device because of the assisted movement. A peak at approximately 0.8 Hz was observed, although it was not a clear peak compared to the peak before the assist device was attached. A peak at approximately 1.6 Hz was also observed. Five minutes after the assist device was removed, not only a peak at approximately 0.8 Hz but also 0.9 Hz was observed, whereas a peak at approximately 1.6 Hz was observed; however, its amplitude was smaller. Figure 22 shows the results of the spectral analysis of the right heel of the right foot while wearing the assistive device, with peaks at approximately 0.4 Hz and 0.8 Hz. This suggests that these two peaks were caused by leg motion.

F Advantages and disadvantages of software implementation

Because this software can be installed on tablets and smartphones, we believe that the skeleton analysis screen can be effective as a simple check tool at rehabilitation sites. In the case of a detailed numerical analysis, there are differences in the numerical values obtained owing to differences in the camera angles, necessitating the use of a camera with a sufficiently wide angle at the time of measurement or having the camera fixed to eliminate shaking of the camera during movement. The current experiment only shows the results of the analysis of one subject with and without pseudo limitations of movement. Data from two subjects of different ages and genders measured simultaneously are currently being analyzed. Based on the above, we believe that the conditions necessary for using this software in the field can be determined by accumulating more data and adapting it to subjects with gait disorders.

IV. CONCLUSION AND FUTURE WORK

With the widespread use of smartphones, it is very easy to record videos of a person's walking condition and to ask for a diagnosis from a medical professional. The ability to obtain skeletal displays and numerical data, similar to this software, is expected to rapidly improve the potential of video analysis in the medical insurance field.

However, the limitations of shooting conditions when introducing this software should be considered. For example, the shooting angle and location on which the analysis should be focused are important. In the future, we will improve the optimization of the video shooting conditions

and correction methods for all shooting angles. In addition, these corrections will be made and adapted for each subject.

We compared the foot movements of the Orthobot, an assistive device, before, during, and after 5 min of using MediaPipe and ORPHE ANYTICS. It was deduced that MediaPipe could obtain data over a considerable area. However, there are many areas where it is difficult to obtain the desired data through programming and to interpret the data; therefore, it is necessary to clarify the purpose of data collection for use in the field.

ACKNOWLEDGMENT

This work was supported by JAPS KAKENHI (grant number JP20K11924).

REFERENCES

- [1] Y. Uchida, T. Funayama, Y. Kogure, "Investigation of the Application of MediaPipe to Gait Analysis," pp. 1-6, IARIA, GLOBAL HEALTH 2022. ISBN: 978-1-61208-995-9.
- [2] L. G-Villanueva, S. Cagnoni, and L. Ascari, "Design of a Wearable Sensing System for Human Motion Monitoring in Physical Rehabilitation," *Sensors*, vol. 13, pp. 7735-7755, 2013.
- [3] Y.-L. Zheng, X.-R. Ding, C. C. Y. Poon, B. P. L. Lo, H. Zhanf, and G.-Z. Yang, "Unobtrusive Sensing and Wearable Devices for Health Informatics," *IEEE Transactions Biomedical Engineering*, vol. 61, pp. 1538-1554, 2014.
- [4] M. M. Alam and E. B. Hamida, "Surveying Wearable Human Assitive Technology for the Life and Safty Critical Applcations: Standards, Challenges and Opportunities," *Sensors*, pp. 9153-9209, 2014.
- [5] M. J. Deen, "Information and Communications Technologies for Elderly Ubiquitous Healthcare in a Smart Home," *Personal and Ubiquitous Computing*, pp. 573-599, 2015.
- [6] S. Hong and K. S. Park, "Unobtrusive Photoplethymographic Monitoring Under the Foot Sole while in a Standing Posture," *Sensors*, 3239, 2018.
- [7] V. Bucinkas, et al., "Wearable Feet Pressure Sensor for Human Gait and Falling Diagnosis," *Sensors*, vol. 21, 5240, 2021.
- [8] P. M. Riek, A. N. Best, and R. Wu, "Validation of Inertial Sensors to Evaluate Gait Stability," *Sensors*, vol. 23, 1547, 2023.
- [9] Y. Uchida et al., "Feature Value Extraction for Body Condition Change Measurement System Using Pressure Sensor Array," *Human Interface Society in Japanese*, vol. 24, No.1, pp. 79-82, 2022, ISSN 2188-6652.
- [10] Y. Uchida, T. Funayama, K. Hori, M. Yuge, N. Shinozuka and Y. Kogure, "Possibility of Detecting Changes in Health Conditions using an Improved 2D Array Sensor System," *Sensors & Transducers*, vol. 259, pp. 29-36, 2022.
- [11] Q. Zou, Y. Wang, Q. Wang, Y. Zhao, and Q. Li, "Deep Learning-Based gait Recognition Using Smartphones in the Wild," *IEEE Transactions on Information Forensics and Security*, pp. 1-15, 2020, arXiv:1811.00338v3 [cs.LG].
- [12] F. Wang, A. Dong, K. Zhang, D. Qian, and Y. Tian, "A qualitative Assessment Grading Study of Balance Performance Based on Lowe Limb Dataset," *Sensors*, vol. 23, 33, 2023.
- [13] V. Bazarevsky et al., "BlazePose: On-device Real-time Body Pose tracking," arXiv:2006.10204v1 [cs.CV] 2020.

- [14] G. Kaur, G. Jaju, D. Agawal, K. Lyer, and C. M. Prashanth, "Implementation of Geriatric Agility Detection Using MediaPipe Pose," *International Journal of Recent Advances in Multidisciplinary Topics*, vol. 3, 119, 2022, ISSN:2582-7839.
- [15] J.-L. Nhung, L.-Y. Ong, and M.-C. Leow, "Comparative Analysis of Skelton-Based Human Pose Estimation," *Future Internet*, vol.14, 380, 2022.
- [16] J.-W. Kim, J.-Y. Choi, E.-J. Ha, and J.-H. Choi, "Human Pose Estimation Using MediaPipe Pose and Optimization Method Based on Humanoid Model," *Applied Sciences*, vol. 12, 2700, 2023. doi.org/10.3390/app13042700.
- [17] Q. Wang, g. Kurilo, F. Ofli, and R. Bajcsy, "Evaluation of Pose tracking Accuracy in the First and Second Generations of Microsoft Kinect," arXiv:1515.04134v1 [cs.CV] 2015.
- [18] P. Plantard, E. Auvinet, A. S. Le Pierres, and F. Multon, "Pose Estimation with a Kinect for Ergonomic Studies: Evaluation of the Accuracy Using a Virtual Mannequin," *Sensors*, vol. 15, pp. 1785-1803, 2015.
- [19] R. A. Clark, B. F. Mentiplay, E. Hough, and Y. H. Pus, "Three-Dimensional Cameras and Skeleton Pose Tracking for Physical Function Assessment: A Review of Use, Validity, Current Developments and Kinect Alternatives," *Gait & Posture*, vol. 68, pp. 193-200, 2019.
- [20] Y. Ma, K. Mithratatne, N. Wilson, Y. Zhang, and X. Wang, "Kinect v2-Based Gait Analysis for Children with Cerebral Palsy: Validity and Reliability of Spacial Margin of Stability ad Spationtemporal Vaibles," *Sensors*, vol. 21, 2104, 2021.
- [21] D. Imoto, S. Hirano, M. Mukaino, E. Saitoh, and Y. Otaka, "A Novel Gait Analysis System for Detecting Abnormal Hemiparetic Gait Patterns during Robo-assisted Gait Training : A Criterion Validity Study among Healthy Adults," *Frontiers in Neurorobotics*, 16:1047376, 2022.
- [22] L. Buker, V. Quinten, M. Hackbarth, S. Hellmers, R. Diekmann, and A. Hein, "How the Processing Mode Influences Azure Kinect Body Tracking Results," *Sensors*, vol. 23, 878, 2023.
- [23] K. Shihomi, K. Ohata, T. Tsuboyama, Y. Sawada, and Y. Higashi, "Development of New Rehabilitation Robot Device that Can be Attached to the Conventional Knee-Ankle-Foot-Orthosis for Controlling the Knee in Individuals After Stroke," 2017 International Conference on Rehabilitation Robotics, pp. 304-307, 2017.
- [24] A. L. Hof, M. G. J. Gazendam, and W. E. Sinke, "the condition for dynamic stability," *Journal of Biomechanics*, vol. 38, pp. 1-8, 2005.
- [25] R. M. Magnani, S. M. Bruijn, J. van Dieen, and M. F. Vieira, "Head Orientation and Gait Stability in Young Adults, Dancers and Older Adults," *Gait & Posture*, vol. 80, pp. 68-73, 2020.
- [26] J. Choi, S. M. Parker, Y. Gwon, and J. Youn, "Wearable Sensor-Based Prediction Model of Time up and Go Test in Older Adults," *Sensors*, vol. 21, 6831, 2021.
- [27] J. Beyea, C.A. McGibon, A. Sexton, J. Noble, and C. O'Connell, "Covergent Validity of a Wearable Sensors Sytem for Measuring Sub-Task Performance during the Timed Up-and-Go test," *Sensors*, vol. 17, 934, 2017.
- [28] J. P. Monteiro, A. T. Magalhaes, and H. P. Oliveira, "Human Pose Estimation, Anthropomorphism and Gamification in Promotion of Physical Activity Among Breast Cancer Survivors," *International Journal on Advances in Life Sciences*, vol. 11, pp. 118-127, 2019.
- [29] F. Buisseret et al., "Time Up and Go and Six-Minute Walking Test with Wearable Inertial Sensor: One Step Futher for Prediction of the Risk of Fall in Elderly Nursing Home People," *Sensors*, vol. 20, 3207, 2020.
- [30] A. L. M. Frangakis, E. D. Lemaire, and N. Baddour, "Subtask Segmentation Method of the Timed Up and Go test and L Test Using Inertial Measurement Units-A Scoping Review," *Information*, vol. 14, 127, 2023.
- [31] Z. Li, R. Zhang, C. H. Lee, and Y. Lee, "An Evaluation of Posture Recognition Based on Intelligenct Rapid Entire Body Assessment System for Determing Musculoskeletal Disorders," *Sensors*, vol. 20, 4414, 2020.
- [32] Y. Ono, O. D. A. Prima, and K. Hosogoe, "Evaluation and Application of Partial Body Joint Model in 3D Human Pose Estimation from Signal Image," *International Journal on Advances in Life Sciences*, vol. 13, pp. 114-123, 2021.
- [33] I. Crombrugg et al., "Accuracy Assessment of Joint Angles Estimated from 2D and 3D Camera Measurements," *Sensors*, vol. 22, 1729, 2022.
- [34] X. Yu, J. Baar, and S. Chen, "Joint 3D Human Shape Recovery and Pose Estimation from a Signal Image with Bilayer Graph," arXiv:2110.8472v2 [cs.CV], 2021.

Examining the Relationship between COVID-19 Mobility and Eviction Rates in Philadelphia

Regina Ruane

The Wharton School
The University of Pennsylvania
Philadelphia, PA, USA
e-mail: ruanej@upenn.edu

Les Sztandera

Kanbar College of Design, Engineering, and Commerce
Jefferson University
Philadelphia, PA, USA
e-mail: Les.Sztandera@jefferson.edu

Abstract—The COVID-19 pandemic has had a significant impact on public health, the economy, and social norms, particularly creating tighter restrictions on the daily lives of millions of people however we do not yet understand what measures are the most effective. Modeling the transmission of the virus has been one method to predict directions. With transmission, the interplay between factors such as age, socioeconomic, susceptibility to infection, and COVID-19 dynamics remains unclear. To address these factors, we analyze eviction and mobility data from Google's COVID-19 Community Mobility Reports before and during the outbreak to explore the relationship between eviction rates and COVID-19 mobility patterns in Philadelphia. We analyzed eviction data from the city of Philadelphia and mobility data from Google's COVID-19 Community Mobility Reports. Our findings suggest that there is a statistically significant relationship between eviction rates and mobility patterns. Specifically, we found that areas with high eviction rates also had a higher level of mobility, which could potentially increase the spread of the virus. Our results highlight the importance of considering the impact of socioeconomic factors on the transmission of COVID-19.

Keywords—COVID-19; eviction; mobility.

I. INTRODUCTION

The coronavirus disease 2019 (COVID-19) pandemic has affected people across the globe, causing millions of deaths and economic instability. The pandemic has caused additional hardships with one of the many consequences of the pandemic has been an increase in eviction rates in many cities in the United States, including Philadelphia. With people losing their jobs or experiencing reduced income, many have been unable to pay rent or mortgage, leading to eviction. Eviction not only has social and economic implications but can also impact public health by forcing people into crowded living conditions, which can increase the transmission of COVID-19. The COVID-19 pandemic brought about unprecedented mobility restrictions to prevent the spread of the virus. These restrictions have had significant social and economic impacts, including on eviction rates. Questions remain about the socioeconomic profile of susceptibility to infection, how social distancing and specific social distancing practices alters contact patterns, and how these factors come together to affect transmission. These questions are particularly relevant to

policy development and implementation for governments and policy-makers. In this study, we evaluate changes in mixing patterns linked to social distancing by collecting eviction and Google mobility data in the midst of the epidemic in Philadelphia, PA, USA. This paper examines the impact of COVID-19 mobility restrictions on eviction rates in Philadelphia, Pennsylvania. Using eviction data from the Eviction Lab and the City of Philadelphia as well as mobility data from Google's COVID-19 Community Mobility Reports, we conduct a comparative analysis of eviction rates before and after the implementation of mobility restrictions in Philadelphia. Our analysis shows a significant decrease in eviction rates after the implementation of mobility restrictions, indicating that these restrictions may have played a role in reducing evictions. We also explore the potential implications of these findings for policymakers and advocates seeking to address the eviction crisis in Philadelphia and beyond, developing a mathematical model to predict how transmission is affected by and altered eviction patterns.

To estimate changes in eviction patterns associated with COVID-19, we conducted network mapping of the sampled eviction data. To understand the interplay between social distancing, changes in human mixing patterns, and outbreak dynamics, potential age differences in susceptibility to infection must also be considered. To advance this goal, we analyzed COVID-19 mobility information gleaned from detailed Google mobility data.

The COVID-19 pandemic has exposed and exacerbated existing socioeconomic and health disparities, including disparities in health and well-being. Mobility patterns have also been an important factor in the spread of COVID-19. Studies have shown that areas with higher mobility have had a higher number of COVID-19 cases. Understanding the relationship between eviction rates and mobility patterns can provide insights into how socioeconomic factors can impact the transmission of COVID-19.

Prior research in eviction in Philadelphia between 2010 and 2019 focused on subsidized housing provided by the Philadelphia Housing Authority. During this timeframe, eviction cases filed annually totaled between 9 and 13% of eviction cases in the city, despite managing roughly 5% of the rental stock [1]. While the residing in subsidized

housing in Philadelphia was associated with lower risk of eviction filings when accounting for other building and neighborhood characteristics, public housing buildings had higher eviction filing risk compared with other types of subsidized properties [2].

The COVID-19 pandemic has disrupted life as we know it, with governments around the world implementing unprecedented measures to limit the spread of the virus. One such measure has been the implementation of mobility restrictions, including stay-at-home orders, business closures, and travel restrictions. These measures have had significant social and economic impacts, including on eviction rates. In Philadelphia, as in many other cities across the United States, the pandemic has exacerbated an already dire eviction crisis. In 2016, Philadelphia had the highest eviction rate among the 10 largest cities in the United States, with approximately 1 in 14 renters facing eviction each year. Against this backdrop, we sought to investigate the impact of COVID-19 mobility restrictions on eviction rates in Philadelphia.

II. METHODOLOGY

We collected eviction data from the city of Philadelphia for the period between January 2019 and December 2021. We also obtained data from the Eviction Lab, a research group that collects and analyzes eviction data from across the United States, and Google's COVID-19 Community Mobility Reports for the same period. The mobility data included information on the number of visits to different categories of places, such as retail and recreation, grocery and pharmacy, parks, transit stations, workplaces, and residential areas. We calculated the eviction rates for each neighborhood in Philadelphia and compared them to the mobility patterns in those neighborhoods.

Our first source of data consisted of individual-level records from eviction cases filed from 1964 to present across the City of Philadelphia. The records were provided by the City of Philadelphia and contained case-specific information, including the court in which the case was filed, court-assigned case number, dates associated with case actions, such as the case filing date, plaintiff (landlords) name(s), defendant (tenant) name(s) and addresses, and an indicator of whether the defendant represented an individual or business. Plaintiff names recorded the party who filed the case.

Case filings were represented by the court identifier and case number. Many cases were represented by multiple individual-level records associated with different defendants or actions. We aggregated filings annually by the earliest date on a record associated with a case. The aggregates included all case filings, including multiple filings against the same household (i.e., serial filings). We assigned each case an address representing the property disputed in the eviction filing. Addresses were cleaned and geocoded. We excluded any cases that had one or more commercial

defendants as identified by the existing "business" indicator. We also removed cases that duplicated the same dates, plaintiff names, and tenant addresses across cases.

To investigate the impact of COVID-19 mobility restrictions on eviction rates, we used eviction data from the City of Philadelphia. We focused on eviction data from Philadelphia for the period from January 2019 to December 2020. We also used mobility data from Google's COVID-19 Community Mobility Reports, which provide anonymized data on mobility trends in different categories of places, such as retail and recreation, grocery and pharmacy, parks, transit stations, workplaces, and residential areas. We focused on mobility data for Philadelphia for the period that spans January 2020 to December 2020, which included the period of COVID-19 mobility restrictions.

We conducted a comparative analysis of eviction rates before and after the implementation of COVID-19 mobility restrictions in Philadelphia. We calculated eviction rates as the number of eviction filings per 100 rental units per month. We also calculated the percentage change in eviction rates from the pre-COVID-19 period (January 2019 to February 2020) to the COVID-19 period (March 2020 to December 2020). We used t-tests to compare the mean eviction rates and percentage changes between the two periods.

To investigate the impact of COVID-19 mobility restrictions on eviction rates, we used eviction data from the Eviction Lab, a research group that collects and analyzes eviction data from across the United States. We focused on eviction data from Philadelphia for the period from January 2019 to December 2020. Additionally, we used mobility data from Google's COVID-19 Community Mobility Reports, which provide anonymized data on mobility trends in different categories of places, such as retail and recreation, grocery and pharmacy, parks, transit stations, workplaces, and residential areas. The focus with this mobility data was the location of Philadelphia for the period from January 2019 to December 2020, which included the period of COVID-19 mobility restrictions.

We used a network-generating approach which consisted of factors assuming to have a fixed geographic location, as determined by coordinates in a two-dimensional space [4]. The network composition consists of actors who are members of groups, e.g., households, and institutions, e.g., schools or places of work, and have individual attributes, i.e., age, education or income. We generated network ties so that actors have some connections to geographically close alters, i.e., ties to members of the same groups like co-workers, some ties to alters with similar attributes, age, and some ties to alters in the population with no defined attribute. Together, this layered approach creates multi-layered networks that have realistic values of local clustering, path lengths and homophily.

The tie formation is based on geographic proximity, where the network consists of random placement of actors into a two-dimensional square. Each actor draws the

number of contacts it forms in this sub-process $d_{geo,i}$ from a uniform distribution between $d_{geo,min}$ and $d_{geo,max}$; for example, if $d_{geo,min} = 10$ and $d_{geo,max} = 20$. The density is user-defined to form ties geographically d_{geo} defines the geographic proximity of contacts as mapped, so that actor i randomly forms $d_{geo,i}$ ties among those $d_{geo,i}/d_{geo}$ who are in close Euclidean distance to actor i . The binary network x represents interaction potential between n individuals. These individuals shall have labels ranging from 1 to n . Each node i can have a set of attributes (aki), e.g., age or location.

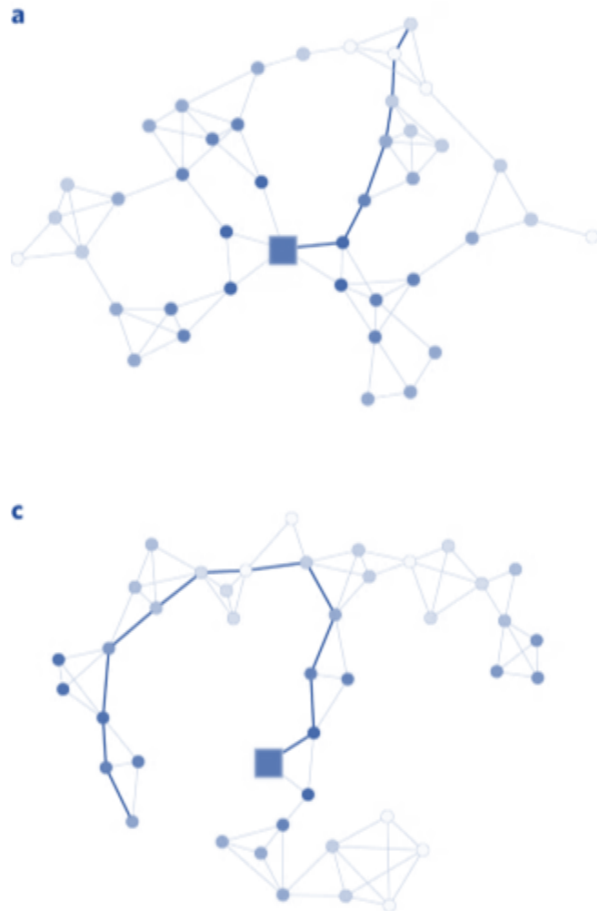


Figure 1. This figure depicts two example networks a) and c) both have the same number of nodes (individuals) and ties, which indicate social interactions, but the networks have different structures, which are depicted by shorter path lengths. Network a) has longer path lengths, which implies different infection curves. Bold ties showcase the shortest infection path from the infection source to the last infected individual in the respective networks.

This network approach aims to represent individuals interacting with some potential contacts similarly to the classic SIR model [5], where individuals are susceptible/infective/removed. These models can be applied on a wide variety of networks, where individuals are susceptible, infectious or recently recovered as well as to its SEIR extension [6], where individuals are susceptible, have been exposed, are infectious and recovered. Individuals can be in four different categories: susceptible to contracting the disease, having been exposed, i.e., infected but not yet infectious, infectious or recovered. We surmise that infection would occur through social interactions. These interactions are modelled in similar ways to the dynamic actor-oriented model which represents relational events. In this model, the probabilities, $\pi_{contact}$ and $\pi_{infection}$, have a similar role with regard to the classic rate of infection, β , in SIR and SEIR models. The β rate demonstrates the average number of contacts per person and the likely rate of infection, which is represented by $\pi_{infection}$. The caveat is that equivalence is not direct due to interaction probability p . Additional model characteristics include classic exposure and recovery rates (often traditionally denoted as σ and γ) in a straightforward manner.

Next, we will define the probability model p , where N_i will be the set of potential contacts, or alters j of a given individual i in the network x . The definition for each step t of the process is $Li(j, t)$, where the previous interactions occurring between i and an alter $j =$ within the past λ interactions of i . In our simulations, λ is arbitrarily arranged to be 2, but this can be modified.

For each alter $j \in N_i$, the value $s(i, j)$ represents the driver for the strategic statistical choice of i to pick j . We define three different approaches and choose the particular approach of homophily. The statistic $ssimilarity$ accounts for the level of similarity between i and j given a set of attributes; $scommunity$ corresponds to the number of alters they share, and $srepetition$ is the count of previous interactions within the past λ contacts of i .

The experiment with geography as the basis and a homophily strategy was developed according to the '1: baseline' parameter. The basis for this experiment in terms of interaction choice partners was the Euclidean distance in geographic placement in the homophily strategy. The two experiments on multidimensional homophily used underlying networks which resulted in the following baseline parameters: two attributes were defined and the number of ties created according to the homophily parameter have been split evenly between the two dimensions. The homophily strategy is used for the simulated infection curves in the two scenarios. This strategy differs in that individuals interact according to the minimization of the absolute difference in both attributes. In the second scenario, only the first attribute is used as the

basis of the homophily strategy and the second attribute is overlooked.

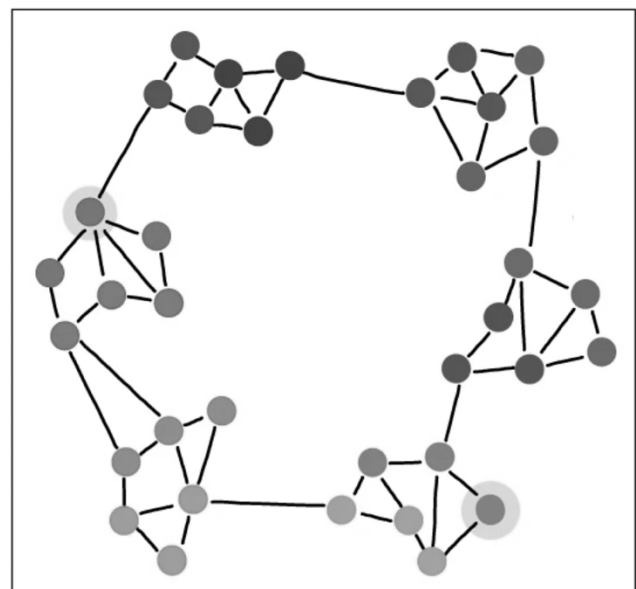
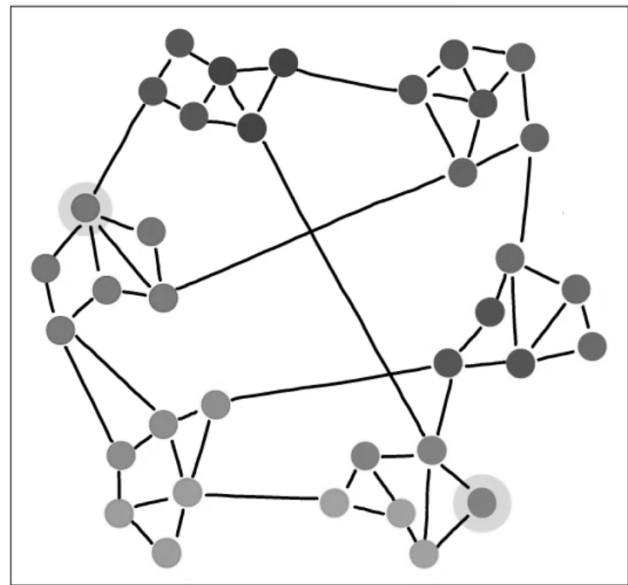
We applied insights from social and statistical network science, illustrating how modification of network configurations individual contact selections and organizational routines can change the rate and spread of the virus through the provision of guidelines, which differentiates the rate of high- and low-impact contacts for disease spread.

Using a social network perspective can show the ways that the shape of the infection curve can be closely related to the concept of network distance or path length, demonstrating the number of network steps necessary to connect two nodes. Specific examples of network distance include the six degrees of separation phenomenon [7], which claims that any two people are connected through at most five acquaintances.

The relationship between infection curve rates and network distance can be illustrated with a simple network infection model as is illustrated in Figure 1. In Figure 1, there are two networks (a and c) with different path lengths, each with one hypothetically infected COVID-19 seed node. At each time step, the disease spreads from infected nodes to every node to which they are connected. The disease spreads would spread from the seed node to its direct neighbors. In the second step, the disease would spread to the direct neighbors' neighbors, who are at network distance 2 from the seed node, and so on. Over time, the virus transgresses among the network ties until all nodes are infected. The example shows that the network distance of a node is identical to the number of time steps it would take the virus to reach all nodes in the network. The distribution of the network distances to the source thus directly maps onto the curve of new infections.

In Figure 1, both networks have the same number of nodes (individuals) and edges (interactions). The network in Figure 1c has a much flatter curve than the network in Figure 1a even though all nodes are eventually infected in both cases. The network in Figure 1c has longer path lengths than the one illustrated in Figure 1a. The networks show more distance between nodes due to differences in the structure of interaction among the nodes even though the same absolute contact prevalence was pervasive. When adopting a network perspective, an approach which flattens the curve in the network is thus equivalent to an increase of tie length from an infected individual to all others, which can be achieved by restructuring contact even though there is a general reduction of contact. Subsequently, one aim of social distancing should be to increase the average network distance between individuals by smartly and strategically manipulating the structure of interactions. Our illustration shows a workable path to maintain a flattening curve, while allowing for some social interaction. To be successful, we must create interaction strategies that allow real-life networks to mirror those the network in Figure 1c and less like Figure 1a.

In Figure 2, we depict a network in which densely tied communities are bridged by random, long-range ties. This kind of network symbolizes the core features of real-world contact network [8] and is commonly referred to as a small-world network [9]. In communities, individuals exhibit homophilic qualities and adjacent communities are geographically close. In terms of geographic distance, the further away two clusters are in the figure, the further they live from each other and the more dissimilar their members become. In Figure 2, the networks depict the successive, the results of contact reduction strategies, creating clusters of individuals with removal of the bridging nodes that would normally connect these clusters. Similar methods have been used as a strategy to disband terrorist groups.



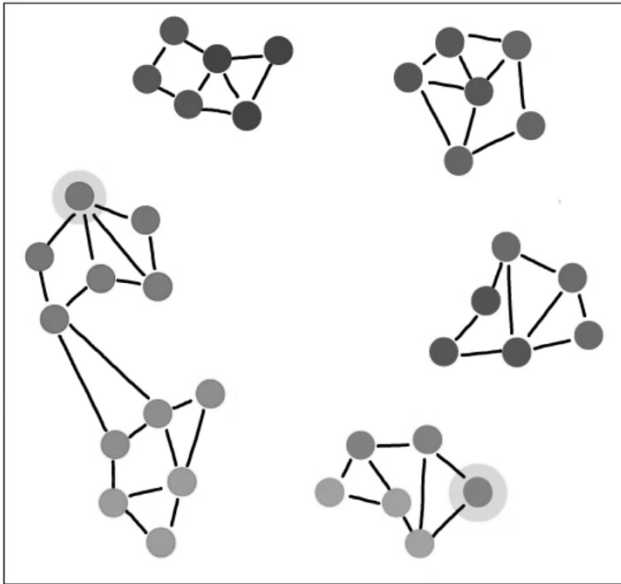


Figure 2. Based on the initial small-world network (a), these example networks are drawn based on the removal of ties from others who live far away and are dissimilar (b), removal of non-embedded ties that are not part of triads (c) repeating rather than extending contact (d). Node placement represents geographic location of residence. Ties to dissimilar others who live far away are indicated by ties substantially longer than the average.

Our network approach uses formal stochastic infection models that incorporate core elements from infection modeling with ideal-type network models and statistical relational event models. Stemming from classical disease modelling in which individuals or actors can be in four categories: susceptible; exposed (infected but not yet symptomatic); infectious; or recovered (no longer susceptible to the disease). With this model, q actors are infectious while all other actors are susceptible to the disease. Susceptible actors can become exposed by having contact with others who are infectious, no matter if this contact results in contagion and is calculated probabilistically. Within a designated amount of time following exposure, an actor becomes infectious, and later moves to the recovered state.

Epidemic modeling shows that contact probabilities in a population are imposed by network structure, which can create contact opportunities and inopportunities among actors. A robust network depicts the typical contact people had in a pre-COVID-19 world in different so-called social circles. It consists of network ties between individuals who live in close proximity to one another with individuals who are similar in terms of individual attributes, such as age, education or socioeconomic status, and individuals who are members of similar groups, such as organizations, social institutions (including schools and workplaces).

Additionally, this type of network includes random connections that may emerge in the population.

Lastly, we conducted a comparative analysis of eviction rates before and after the implementation of COVID-19 mobility restrictions in Philadelphia. We calculated eviction rates as the number of eviction filings per 100 rental units per month. We also calculated the percentage change in eviction rates from the pre-COVID-19 period (January 2019 to February 2020) to the COVID-19 period (March 2020 to December 2020). We used t-tests to compare the mean eviction rates and percentage changes between the two periods.

III. RESULTS

A. Analysis

Our analysis revealed that areas with high eviction rates had a higher level of mobility, particularly in places such as retail and recreation, grocery and pharmacy, and parks. Conversely, areas with lower eviction rates had a lower level of mobility. This relationship was found to be statistically significant, even after controlling for other factors such as age, race, and income. These results suggest that the eviction rates and mobility patterns are closely linked, and areas with high eviction rates may experience increased transmission of COVID-19 due to higher mobility.

The network analysis demonstrated that individual adoption was much more likely when participants received social reinforcement from multiple neighbors in the social network. The patterns of behavior spread were significantly farther and faster across clustered-lattice networks than across corresponding random networks.

Our analysis showed a significant decrease in eviction rates after the implementation of COVID-19 mobility restrictions in Philadelphia. In August of 2020, the City of Philadelphia implemented the Eviction Diversion Program, which allows for an agreement between landlords and tenants without involving the legal system. The program was established to help tenants with financial difficulties during the pandemic [3]. Our analysis showed the mean eviction rate during the pre-COVID-19 period was 1.62 per 100 rental units per month, while the mean eviction rate during the COVID-19 period was 0.96 per 100 rental units per month. This represents a 41.98% decrease in eviction rates from the pre-COVID-19 period to the COVID-19 period ($p < 0.001$). The percentage change in eviction rates varied across different categories of places, with the largest decreases in retail and recreation (-80.23%), transit stations (-72.27%), and workplaces (-54.06%) ($p < 0.001$ for all).

Since most individuals in a post-lockdown world need to interact across multiple social circles, adopting only one strategy to prevent the disease spread may not be practical. A mix of different strategies could therefore be more realistic to account for the multifaceted nature of human

interaction. In our network analyses, we found that mixing strategies, using three, two-faceted combinations and one three-faceted combination, compared with the single strategies that aim for similarity and also community building. Our work shows that using strategies that are multifaceted are comparably as effective as single strategies and can be recommended as alternatives if single strategies are not practicable in some settings. Each combination performs better in limiting infection spread than the naive contact reduction strategy.

Governments and organizations faced economic and social pressure to gradually and safely open up societal activity, yet they lacked scientific evidence on how to successfully do this. Using social network-based strategies empowers individuals and organizations to adopt safer contact patterns across multiple domains by as it provides individuals with ways to differentiate between high- and low-impact contacts. This system gives them a structure with which to operate and confidently begin to interact societally. The result may also empower individuals to strategically adjust and control their own interactions without being requested to fully isolate, giving them decision-making power. The emphasis in this approach makes distancing measures more palatable and sustainable over longer periods of time.

This approach is one that has real-world application, providing individuals opportunities to interact in different social circle in the workplace or with family and friends. Our analysis using mixed strategies addresses the concern over the general population being able to adopt one rigid lockdown-type approach. Our results show that a mix of strategies are a considerably better approach than simply releasing one non-strategic approach; however, further modelling is needed to determine the performance across a variety of contexts. When approaching this issue from a policy perspective, the design of steps to ease lockdowns can be done with potential behavioral recommendations in mind. This approach should consider network structures and demographic characteristics of individuals to determine how the use of one strategy will yield the best results. Decisions on which approaches to utilize and the coupling of these approaches will need to consider the population and their patterns of behavior.

IV. CONCLUSION

Determining strategies for contact reduction and social distancing can help to inform policy changes ranging from short-term, e.g., complete lockdown, to more long-term approaches. Contact reduction strategies that stem from insights into individual network contact, such as diseases, memes, information or ideas, can greatly decrease the propensity for the spread of the disease [9,10]. This type of spread is generally preventable with networks that consist of groups that are densely connected and have only a few connections in-between. An example of this type of network

would be one that has individuals living in isolated villages that are scattered over sparse rural areas [11]. Such knowledge can aid in the avoidance of rapid contagion levels through the encouragement of social distancing. This approach can provide an increase in clustering patterns to ensure the largest benefit of reduction in social contact, which will help to limit disease spread.

Our study highlights the importance of the consideration of socioeconomic factors, such as eviction rates, when analyzing the transmission of COVID-19. Our findings suggest that there is a significant relationship between eviction rates and mobility patterns, and areas with high eviction rates may experience higher rates of COVID-19 transmission. Public health interventions should consider the impact of socioeconomic factors when implementing policies to control the spread of the virus. Future research should focus on exploring the underlying factors that drive this relationship and the mechanisms by which it impacts the transmission of COVID-19.

A shortcoming of our study is the limited number of network actors due to the confinement of the city limits of Philadelphia. While we varied the number of nodes and found no substantial difference in the results, the dynamics of the model in large networks of, for example, 100,000+ actors is not known. In the current implementation of the model, the computational complexity increases with the number of actors, which makes simulations with such numbers unrealistic. Subsequently, additional work on the model implementation is needed to extend its applicability to large, real-world networks, offering clearer extensions for future research.

Despite these limitations, some concrete policy guidelines can be deduced from our network-based strategies. In workplaces and schools, staggering shifts and start and end times will keep contact in small groups at a minimum and reduce contact between those present. Additionally, repeated social meetings of individuals of similar ages who live alone carry a comparatively low risk. However, in a household of five, when each person may interact with different sets of friends, many shortcuts are being formed that are potentially connected to a very high risk of spreading the disease.

In summary, simple behavioral policies can go a long way in keeping spread of disease at a minimum. For disease containment, our approach provides insights to individuals, governments and organizations regarding strategies to enable contained activity: seeking similarity; strengthening interactions within communities; and repeated interaction with the same people to create bubbles, reducing the higher levels of mobility, particularly in places such as retail and recreation, grocery and pharmacy, and parks. This will aid in helping to reduce the eviction rates since eviction rates and mobility patterns are closely linked and greatly reduce the transmission of disease spread.

REFERENCES

- [1] I. Goldstein, E. Dowdall, C. Weidig, J. Simmons, and B. Carney, "Evictions in Philadelphia: A data & policy update," *The Reinvestment Fund*. Available from https://www.reinvestment.com/wp-content/uploads/2019/10/ReinvestmentFund__PHL-Evictions-Brief-Oct-2019.Pdf, 2019.
- [2] G. Preston and V. J. Reina. "Sheltered from eviction? A framework for understanding the relationship between subsidized housing programs and eviction," *Housing Policy Debate*, vol. 31, no. 3-5, pp. 785-817, 2021.
- [3] A. Heinrichs and M. Treskon, "Diverting Eviction-Related Cases Away from Courts," 2023.
- [4] P. Block, M. Hoffman, I. J. Raabe, et al., "Social network-based distancing strategies to flatten the COVID-19 curve in a post-lockdown world," *Nat. Hum. Behav.*, vol. 4, pp. 588–596, 2020. <https://doi.org/10.1038/s41562-020-0898-6>
- [5] M. E. J. Newman, "Spread of epidemic disease on networks," *Phys. Rev. E* 66, 016128, 2002.
- [6] R. M. Anderson and R. M. May, *Infectious Diseases of Humans: Dynamics and Control*, Oxford Univ. Press, 2002.
- [7] S. Milgram, "The small world problem," *Psychol. Today*, vol. 2, pp. 60–67, 1967.
- [8] D. J. Watts and S. H. Strogatz, "Collective dynamics of 'small-world' networks," *Nature*, vol. 393, pp. 440–442, 1998.
- [9] D. J. Watts, "Networks, dynamics, and the small-world phenomenon," *Am. J. Sociol.*, vol. 105, pp. 493–527, 1999.
- [10] D. Centola, "The spread of behavior in an online social network experiment," *Science*, vol. 329, pp. 1194–1197, 2005.
- [11] H. B. Shakya, D. Stafford, D. A. Hughes, T. Keegan, R. Negron, J. Broome, M. McKnight, L. Nicoll, J. Nelson, E. Iriarte, and M. Ordonez, "Exploiting social influence to magnify population-level behaviour change in maternal and child health: study protocol for a randomised controlled trial of network targeting algorithms in rural Honduras," *BMJ open*, vol. 7, p. e012996, 2017.